Universidad de Deusto

Design and Development of a passive computational UHF RFID platform using vector backscatter modulation on the uplink

Doctoral thesis presented by Florian Muralter
in the PhD program in Engineering for the Information Society and Sustainable Development

Directed by Dr. Hugo Landaluce Simon
and Dr. Asier Perallos Ruiz

Universidad de Deusto

Design and Development of a passive computational UHF RFID platform using vector backscatter modulation on the uplink

Doctoral thesis presented by Florian Muralter
in the PhD program in Engineering for the Information Society and Sustainable Development

Directed by Dr. Hugo Landaluce Simon and Dr. Asier Perallos Ruiz

PhD candidate

	Signatory	Florian Muralter
	Date/Time-UTC	2021-05-14T05:27:54Z
Note	This document is signed with a qualified electronic signature and is legally equivalent to a handwritten signature. https://sign.sproof.io	

PhD supervisor

Hugo Landaluce

Firmado digitalmente por Hugo Landaluce
Nombre de reconocimiento (DN): cn=Hugo Landaluce, o=Universidad de Deusto, ou=Facultad de Ingeniería, email=hlandaluce@deusto.es, c=ES
Fecha: 2021.05.13 10:50:08 +02'00'

PhD supervisor

Firmado digitalmente por PERALLOS RUIZ ASIER - 449761935
Nombre de reconocimiento (DN): c=ES, serialNumber=IDCES-449761935, givenName=ASIER, sn=PERALLOS RUIZ, cn=PERALLOS RUIZ ASIER - 449761935
Fecha: 2021.05.13 09:35:47 +02'00'

Bilbao, May 2021

Design and Development of a passive computational UHF RFID platform using vector backscatter modulation on the uplink

Author: Florian Muralter

Advisor: Hugo Landaluce Simon

Advisor: Asier Perallos Ruiz

Text printed in Bilbao

First edition, May 2021

Abstract

This work presents the steps taken to design and implement a passive, computational Ultra High Frequency (UHF) Radio Frequency Identification (RFID) platform using vector backscatter modulation to increase the data throughput on the reader-to-tag communication link.

Passive UHF RFID represents an automated identification technology operating in the Industrial Scientific and Medical (ISM) band between 860 MHZ and 960 MHZ. One such RFID system consists of an interrogator (reader) and at least one wirelessly powered transponder (tag). The energy needed for the operation of the tag is harvested from the incident electromagnetic wave. After the reader has interrogated the tags, the reader radiated continuous wave is used as the carrier for the tag-to-reader backscatter communication. This technology uses antenna load modulation to reflect a distinct part of the incident wave corresponding to the transmitted data sequence. Due to recent advances in the area of RFID, transponders are no longer used for identification only. With the availability of low-power sensors and microcontroller units (MCUs), sensoric and computational capabilities have been added to attract a wider field of applications. The additional need of being able to backscatter the data collect by a sensor, or computed by the MCU to the reader requires further advances considering the backscatter communication link.

As part of this thesis we have presented a thorough study of State-of-the-Art passive computational RFID. This theoretical and experimental investigation of the performance limitations, has fruited

in the identification of gaps considering the typically used impedance measurement methodologies. Thus, we have proposed an alternative method for measuring the chip impedance of an UHF RFID chip, as well as an alternative approach to measuring the reflected harmonic power using a Digital Sampling Oscilloscope. As a result, the reflected harmonics at low input power levels could be neglected when designing the presented modular passive UHF RFID platform with easily exchangable modules. This research platform facilitates the design process when developing novel UHF RFID solutions. The further proposed passive computational UHF RFID platform using backscatter communication represents a complete RFID system consisting of a tag with the ability to transmit 2-bits at a time and a Software Defined Radio reader being able to demodulate the tag response.

Acknowledgements

The authoring of this PhD thesis is not only the work of the sole author, it also reflects the guidance, support and help of a number of close individuals which were instrumental to this outcome.
First of all, I would like to express my gratitude to my supervisors Hugo Landaluce and Asier Perallos. Thank you for giving me the opportunity to spend this time in DeustoTech and the University of Deusto. The numerous short or long, personal or work-related meetings with Hugo have definitely shaped my thinking and often calmed my enthusiastic outbreaks, where the always objective and solution-oriented approach of Asier has often helped me re-find the continuous thread in my work.
I am also grateful to all the members of the DeustoTech Institute of Technology, especially Laura, Luis, Ruben, Aimar, Juan and Timothy, who have from the very beginning made me feel welcome and incorporated.
I would like to extend my sincere thanks to the researchers at the Associate Professorship for Microwave Engineering at the Technical University Munich led by Prof. Erwin Biebl. The possibility to spend 6 months at the TUM and to have access to all the lab facilities has improved my progress. The fruitful discussions in either physical or virtual coffee breaks have helped me widen my scope in other RF areas and refine my thoughts on my research topics.
Finally, I would like to say "Danke!" to my family. A huge part of what I am today, both in my leisure time, as well as at work is influenced by the opportunities offered by my parents, who always

appreciate the traveling and visiting of new places, even though sometimes they'd just like us to be a bit closer. Special thanks also to my brother Fabian, who never ceases to amaze me, with how little words are needed to make me understand a topic, he probably didn't even understand. The completion of this dissertation would definitely not have been possible without the help of my wife Tessa, who, with her concise responses and straight-forward solutions often helps me to simplify my thinking.

Thank you!

Florian Muralter

May 2021

Contents

List of Figures

List of Tables

Acronyms

CRC Cyclic-redundancy Check.

EIRP Effective Isotropic Radiated Power.

EM Electromagnetic.

EPC Electronic Product Code.

EPC-C1G2 EPC Class 1 Generation 2.

ETSI European Telecommunications Standards Institute.

FCC Federal Communications Commission.

GPS Global Positioning System.

HF High Frequency.

IC Integrated Circuit.

IoT Internet of Things.

ISM Industrial Scientific and Medical.

LF Low Frequency.

MCU Microcontroller Unit.

Acronyms

PC Protocol Control.

RFID Radio Frequency Identification.

SHF Super High Frequency.

UHF Ultra High Frequency.

VLF Very Low Frequency.

WSN Wireless Sensor Network.

chapter 1 Introduction

The following chapter provides a short introductory overview of the topics investigated in this thesis. The motivational background, as well as current trends in computational passive UHF RFID are presented. This section is followed by the thesis statement, including the proposed hypothesis, the defined objectives, and the achieved contributions. Subsequently this thesis' structure is presented, providing the reader with a continuous thread running through all published manuscripts. Finally, a short introduction into the scientific research articles written as part of this thesis is provided.

1.1 The Evolution of RFID

RFID: Enabling Industry 4.0 [1] and the Internet of Things (IoT) [2].

This technology, now being key to some of the most recent additions to making the world a smarter place, has a long history [3]. As the fundamental technology of RFID, reflective-power communication was first mentioned in Harry Stockman's 1948 landmark paper [4]. However, his statement, "Evidently considerable research and development work has to be done before the remaining basic problems in reflected-power communication are solved, and before the field of useful applications is explored."[4], has deemed to be true, as, for the following twenty years, the research world was lacking progress in this field. Given the development of the transistor, the Integrated Circuit (IC) and many more inevitable inventions, the 1970s and 1980s were off to an RFID boom.

The term RFID refers to all identification systems operating using radio frequency communication. Such an RFID system typically consists of an interrogator (reader) and at least one transponder (tag), where the reader refers to a typically stationary base station and the responding tags, placed on objects, are contactless and movable (see Figure 1.1). [5]

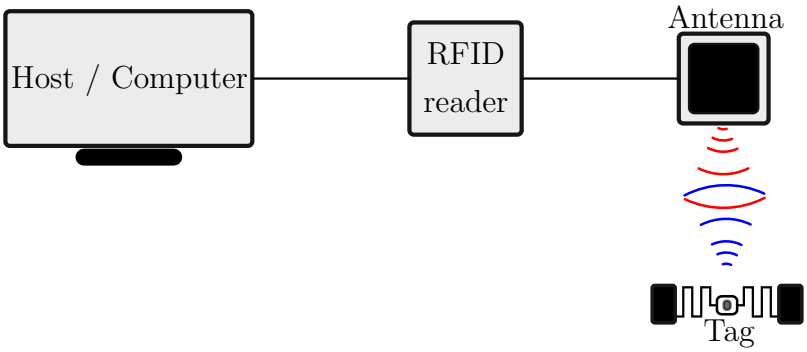

Figure 1.1: Visualization of a typical RFID system.

Being designed for identification processes, the first major fields of deployment were asset tracking and factory automation. Until now, the areas where RFID is deployed are continuously evolving. Everyday life, even though hardly

ever noticed, is packed with RFID applications ranging from automated toll collection and access control to dispensing goods or boarding a plane. Yet, being already considered mainstream in the 1990s, the evolution of RFID is still in progress, and the technologies are being adapted to the emerging disciplines and needs [3].
An RFID tag can be powered by an external power source (active) or by harvesting the incident electromagnetic wave (passive). Improvements in passive RFID and the development of improved ICs for energy harvesting have yielded a technology being considered fully contactless [6]. Three further additions to the area of passive RFID, apart from its traditional use in asset tracking, are:

- ◇ RFID sensing and computational RFID:
  While RFID is commonly used to identify and track objects, Wireless Sensor Network (WSN)s are typically used to collect data from their sensor nodes. Recent additions to the IoT have seen a fusion of these two disciplines, benefiting from the potentials and possibilities of either of them. RFID sensing represents a subarea of RFID, where the deployed RFID tag incorporates an external sensor. On the other hand, in computational RFID systems an additional microcontroller is connected to implement simple computational tasks. [7]

- ◇ RFID based localization:
  Given the inherent localization problem of the Global Positioning System (GPS) in indoor scenarios, recent developments in the area of RFID based indoor localization have widened the scope of this technology. [8]

- ◇ Chipless RFID:
  The main drawback of RFID tags compared to its antecessor, the barcode, is the cost of the tag itself, which is mainly dictated by the price of the deployed RFID chip. Chipless RFID, thus, is focused on getting rid of the IC, by developing planar encoders. [9]

All these advances will not be the last additions to the growing field of RFID research. Latest advances in material science and antenna design have shown that biodegradable RFID [10] might just be the next stop on this path.

1.2 Thesis Statement

RFID sensing and computational RFID represent emerging areas within the field of RFID. As a result, the amount of data to be transmitted back towards the reader is increasing, yielding the need for faster and more powerful backscatter communication architectures. Vector backscatter modulation, referring to load modulation with a vector difference between the deployed impedance states represents one promising solution. The following section presents the statement of the hypothesis, the addressed objectives and the achieved contributions.

1.2.1 Hypothesis

It is possible to design and develop an UHF RFID research platform using vector backscatter modulation to increase the data throughput on the reader-to-tag communication link.

1.2.2 Objectives

In order to validate the proposed hypothesis, the following objectives have been identified.

Objective 1 To perform an analysis and review of the currently available passive computational UHF RFID tags.

Objective 2 To study and investigate the methodologies used to characterize the chip impedance seen by the tag antenna.

Objective 3 To design and develop a passive, computational UHF RFID platform using vector backscatter modulation.

1.2.3 Contributions

The previously mentioned objectives have resulted in the following five contributions.

Contribution 1 Analysis of the State of the Art in passive, computational UHF RFID by performing an theoretical and experimental evaluation of available passive, computational UHF RFID platforms.

Contribution 2 Development of an alternative procedure for measuring the impedance of passive UHF RFID tags, by using a transmission line transformer test fixture.

Contribution 3 Development of an alternative procedure for measuring the reflection coefficient of passive UHF RFID tags at the frequencies up to the third harmonic, by using a Digital Sampling Oscilloscope (DSO) and a subsequent novel signal processing methodology.

Contribution 4 Design and implementation of a modular, passive, computational UHF RFID platform with easily exchangable modules.

Contribution 5 Design and implementation of a passive, computational UHF RFID tag using vector backscatter modulation.

1.2.4 Structure of the Thesis

Based on the hypothesis, objectives, and contributions mentioned in the previous section, the following part provides a continuous thread throughout the latter chapter containing the scientific publications.

Firstly, a study of the State of the Art in computational, passive UHF RFID has been performed. Three available platforms were studied both theoretically and experimentally to obtain thorough insight into the recent advances in this area. Having achieved publication of this first review as part of the SpliTech 2019 Conference (Publication I), an invitation to extend the work

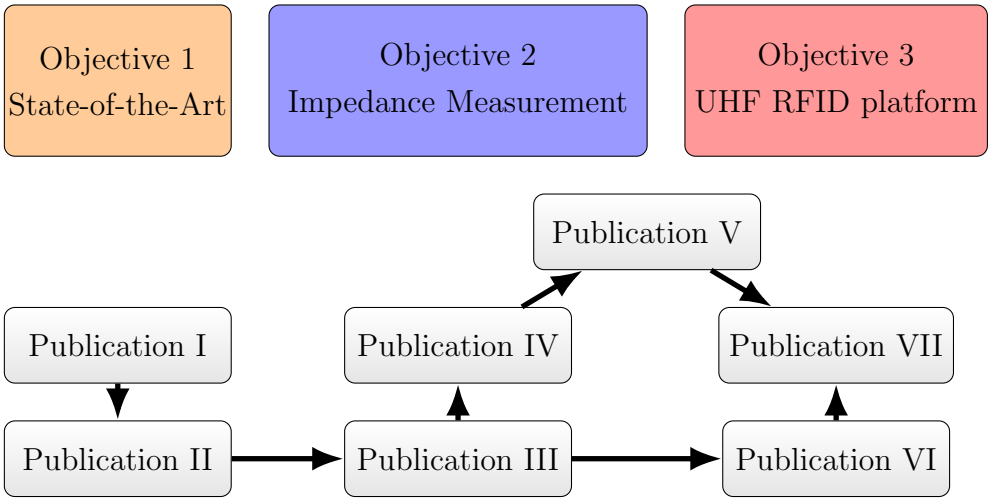

Figure 1.2: Vizusalization of the structure of this thesis.

and submit it to a special issue in the Transactions on Emerging Telecommunications Technologies Journal was pronounced. This extended version, incorporates a total of five investigated platforms and presents a more comprehensive experimental section (Publication II). As a result, the problematic behavior of the UHF RFID chip impedance due to the nonlinear character of the rectifier section was identified as one of the main issues when designing novel UHF RFID solutions. Thus, the next investigations focused on studying the measurement and nonlinear behavior of the chip impedance. This process has fruited in the publication of an alternative approach to measuring the chip impedance based on a transmission line transformer (Publication III). Furthermore, a methodology to study the backscattered harmonics using a time domain reflection coefficient approach has been proposed (Publication IV). Having obtained a more reliable method for measuring the impedance of UHF RFID chips, and knowing, that the reflected power at the harmonic frequencies can be neglected at low power levels, the further work relies on these conclusions drawn from the previous investigations. All further achievements are directly connected to the actual design and implementation process of the passive, computational UHF RFID platform using vector backscatter modulation. Firstly, the process of selecting impedance for achieving a Phase-shift keying (PSK) load modulation constellation has been studied (Publication V).

Next, a passive, modular, computational UHF RFID research platform with easily exchangable modules has been proposed to facilitate the development process of novel UHF RFID solutions (Publication VI). The *passive computational UHF RFID platform using vector backscatter modulation* then presents the fully functional, passive, computational UHF RFID platform using a dual-gate Metal Oxide Semiconductor Field Effect Transistor (MOSFET) as the quaternary modulator to achieve a multi-state backscattering (Publication VII). The corresponding Software Defined Radio (SDR) reader is able to demodulate and decode the received response, yielding an overall shortened response time. Figure 1.2 shows a visualization of the thesis' structure and the assignment of the publications to the different research objectives.

1.3 Publications

This thesis represents a compilation of 7 published research articles. The following list presents the mentioned manuscripts with their corresponding reference and relates its content to one of the defined research objectives.

Publication I

"A theoretical and experimental study of passive computational RFID tags" investigates the RF front-end of 3 State-of-the-Art passive computational RFID tags: AMS SL900a Dev Kit, Farsens Spider Eval, WISP 5.1. Given a module-based approach, the antenna, the power matching, the power harvesting, and the load modulation are reviewed both theoretically and experimentally.
This publication is linked to **Objective 1**.

F. Muralter, L. Arjona, H. Landaluce and A. Perallos, "A theoretical and experimental study of passive computational RFID tags," in *2019 4th International Conference on Smart and Sustainable Technologies (SpliTech),* pp. 1-5, 2019.

Publication II

This paper with the same title as publication 1 represents the extension of the above-mentioned paper presented at the SpliTech 2019 conference. The extended version incorporates an expanded theoretical study, adding further research platforms, and an enlarged experimental section.
This publication is linked to **Objective 1**.

F. Muralter, L. Arjona, H. Landaluce and A. Perallos, "A theoretical and experimental study of passive computational RFID tags," *Transactions on Emerging Telecommunications Technologies,* vol. 31, no. 12, 2020.

Publication III

"UHF RFID chip impedance and sensitivity measurement using a transmission line transformer" describes a simplified procedure for measuring the impedance of an UHF RFID chip and finding its turnon-point.
This publication is linked to **Objective 2**.

F. Muralter, M. Hani, H. Landaluce, A. Perallos and E. Biebl, "UHF RFID chip impedance and sensitivity measurement using a transmission line transformer," in *IEEE International Conference on RFID (IEEE RFID 2021)*, 2021.

Publication IV

"Harmonic Voltage Reflection Analysis of UHF RFID chips" presents a measurement platform for the harmonic characterization of UHF RFID chips. The measurement of the incident and reflected wave at the RFID chip terminals is performed using a digital sampling oscilloscope.
This publication is linked to **Objective 2**.

F. Muralter, M. Hani, H. Landaluce, A. Perallos and E. Biebl, "Harmonic Voltage Reflection Analysis of UHF RFID chips," *IEEE Transactions on Instrumentation and Measurement,* vol. 70, pp. 1–7, 2020.

Publication V

"Selecting impedance states in a passive computational RFID tag backscattering in PSK" proposes a methodology to carefully select the impedance states of a backscatter phase-shift keying (PSK) load modulator in a passive computational UHF RFID tag.
This publication is linked to **Objectives 2 and 3**.

F. Muralter, R. Del-Rio-Ruiz, H. Landaluce and A. Perallos, "Selecting impedance states in a passive computational RFID tag backscattering in PSK," *IEEE Microwave and Wireless Components Letters,* vol. 29, no. 10, pp. 680–682, 2019.

Publication VI

"A Fully Customizable RFID Research Platform with Exchangeable Modules" presents the design and implementation of a passive, modular, computational UHF RFID research platform. The incorporated tag can be subdivided into a number of modules (e.g., Modulator, Rectifier, etc.), which have been separated and optimized for easy connectability using sub-miniature A (SMA) connectors and standard jumper wires.
This publication is linked to **Objective 3**.

F. Muralter, L. Arjona, H. Landaluce and A. Perallos, "A Fully Customizable RFID Research Platform with Exchangeable Modules," *IEEE Sensors Journal,* 2021.

Publication VII

"A passive computational UHF RFID platform using vector backscatter modulation" presents the design and implementation of a passive, computational UHF RFID platform with quaternary backscattering capabilities.
This publication is linked to **Objective 3**.

F. Muralter, L. Arjona, H. Landaluce and A. Perallos, "A passive computational UHF RFID platform using vector backscatter modulation," *IEEE Sensors Journal,* 2021.

References

[1] L. D. Xu, E. L. Xu, and L. Li, "Industry 4.0: state of the art and future trends," *International Journal of Production Research*, vol. 56, no. 8, pp. 2941–2962, 2018.

[2] X. Jia, Q. Feng, T. Fan, and Q. Lei, "RFID technology and its applications in Internet of Things (IoT)," in *2012 2nd International Conference on Consumer Electronics, Communications and Networks (CECNet)*, 2012, pp. 1282–1285.

[3] J. Landt, "The history of RFID," *IEEE Potentials*, vol. 24, no. 4, pp. 8–11, 2005.

[4] H. Stockman, "Communication by Means of Reflected Power," *Proceedings of the IRE*, vol. 36, no. 10, pp. 1196–1204, 1948.

[5] K. Finkenzeller, *RFID Handbook: Fundamentals and Applications in Contactless Smart Cards, Radio Frequency Identification and Near-Field Communication, 3rd Edition*. John wiley & sons, 2010.

[6] D. Paret, *RFID at Ultra and Super High Frequencies: Theory and Application*. John Wiley & Sons, 2009.

[7] H. Landaluce, L. Arjona, A. Perallos, F. Falcone, I. Angulo, and F. Muralter, "A Review of IoT Sensing Applications and Challenges Using RFID and Wireless Sensor Networks," *Sensors*, vol. 20, no. 9, p. 2495, 2020.

[8] C. Li, L. Mo, and D. Zhang, "Review on UHF RFID Localization methods," *IEEE Journal of Radio Frequency Identification*, vol. 3, no. 4, pp. 205–215, 2019.

[9] C. Herrojo, F. Paredes, J. Mata-Contreras, and F. Martín, "Chipless-RFID: A Review and Recent Developments," *Sensors*, vol. 19, no. 15, 2019.

[10] F. Costa, E. Perret, S. Genovesi, S. Tedjini, A. Lazaro, D. Girbau, R. Villarino, M. Borgese, A. Dicandia, and G. Manara, "Progress in green chipless RFID sensors," in *2017 11th European Conference on Antennas and Propagation (EUCAP)*. IEEE, 2017, pp. 3917–3921.

CHAPTER 2 Fundamentals

The following chapter introduces the basics and fundamentals necessary and relevant to understanding the scientific work presented in the latter chapters of this thesis. First, Reflection Coefficient Analysis, Backscatter Communication, and the Friis Equation, which are common RF engineering topics and their relation to RFID technology, are introduced. The following section about RFID identifies this thesis' position within the area of RFID. Subsequently, a concise State of the Art in passive computational UHF RFID is presented.

2.1 Reflection Coefficient Analysis

S-parameters describe the response of an N-port network to signals applied to any of its ports. The first number in the subscript refers to the responding port, while the second number indicates the incident port. [1]

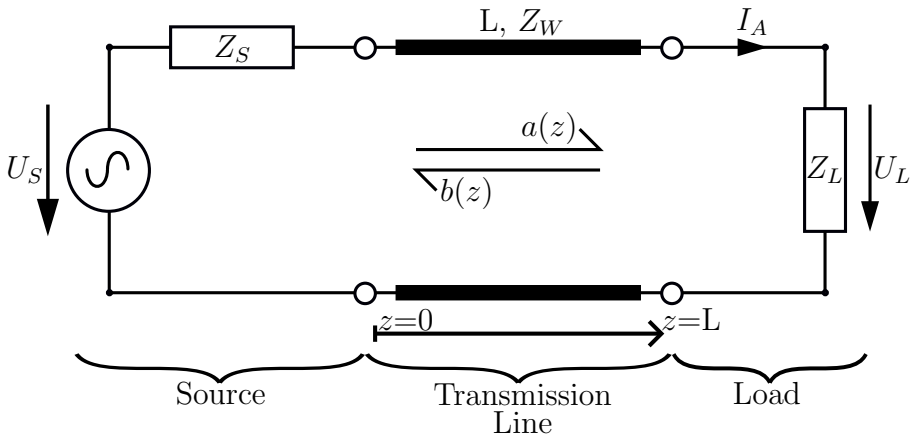

Figure 2.1: Transmission Line fed by a Source and terminated by a Load.

Given a 1-port device, the only existing S-parameter would be S_{11} referred to also as the reflection coefficient Γ with alternative symbols being r, ρ. This key term of transmission line theory can be derived from the voltage and current waves $a(z)$ and $b(z)$ (see Figure 2.1) traveling in opposite directions on the transmission line at point z [2]:

$$U(z) = U_p(z) + U_r(z) = \sqrt{Z_W}[a(z) + b(z)], \tag{2.1}$$

$$I(z) = I_p(z) + I_r(z) = \frac{1}{\sqrt{Z_W}}[a(z) - b(z)], \tag{2.2}$$

where $U(z)$ and $I(z)$ represent the superposition of the forward propagating waves U_p, I_p and the reflected waves U_r, I_r. Z_W stands for the wave impedance. At the load $z = L$ with impedance Z_L, the relation of voltage and current is given as [3]

$$Z_L = \frac{U(L)}{I(L)}. \tag{2.3}$$

Substituting $U(L)$ and $I(L)$ using Equations 2.1 and 2.2 results in the following relation:

$$Z_L = \frac{\sqrt{Z_W}[a(z) + b(z)]}{\frac{1}{\sqrt{Z_W}}[a(z) - b(z)]}, \tag{2.4}$$

which by rearranging the formula yields

$$\frac{b(L)}{a(L)} = \frac{Z_L - Z_W}{Z_L + Z_W}. \tag{2.5}$$

With the reflection coefficient Γ defined as the ratio of the reflected to the incident wave, Γ can be calculated as

$$\Gamma = \frac{Z_L - Z_W}{Z_L + Z_W}, \tag{2.6}$$

depending on both the load impedance Z_L and the wave impedance Z_W.

2.1.1 Reflection Coefficient in RFID

Considering a typical RFID tag, consisting of an antenna and an RFID chip results in a system similar to the one presented in Figure 2.1. The part missing between the terminals of the source and the load is the transmission line, thus, yielding a direct connection of two complex impedances.

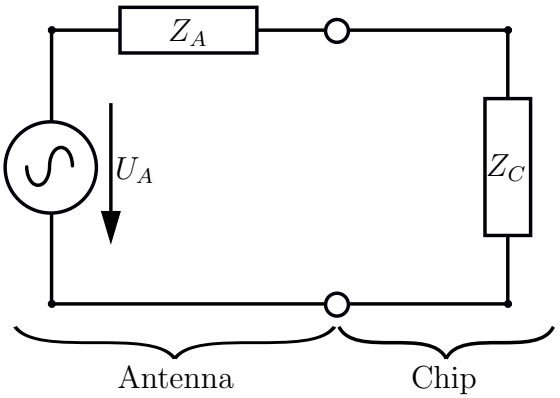

Figure 2.2: Equivalent circuit of a receiving RFID tag.

The equivalent circuit representing an RFID tag in the receiving mode is shown in Figure 2.2 and results in a voltage reflection coefficient of

$$\Gamma = \frac{Z_C - Z_A}{Z_C + Z_A}. \tag{2.7}$$

To allow for a maximum power transfer, Γ has to be minimized. According to the maximum power theorem this is achieved by designing the antenna to have an impedance of $Z_A = Z_C^*$, with Z_A and Z_C denoting the antenna and RFID chip impedance, respectively. Another option is to design a suitable impedance matching network and connecting it between antenna and chip. Due to size and fabrication constraints, commercial RFID tags usually use impedance matched antenna designs.

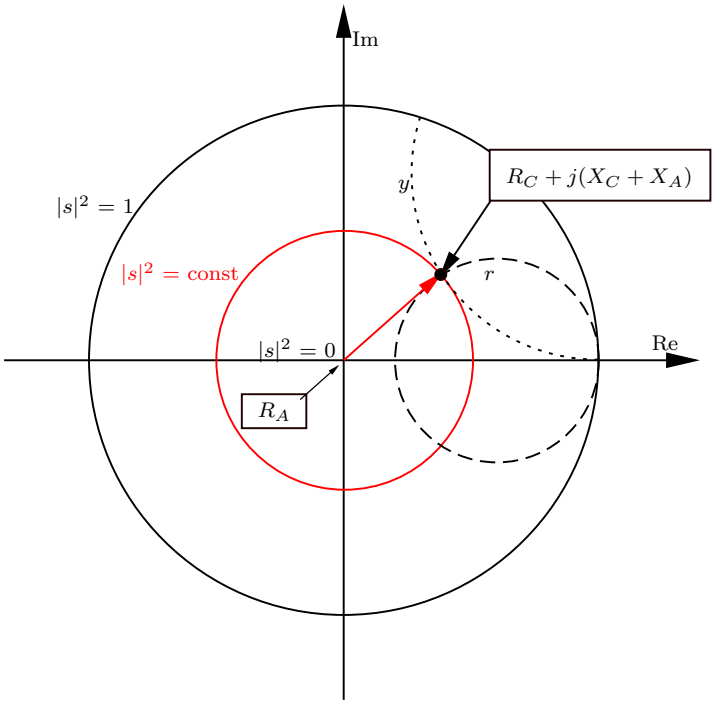

Figure 2.3: Visualization of the method proposed in [5] (with permission).

The Smith chart [4] represents a visual tool for designing impedance matching networks. This approach is typically used to match a complex load to a solely resistive transmission line. The process involves a normalization of the diagram to the real wave impedance, making it cumbersome to design a

matching network to interconnect two devices with complex impedances. In [5], a method to deploy the adapted Smith chart matching approach presented in [6] to RFID tag design and allowing the extraction of the power reflection coefficient $|\Gamma|^2$ from the Smith chart.
Figure 2.3 shows a visualization of the method proposed in [5]. By normalizing the Smith chart with the real part of the antenna impedance $\Re\{Z_A\}$ the contours of constant reactance become contours of modified reactance $X_C + X_A$. Concentric circles represent contours of constant power reflection. Thus, the minimum of a plotted trace of Γ as a function of frequency can easily be distinguished by finding the data point closest to the center of the Smith chart.

2.2 Backscatter Communication

Backscatter communication, first referred to as *Communication by Means of Reflected Power* [7], is a communication technology reflecting or backscattering a controlled part of an incident Electromagnetic (EM) wave to transmit data [8]. The antenna scattering theorem [9] represents the physical foundation to this technology. An antenna, if illuminated by an incident wave scatters EM energy corresponding to two different scattering modes. Thus, the backscattered field $E_{\mathrm{SCAT}}(Z_L)$ can be described as a superposition of both structural and load dependent scattering as [10]:

$$E_{\mathrm{SCAT}}(Z_L) = E_{\mathrm{SCAT}}^{\mathrm{REF}} + \Gamma_{\mathrm{MOD}} I_{\mathrm{REF}} E_{\mathrm{RAD}}, \tag{2.8}$$

with

$$\Gamma_{\mathrm{MOD}} = \frac{Z_L - Z_A^*}{Z_L + Z_A}, \tag{2.9}$$

where I_{REF} is the terminal current when the antenna is conjugate-matched and E_{RAD} stands for the field radiated by the scattering antenna considering a unit current source. Γ_{MOD} is a modified version of the voltage reflection coefficient presented in Equation 2.7. For a real valued Z_A, Γ_{MOD} reduces to its typical form. By refactoring Equation 2.8

$$E_{\mathrm{SCAT}}(Z_L) = I_{\mathrm{REF}} E_{\mathrm{RAD}} (A - \Gamma_{\mathrm{MOD}}), \tag{2.10}$$

with

$$A = \frac{E_{\mathrm{SCAT}}^{\mathrm{REF}}}{I_{\mathrm{REF}} E_{\mathrm{RAD}}}. \tag{2.11}$$

A is a complex, load-independent coefficient related to the geometrical and EM material characteristics of the used antenna design.

2.2.1 Backscatter Communication in RFID

Considering a typical thin dipole antenna as commonly used in UHF RFID tags, Equation 2.10 further reduces to

$$E_{\mathrm{SCAT}}(Z_L) = I_{\mathrm{REF}} E_{\mathrm{RAD}} (1 - \Gamma_{\mathrm{MOD}}), \tag{2.12}$$

as $A = 1$ yields a reasonable approximation [11].
A modulation of the backscattered field is then achieved by changing the impedance (load) at the terminals of the tag antenna, yielding the commonly used backscatter load modulation. With the antenna impedance not depending on the chip impedance connected to its ports, the modified reflection coefficient Γ_{MOD} is, thus, changed corresponding to the data sequence transmitted towards the reader.

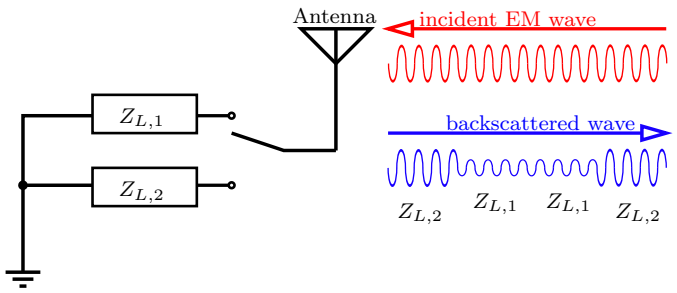

Figure 2.4: Visualization of backscatter load modulated communication.

To achieve a maximum power transfer to the chip circuitry during reader-to-tag communication, the first load impedance $Z_{L,1}$ is often named the absorbing state, as it is designed to be conjugate matched to the tag antenna impedance. The second load modulation state corresponding to $Z_{L,2}$ is then selected to manage a trade-off between power harvesting efficiency during tag-to-reader (uplink) communication and a high modulation depth. Considering this explanation the impedance state $Z_{L,1}$ corresponds to a logic LOW (minimum power reflected) and $Z_{L,2}$ a logic HIGH received by the reader.

2.3 Friis Equation

The Friis equation [12] represents a simple transmission formula for radio communication environments consisting of a transmitting and a receiving antenna. Considering free space propagation the power at the terminals of the receiving antenna P_R can be calculated as:

$$P_R = P_T \frac{A_R A_T}{d^2 \lambda^2}, \tag{2.13}$$

where P_T denotes the power fed to the terminals of the transmitting antenna, and A_R and A_T refers to the apertures (effective areas) of the receiving and transmitting antennas, respectively. λ denotes the free space wavelength and d represents the distance between the two considered antennas.
The aperture A of an antenna is defined as the ratio of the power available at the terminals of a receive antenna to the power flux density of a polarization-matched plane wave incident on the antenna from the same direction [13]. A is related to the antenna gain as

$$G = \frac{A}{A_{\mathrm{ISO}}}, \tag{2.14}$$

with the aperture of an isotropic antenna being

$$A_{\mathrm{ISO}} = \frac{\lambda^2}{4\pi}. \tag{2.15}$$

Thus, substituting the antenna apertures A_R and A_T in Equation 2.13 by the corresponding gain parameters G_R and G_T yields the version of the Friis equation most commonly used in communications engineering:

$$P_R = P_T G_T G_R \left(\frac{\lambda}{4\pi d}\right)^2 \tag{2.16}$$

2.3.1 Read Range Evaluation in UHF RFID

UHF RFID is considered a long-range automatic identification technology [14]. Thus, the maximum distance at which a tag can be identified by a reader, the so-called read range represents one of the most important tag performance

characteristic. Both the reader sensitivity $P_{\mathrm{th,R}}$ and the chip sensitivity $P_{\mathrm{th,C}}$ can be the limiting factor. However, in passive UHF RFID the read range is typically restricted by the tag's sensitivity influenced by the chip sensitivity and the impedance matching factor between the tag antenna and the RFID chip. As an RFID system refers to a radio communication environment consisting of two antennas, the Friis equation deems very useful for the estimation and evaluation of the read range r_{max} in a laboratory environment [5]:

$$r_{\mathrm{max}} = \frac{\lambda}{4\pi}\sqrt{\frac{P_T\, G_T\, G_R\, PLF\, \tau}{P_{\mathrm{th,C}}}}, \tag{2.17}$$

with

$$\tau = |1 + \Gamma|^2, \tag{2.18}$$

where τ represents the power transmission coefficient which is related to the tag's impedance matching. PLF denotes the polarization loss factor which considering a circularly polarized reader antenna and a linearly polarized tag antenna is $PLF = 0.5$.

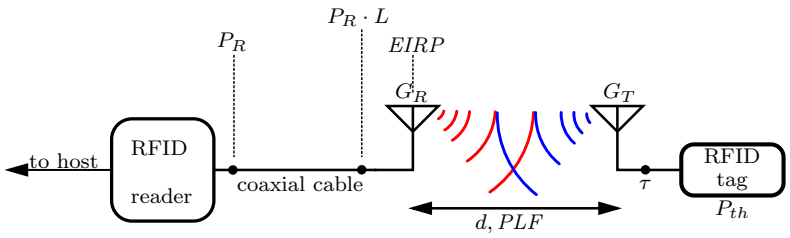

Figure 2.5: Visualization of the methodology used for measuring the read range of a UHF RFID tag.

This theoretical estimation can further be evaluated experimentally using an experimentation setup as sketched in Figure 2.5. The investigated tag is placed at a defined distance d from the reader antenna with gain G_T. Using a stepped transmit power, the minimum power P_{min} required for communication is evaluated. Given an Effective Isotropic Radiated Power (EIRP), which

typically is considered the maximum value allowed by local standards, the maximum read range can be computed using [5]

$$r = \sqrt{\frac{EIRP}{P_{\min} L G_T}}, \tag{2.19}$$

where L represents the losses introduced by the cable between the reader and the reader antenna.

2.4 Radio Frequency Identification

The following section tries to give a presentation of the research area of RFID. The methodology used for this purpose is visualized by the tree diagram shown in Figure 2.6.

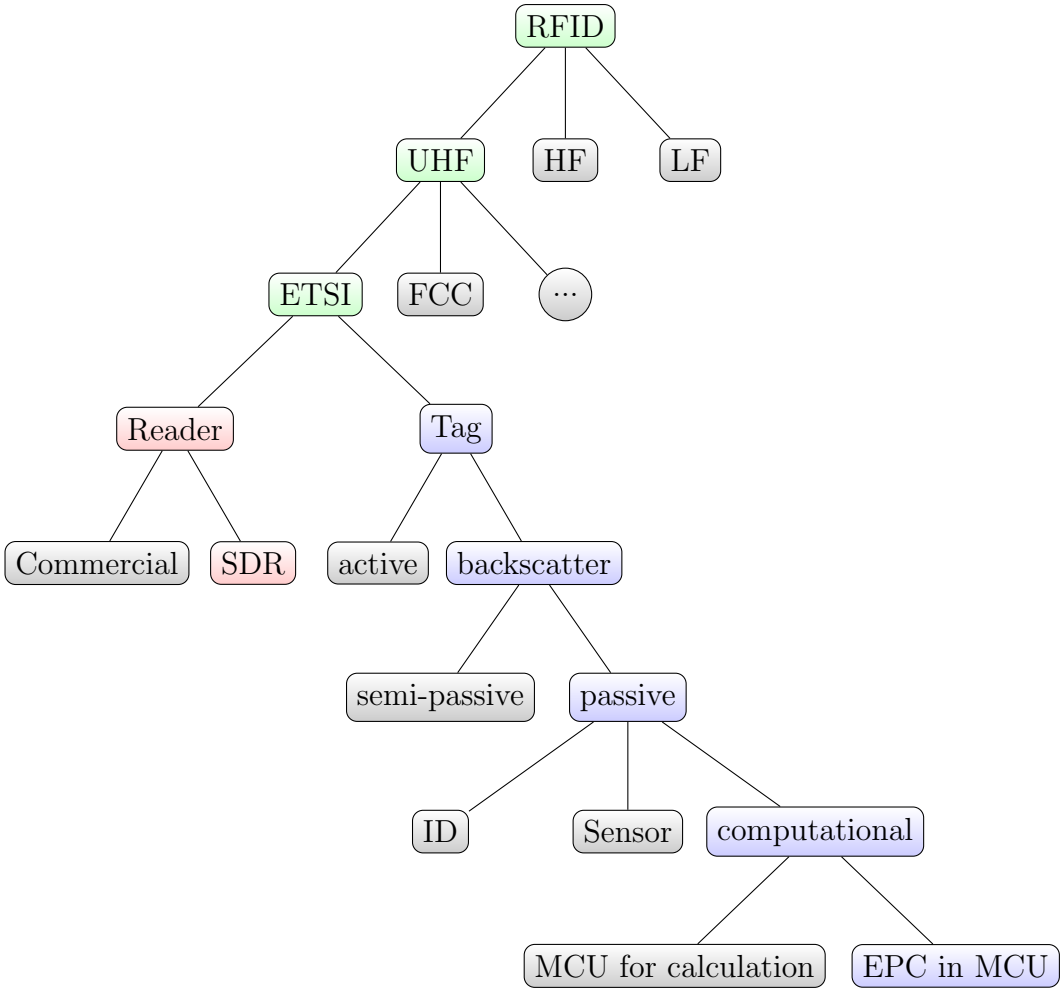

..

Figure 2.6: Tree Diagram of the research area of RFID

Starting from a very global perspective of RFID, the description follows a continuous path to, in the end, localize the position of this thesis within the field of RFID. RFID is first divided according to the operational frequency

band (UHF). Considering the usage of the platform mainly in Europe, it has to comply with the European Telecommunications Standards Institute (ETSI) regulations. Any RFID platform consists of at least one reader and a minimum of one tag. The focus on one of these topics further narrows the research area. Tags can be separated according to their power source (e.g., passive). These passive RFID tags are further subdivided by their functionality (e.g., computational), where some of the computational tags yield the possibility to adapt the communication protocol as it is firmware implemented (e.g. EPC in MCU). This general section on the research area of RFID is followed by a short review of the State of the Art in passive computational RFID.

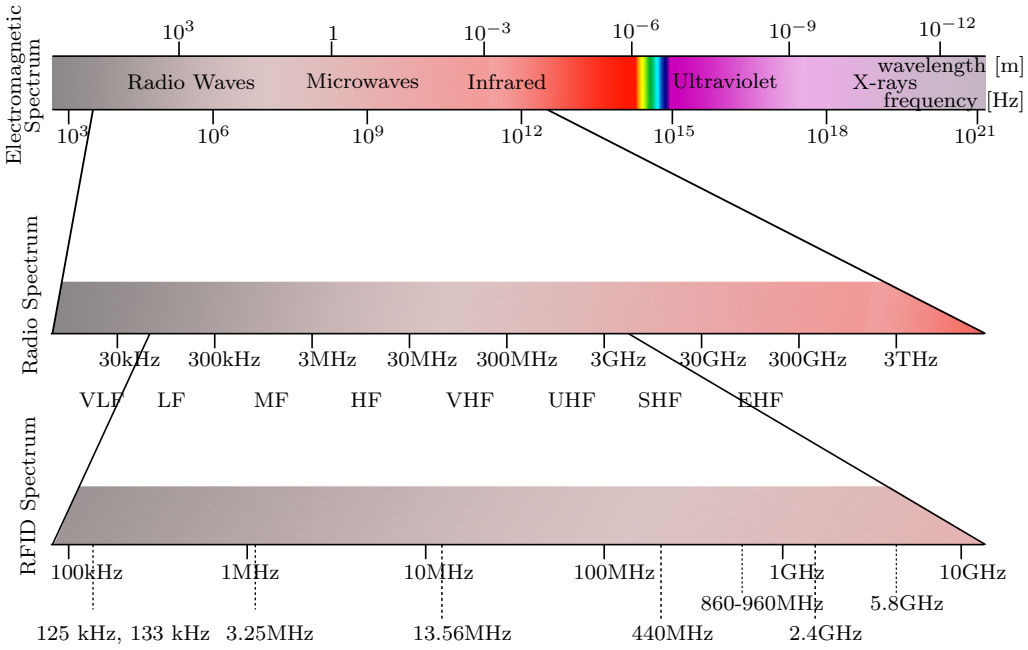

Figure 2.7: Used RFID frequency bands

2.4.1 UHF RFID

The Frequency f is a common characteristic to classify radio communication systems. As shown in Figure 2.7, the radio spectrum only forms a small part of the wide band of electromagnetic waves. Within this approximate range from 10 kHz to 3000 GHz, narrower frequency bands are named according to their frequency (Very Low Frequency (VLF), Low Frequency (LF), ...). Only

certain frequency bands within this range are accepted and/or authorized by national and international regulatory bodies for RFID applications [15]. Where LF and High Frequency (HF) RFID is typically using inductive coupling (near-field) between the reader and the tag, RFID systems in higher frequency band (UHF and Super High Frequency (SHF)) use electromagnetic coupling (far-field), thus, allowing for a longer read range at higher frequencies. [14]

The further part of this thesis is focussed on UHF RFID using frequencies in the Industrial Scientific and Medical (ISM) band between 860 MHz and 960 MHz. Within this range, regional regulatory authorities specify the authorized frequency bands and maximum limits of radiated power, commonly stated as EIRP. Figure 2.8 shows a visualization of the authorized UHF RFID frequency bands assigned to different regions of the world [16].

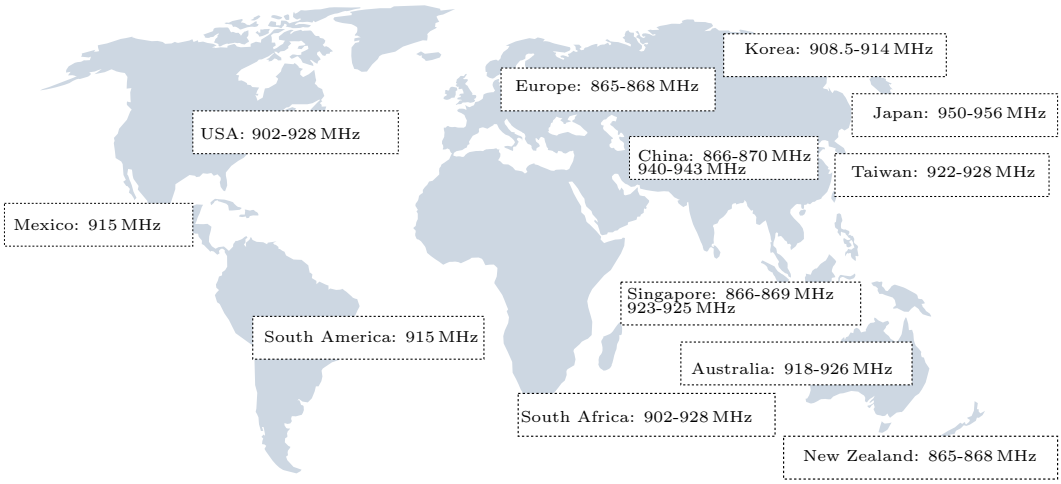

Figure 2.8: Authorized UHF RFID frequency bands by region

The two frequency bands most relevant to the latter part of this work, will be referred to by their standardization organization: The European 865 MHz-868 MHz band as ETSI and the Northern American 902 MHz-928 MHz band as Federal Communications Commission (FCC).

2.4.2 EPC Class 1 Generation 2

To allow for the compatibility of different RFID systems, communication protocols define the physical and logical requirements of an RFID system operating in a certain frequency band with a given power source. Table 2.1 shows a collection of available communication protocols and their assigned operation scenario.

Table 2.1: Available communication protocols for certain frequency bands and power sources [16].

Power Source	Frequency			
	124/134 kHz	13.56 MHz	860-960 MHz	2.4 GHz
passive	ISO 11784/5 ISO 14223 ISO 18000-2	ISO 14443 ISO 15693 ISO 18000-3	ISO 18000-6A, B, C EPC Class 0, Class 1 AAR S918	ISO 18000-4 Intellitag Mu-chip
semi-passive			California Title 21 EZ Pass AR S918	ISO 1800-4 Alien BAP
active	Rubee			ANSI 371.1 ISO 18000-4

The Electronic Product Code (EPC) Class 1 Generation 2 "defines the physical and logical requirements for a passive-backscatter, Interrogator-talks-first (ITF), radio-frequency identification (RFID) system operating in the 860 MHz-960 MHz frequency range."[17] The further part of this section provides a short description of the parts of the EPC Class 1 Generation 2 (EPC-C1G2) communications protocol most relevant to the remainder of this thesis.

Interrogator-to-Tag (R→T) communications

The reader interrogates one or more tags by transmitting a modulated RF signal using a DSB-ASK, SSB-ASK, or PR-ASK modulation format with PIE encoding. Figure 2.9 shows the corresponding PIE symbols, where a Tari is the reference time interval for the downlink (R→T) signaling, and is defined

as the duration of a data-0. Tari values in the range of 6.25 μs to 25 μs are EPC-C1G2 compliant.

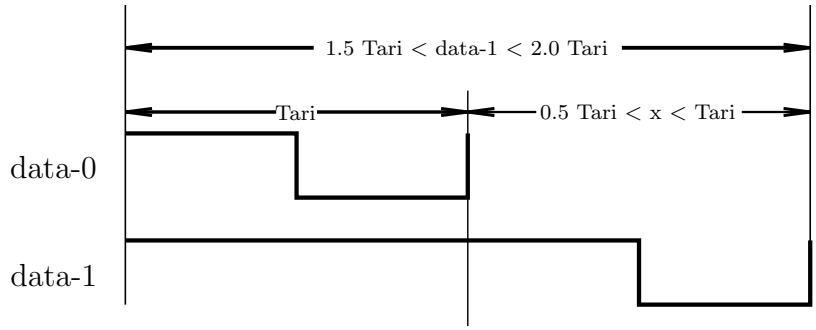

Figure 2.9: Baseband PIE symbols in R→T communication.

An interrogator command shall always begin with either a preamble or a frame-sync. A preamble is used for the Query command and refers to the start of an inventory round, where all other commands are prepended with a frame-sync, which is identical to a preamble, minus the TRcal symbol (see Figure 2.10).

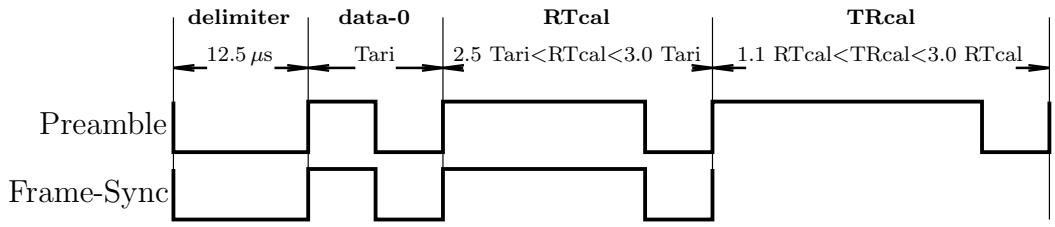

Figure 2.10: Prepended data sequences for R→T signaling.

Tag-to-Interrogator (T→R) communications

A tag responds to an interrogator command using backscatter communication as described in section 2.2.1, where the tag selects the modulation format and the interrogator choses both the encoding and the data rate by means of the Query command. The uplink (T→R) shall use either ASK and/or PSK

modulation encoding the data as FM0 or Miller. An encoding type specific preamble is prepended to every T→R message transmitted by the tag. To ensure the validity of certain R→T and T→R commands a Cyclic-redundancy Check (CRC) is used.

Inventory Round

An inventory round is "the period initiated by a Query command and terminated by either a subsequent Query command (which also starts a new inventory round) or a Select command. [...] The inventory command set includes Query, QueryAdjust, QueryRep, ACK, and NAK."[17] Assuming a single tag reply, the inventory round is visualized in Figure 2.11 and proceeds as follows:

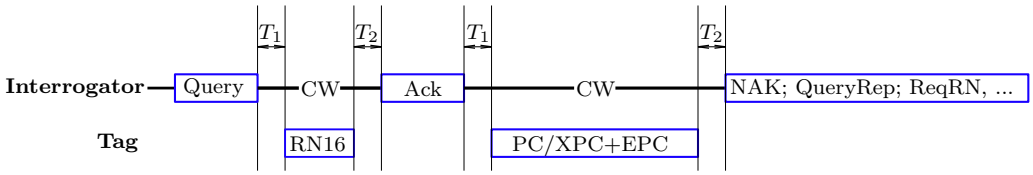

Figure 2.11: Visualization of inventory round timing for a single tag reply.

(1) The reader opens the inventory round by transmitting a Query command, followed by a Continuous Wave (CW) to allow backscatter communication.

(2) The tag backscatters an RN16 as a response to the received and decoded Query command.

(3) The interrogator then acknowledges the transponder with an ACK message containing this same RN16.

(4) The acknowledged Tag transitions to the acknowledged state, backscattering its Protocol Control (PC)/Extended Protocol Control (XPC) and EPC.

(5) Depending on the received response the reader then issues a QueryAdjust or QueryRep, causing the identified tag to invert its flag and transition to ready, potentially causing another tag to enter the inventory round, jumping back to step (2).

The time parameters relevant when designing and developing interrogators and transponders, partly shown in Figure 2.11 are described as follows:

T_1 Time between the end of the interrogator transmission and the corresponding tag response.

T_2 Interrogator response time, measured from the end of the last bit of the tag response to the first falling edge of the next interrogator transmission.

T_3 Time an interrogator waits, after T_1, before it issues another command.

T_4 Minimum time between interrogator commands.

Read Command

The Read command belongs to the set of Access commands and, in combination with the Req_RN command allows to request data from a specified register of the RFID chip, after having received its PC and EPC. The corresponding command sequence is visualized in Table 2.2. The Read command transmitted by the reader, thus, specifies both the number of words to read (Word-Count), the starting address pointer (Word-Pointer) and the memory bank to read from (Memory-Bank).

Table 2.2: Set of commands necessary for an RFID data read.

Req_RN		Handle		Read		Data	
# bits	description	# bits	description	# bits	description	# bits	description
8	1100 0001	16	Handle	8	1100 0010	1	0
16	prior RN16	16	CRC-16	2	Memory-Bank	Var	Data
16	CRC-16			EBV	Word-Pointer	16	Handle
				8	Word-Count	16	CRC-16
				16	Handle		
				16	CRC-16		

2.4.3 Power sources of RFID tags

RFID tags can further be separated according to their power source. Figure 2.12 shows a comparison of the three different types of power sources used in UHF RFID tags.

Active

Active RFID tags use a power supply to provide sufficient energy to the RFID chip and incorporate an active transmitter to respond to the messages received from the reader. (e.g., Nordic Semiconductor nRF52832 [18]) [19]

Semi-passive

Semi-passive RFID tags also use backscattering to communicate with the interrogator but are provided with an external (e.g., battery) power source as the power supply. Most of these chips can be used passively, but an external power source can be connected to extend their read range. (e.g., Impinj Monza-8k [8], Farsens Rocky100 [20]) [19]

Passive

Passive RFID tags typically consist of an antenna and the RFID chip. The tag-to-reader communication is achieved by backscattering a certain part of

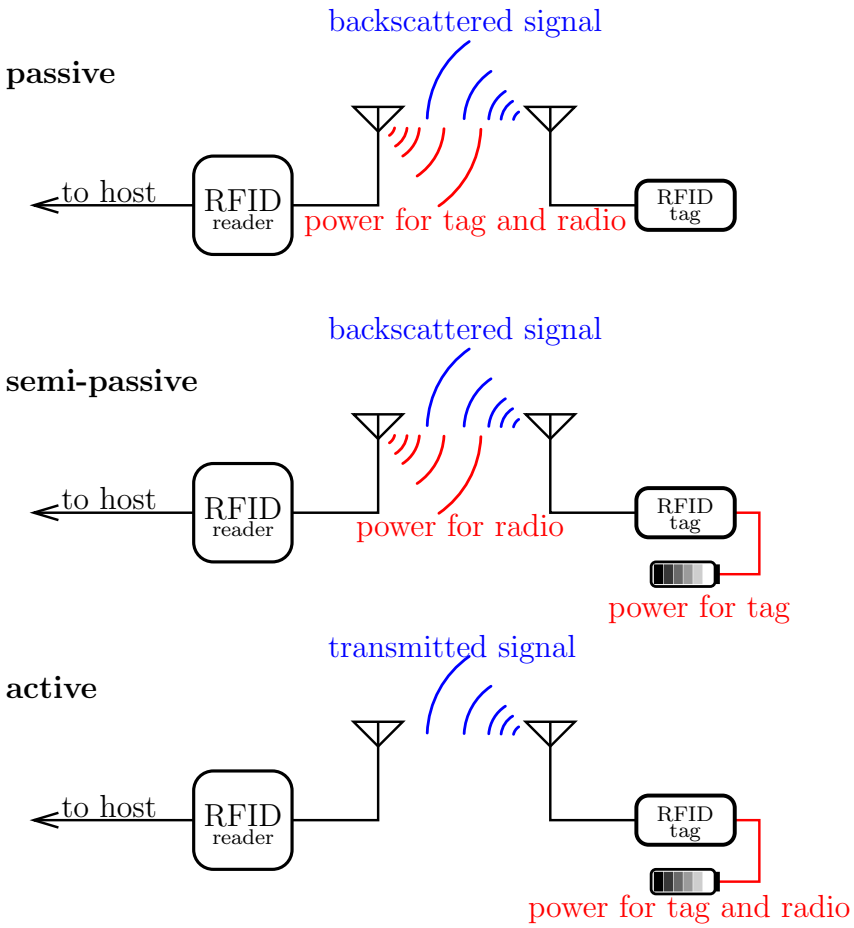

Figure 2.12: RFID tag classification due to power sources during uplink communication.

the incident electromagnetic wave using load modulation at the antenna terminals. The energy needed for the RFID chip to operate is harvested from the incident electromagnetic wave. (e.g., NXP Ucode 8 [21], Impinj M700 Series [22]) [19]

The typical architecture of a passive RFID tag is shown in Figure 2.13, where the tasks performed by the modules presented in the block chart are as follows:

- ◇ Antenna: The tag antenna is used to transform the electromagnetic waves emitted by the reader into electric waves. Due to the influence

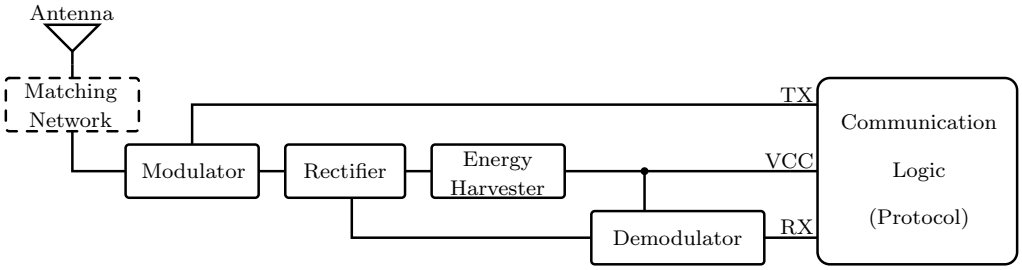

Figure 2.13: Passive RFID tag architecture

of the antenna impedance on the reflection coefficient Γ, it influences both the backscattered signal strength, as well as the energy harvesting performance of the tag.

◇ Matching Network (optional): A matching network is mainly used in computational RFID and RFID sensing. Due to size restrictions in commercial RFID tags, the matching network is typically omitted by using a conjugate-matched antenna design.

◇ Modulator: The load modulator represents the main part of the uplink communication. Typically, a MOSFET is used to short the antenna terminals creating a deliberate mismatch.

◇ Rectifier: The UHF radio wave incident at the tag is rectified by the rectifier section, typically consisting of a Schottky diode circuitry. Part of the rectified Direct Current (DC) voltage is then fed to the energy harvester to power the chip, where the rest is used to demodulate the reader's incoming message.

◇ Energy Harvester: The energy harvester section provides the circuitry incorporating the communication protocol with the operating power. This is achieved, by stepping up the DC voltage output from the rectifier section to the voltage needed to power the rest of the tag.

◇ Demodulator: The demodulation of the incident reader message is typically achieved using an envelope detector, followed by a comparator

to obtain a digital logic signal at the input of the section hosting the protocol layer.

- ◇ Communication Logic (Protocol): A communication standard (e.g., EPC-C1G2) is then used to decode and process the protocol compliant command to backscatter the requested response.

2.4.4 Computational and Sensor RFID

In recent years, the field of RFID communications, intentionally developed for identification purposes only, has been expanded to providing sensoric and computational capabilities [23]. Due to the increased efficiency of Radio Frequency (RF) energy harvesters, their output power can now be sufficient for the operation of an external low power sensor and/or microcontroller.

Sensor RFID

Sensor RFID can be further separated into two types of sensing [24]:

- **Analog RFID sensing**: These implementations use device specific backscattering characteristics to obtain information about the sensor's environment. Sensitive coatings are used to further alter the backscatter response to obtain information about the desired parameter [25]
- **Digital RFID sensing**: These systems perform sensing tasks by using external low power sensors to write data to the internal memory via a standard communication protocol (e.g., I2C, SPI, ...). Examples for RFID chips allowing the incorporation of external sensors are: Impinj Monza X-8k Dura [26], Farsens Rocky100 [20].

Computational RFID

Computational RFID refers to a niche within the area of RFID, where the tags provide computational power to solve simple calculations. This behaviour is mainly achieved by using an external Microcontroller Unit (MCU) to perform the computation task and store the information in the intrinsic memory of the RFID chip to be then read by the reader using the previously explained EPC-C1G2 Read command (e.g., Farsens Medusa [27]).
Further flexibility is achieved by research platforms, where the communication protocol is also implemented in the MCU. Thus, the communication logic can be adapted easily to allow for the development of novel approaches in the protocol layer. [23; 28]

References

[1] F. Gustrau, *RF and Microwave Engineering: Fundamentals of Wireless Communications*. John Wiley & Sons, 2012.

[2] G. Gronau, *Höchstfrequenztechnik: Grundlagen, Schaltungstechnik, Messtechnik, Planare Antennen*. Springer-Verlag, 2013.

[3] H. Heuermann, *Hochfrequenztechnik: Komponenten für High-Speed-und Hochfrequenzschaltungen*. Springer-Verlag, 2018.

[4] P. H. Smith, "Transmission line calculator," *Electronics*, vol. 12, no. 1, pp. 29–31, 1939.

[5] P. V. Nikitin, K. S. Rao, S. F. Lam, V. Pillai, R. Martinez, and H. Heinrich, "Power reflection coefficient analysis for complex impedances in RFID tag design," *IEEE Transactions on Microwave Theory and Techniques*, vol. 53, no. 9, pp. 2721–2725, 2005.

[6] K. Kurokawa, "Power waves and the scattering matrix," *IEEE Transactions on Microwave Theory and Techniques*, vol. 13, no. 2, pp. 194–202, 1965.

[7] H. Stockman, "Communication by Means of Reflected Power," *Proceedings of the IRE*, vol. 36, no. 10, pp. 1196–1204, 1948.

[8] J. Niu and G. Y. Li, "An Overview on Backscatter Communications," *Journal of Communications and Information Networks*, vol. 4, no. 2, pp. 1–14, 2019.

[9] R. C. Hansen, "Relationships between antennas as scatterers and as radiators," *Proceedings of the IEEE*, vol. 77, no. 5, pp. 659–662, 1989.

[10] C. Yen, A. E. Gutierrez, D. Veeramani, and D. van der Weide, "Radar Cross-Section Analysis of Backscattering RFID Tags," *IEEE Antennas and Wireless Propagation Letters*, vol. 6, pp. 279–281, 2007.

[11] F. Fuschini, C. Piersanti, F. Paolazzi, and G. Falciasecca, "Analytical Approach to the Backscattering from UHF RFID Transponder," *IEEE Antennas and Wireless Propagation Letters*, vol. 7, pp. 33–35, 2008.

[12] H. T. Friis, "A note on a simple transmission formula," *Proceedings of the IRE*, vol. 34, no. 5, pp. 254–256, 1946.

[13] C. A. Balanis, *Antenna Theory: Analysis and Design*. John wiley & sons, 2016.

[14] K. Finkenzeller, *RFID-Handbuch: Grundlagen und praktische Anwendungen von Transpondern, kontaktlosen Chipkarten und NFC*. Carl Hanser Verlag GmbH Co KG, 2015.

[15] D. Paret, *RFID at Ultra and Super High Frequencies: Theory and application*. John Wiley & Sons, 2009.

[16] "3. Types of RFID," https://polygait.calpoly.edu/what-rfid/types-of-rfid, Accessed: 2020-11-30.

[17] GS1, "EPC Radio-Frequency Identity Protocols Class-1 Generation-2 UHF RFID Protocol for Communications at 860 MHz–960 MHz Version 1.2.0," 2008.

[18] "Nordic Semiconductor nRF52832 Product Brief," https://www.nordicsemi.com/-/media/Software-and-other-downloads/Product-Briefs/nRF52832-product-brief.pdf?la=en&hash=2F9D995F754BA2F2EA944A2C4351E682AB7CB0B9, Accessed: 2020-11-30.

[19] F. Muralter, L. Arjona, H. Landaluce, and A. Perallos, "Modular UHF RFID research platform," *IEEE Sensors Journal*, vol. NA, no. NA, p. NA, 2021.

[20] "Farsens Rocky 100; RFID tag ICs for IoT solution development," http://www.farsens.com/en/products/rocky100/, Accessed: 2020-11-30.

[21] "NXP UCODE 8/8m Datasheet," https://www.nxp.com/docs/en/data-sheet/SL3S1205-15-DS.pdf, Accessed: 2020-11-30.

[22] "Impinj M700 Series Datasheet," https://support.impinj.com/hc/article_attachments/360016110979/Impinj_M730_and_M750_Tag_Chip_Datasheet_20200902_R4.pdf, Accessed: 2020-11-30.

[23] A. P. Sample, D. J. Yeager, P. S. Powledge, A. V. Mamishev, and J. R. Smith, "Design of an RFID-based battery-free programmable sensing platform," *IEEE Transactions on Instrumentation and Measurement*, vol. 57, no. 11, pp. 2608–2615, 2008.

[24] H. Landaluce, L. Arjona, A. Perallos, F. Falcone, I. Angulo, and F. Muralter, "A Review of IoT Sensing Applications and Challenges Using RFID and Wireless Sensor Networks," *Sensors*, vol. 20, no. 9, 2020.

[25] C. Occhiuzzi, S. Caizzone, and G. Marrocco, "Passive UHF RFID antennas for sensing applications: Principles, methods, and classifcations," *IEEE Antennas and Propagation Magazine*, vol. 55, no. 6, pp. 14–34, 2013.

[26] "Impinj Monza X-8k Dura Datasheet," https://support.impinj.com/hc/article_attachments/360016110999/Impinj_Monza_X-8K_Dura_Tag_Chip_Datasheet_R8_1_20200721.pdf, Accessed: 2020-11-30.

[27] "Farsens EVAL01-Medusa-RM 100," http://www.farsens.com/en/products/eval01-medusa-rm/, Accessed: 2020-11-30.

[28] D. Fabbri, E. Berthet-Bondet, D. Masotti, A. Costanzo, D. Dardari, and A. Romani, "Long range battery-less UHF-RFID platform for sensor applications," in *2019 IEEE International Conference on RFID Technology and Applications (RFID-TA)*. IEEE, 2019, pp. 80–85.

CHAPTER 3 Scientific Publications

This section provides information on the original scientific work arisen from the investigations in the area of passive computational UHF RFID. The results are reproduced from peer-reviewed publications. Permissions related to the material should be directed to the publishing authorities.

The DOIs of the articles are:

(1) 10.23919/SpliTech.2019.8783177

(2) 10.1002/ett.3939

(3) Accepted

(4) 10.1109/TIM.2020.3043942

(5) 10.1109/MWCL.2019.2935303

(6) 10.1109/JSEN.2021.3073421

(7) Under Review

3.1 A theoretical and experimental study of passive computational RFID tags (SplitTech)

Conferences > 2019 4th International Confer...

A theoretical and experimental study of passive computational RFID tags

Publisher: IEEE

Florian Muralter ; Laura Arjona ; Hugo Landaluce ; Asier Perallos **All Authors**

Published in: 2019 4th International Conference on Smart and Sustainable Technologies (SpliTech)

Date of Conference: 18-21 June 2019

INSPEC Accession Number: 18883323

Date Added to IEEE *Xplore*: 01 August 2019

DOI: 10.23919/SpliTech.2019.8783177

Publisher: IEEE

3.1.1 Preface

The theoretical and experimental study published in this manuscript was performed by the author of this thesis in the microwave laboratory of the DeustoTech Institute of Technology under the supervision of Hugo Landaluce. Laura Arjona from the University of Washington provided access to the WISP 5.1 platform and the necessary know-how to evaluate its performance. Asier Perallos supervised the whole project. All authors were involved in the preparation and revision of the manuscript.

3.1.2 Article

A theoretical and experimental study of passive computational RFID tags

1st Florian Muralter
DeustoTech
University of Deusto
Bilbao, Spain
florian.muralter@deusto.es

2nd Laura Arjona
Paul G. Allen Center
University of Washington
Seattle, USA

3rd Hugo Landaluce
DeustoTech
University of Deusto
Bilbao, Spain

4th Asier Perallos
Faculty of Engineering
University of Deusto
Bilbao, Spain

***Abstract*—Passive computational RFID tags have in recent years created a new perspective of usability in the area of RFID. Researchers profit from the possibility to perform a closer investigation of communication characteristics such as the protocols by adapting the digital, logic communication unit. In industry, the possibility of performing simple computational tasks allows computational RFID tags to be used in wireless sensor networks, with the addition of being battery-free. This work investigates the RF front-end of 3 state-of-the-art passive computational RFID tags: AMS SL900a Dev Kit, Farsens Spider Eval, WISP 5.1. Given a module-based approach, the antenna, the power matching, the power harvesting and the load modulation are reviewed both theoretically and experimentally. The influence of certain properties, assigned to a specific module, on the overall performance is evaluated using a tag read range measurement.**

***Index Terms*—computational radio frequency identification (CRFID), power reflection, tags**

I. Introduction

Ultra-high-frequency (UHF) radio frequency identification (RFID) is an automatic identification technology operating in the industrial, scientific and medical (ISM) radio bands at 865-868 MHz (ETSI - Europe) and 902-928 MHz (FCC - Northern America) [1]. A RFID system typically includes an interrogator (reader) and a transponder (tag). Such a tag consists of an antenna and a chip, which executes the implemented identification task. RFID tags can be subdivided into three categories: (1) passive (battery-free), (2) semi-passive (battery-assisted) and (3) active (with battery). A passive RFID tag does not only receive the data stream via the reader-radiated RF field, it also harvests the energy to operate from the incident wave. The technology used for the uplink (tag to reader) communication is based on the backscattering theorem [2]. While the reader is transmitting a continuous wave, the complex impedance between the terminals of the tag antenna is switched in a determined way, such that a load modulated signal is back-scattered to the receiving antenna of the reader. In recent years, a new discipline within the area of UHF RFID has evolved. Computational passive RFID tags yield the possibility to execute simple computational tasks on a passively powered tag. Thus, they present a tool for researchers to closer investigate the implemented protocol and on the other hand offer the possibility of sensing in hardly accessible places

Fig. 1. Investigated passive computational RFID tags: Farsens Spider (top), AMS SL900A (mid), Wisp 5.1 (bottom)

[3].

This work presents a contemporary study of three state-of-the-art passive computational RFID tags (Fig. 1):

- WISP 5.1: The Wireless Identification and Sensing Platform (WISP) is a passive computational RFID tag, first presented in [3] and investigated in its updated version 5.1 [4].
- Farsens Spider: The EVAL01-Spider-R by Farsens is a development board for the Rocky100 UHF RFID chip by Farsens [5]
- AMS SL900A Demo Kit: This device represents an evaluation tool for the implemented SL900A smart EPC Gen 2 sensor tag IC [6]

The investigated tags all yield the possibility of extending their functionality with external low-power sensors. The WISP 5.1 incorporates a micro-controller to execute the communication protocol, which by the other tags is done by a not accessible state logic. This additional feature allows to easily modify the implemented protocol and the structure of communication.

This work uses a module-based methodology to investigate and compare the RF frontend of the mentioned tags. Fig. 2 shows a block diagram, presenting the different sections of a typical passive computational RFID tag. The modules, which

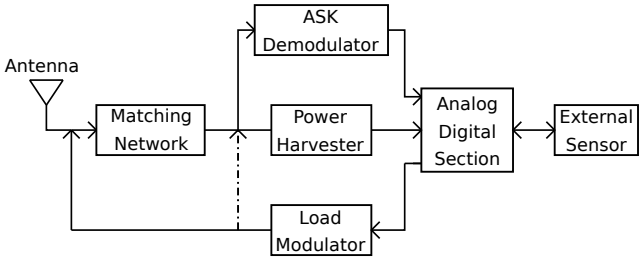

Fig. 2. Modules of a passive computational RFID tag

are part of the RF frontend - antenna, matching network, energy harvester, load modulation - are separately examined and its influence on the overall performance is reviewed. The presented study can serve as a useful tool for researchers to more thoroughly understand the behavior of computational RFID (CRFID) tags and thus, for developing new improved CRFID concepts.

II. Theoretical Study

The tag read range is considered the most significant RFID tag characteristic [7]. According to [8] the maximum read range r_{max} for a free-space environment can be calculated using the Friis equation

$$r_{max} = \frac{\lambda}{4\pi}\sqrt{\frac{P_t \cdot G_t \cdot PLF \cdot G_r \cdot (1-|s|^2)}{P_{th}}} \tag{1}$$

with

$$|s|^2 = \left|\frac{Z_C - Z_A^*}{Z_C + Z_A}\right|^2 \tag{2}$$

where

- P_t - transmitted power
- G_t - gain of transmit antenna
- PLF - polarization loss factor
- G_r - gain of receiving antenna
- λ - wavelength
- $|s|^2$ - power reflection coefficient
- r - distance between reader and tag antenna
- Z_A - complex antenna impedance
- Z_C - complex chip impedance
- P_{th} - power threshold (chip)

Given (1), the occuring variables can be assigned to the different modules of a RFID system presented in Fig. 2 and thus, their influence on the performance characterstic, tag read range, can be evaluated separately.

A. Antenna

The tag antenna represents the first component interacting with the incident RF signal. RFID tag antennas have been discussed in a large number of publications (e.g. [8]–[10]). Considering the antenna design for a passive computational RFID tag, a half-wave dipole is the most common example. For a half-wave dipole, which represents a linear polarized antenna in the field of an often circular polarized reader antenna, the polarization mismatch has to be taken into account. The polarization loss factor given the mentioned scenario is $PLF = 3$dB. Another antenna property, that is directly influencing the value of r_{max} is its gain G_r. The antenna gain is a measure of the directivity and the efficiency of an antenna compared to an isotropic antenna. For a half-wave dipole the gain is considered to be $G_r = 2.15$dBi and constant in the investigated frequency range. A further reason for typically choosing half-wave dipoles is their resistance, which at resonance is considered to be $R_A = 73\,\Omega$. Above its resonant frequency, the antenna impedance is inductive, which allows an easier conjugate matching to the capacitive chip impedance $Z_A^* = Z_C$. The half-wavelength, which is typically considered a starting-point for the antenna design is $\lambda/2 \sim 0.16$m for the UHF band.

B. Matching Network

The power reflection coefficient $|s|^2$ from (2) is a measure for the impedance match between the complex antenna impedance Z_A and the complex chip impedance Z_C [11]. Considering all other variables in (1) slowly varying with frequency, the power reflection coefficient, and thus the power matching between the antenna and the chip, represents the main contribution to the change of the read range as a function of the frequency [12]. Figure 3 shows the decrease of the maximum read range r_{max} with the increase of the power reflection coefficient $|s|^2$. To assure a good matching, either a separate matching network is designed, or as typical in standard RFID tags, the antenna design is adapted, such that it matches the complex impedance of the built chip. This second concept decreases the losses created by a separate matching network and hence, increases the performance.

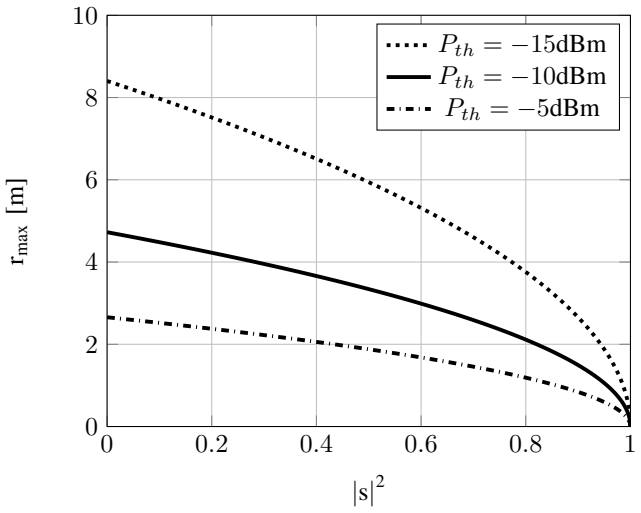

Fig. 3. Read ranges r_{max} as a function of the power reflection coefficient $|s|^2$ for 3 different values of P_{th}

C. Power Harvester

The RF harvesting unit is designed to provide the needed voltage for operation to the digital circuitry and sensors [13]. This module typically consists of (1) RF-DC converter, (2) a step-up converter and (3) a voltage regulator. The input impedance of the energy harvesting unit commonly presents the main part of the chip impedance and thus is the impedance to be matched to the antenna [10].
Depending on the current needed for the operation of the tag, different storage capacitors are included to assure a continuous power supply for the duration of one operation cycle.
Considering the three investigated tags, the power harvesting unit is not accessible, except for the WISP, where it consists of a Greinacher Voltage Doubler, a Boost-Charge-Pump-IC and a voltage regulator.
The harvester-parameter present in (1) is the threshold power P_{th}. This value represents the minimum power that is need for the RFID chip to start operating. With a sensitivity of $P_{th} = -14$dBm, the Farsens tag outperforms the AMS by 7 dB, which results in a significantly higher theoretical read range maximum.

D. Load modulation

Load modulation represents the modulation scheme for backscatter RFID communications. The impedance seen by the antenna terminals is switched between determined states, such that an amplitude shift keying (ASK) or phase shift keying (PSK) signal is back-scattered. The choice of the modulation format depends on several aspects, but according to [10], using PSK results in an increased performance. With PSK communication [14] it is possible to achieve a constant power transfer between the antenna and the chip. As the impedance states can be selected in a way, that they yield the same power reflection coefficient $|s|^2$.
For a RFID system backscattering ASK, the most common method to choose the impedance states is to create a near perfect conjugate match for the main state, and switch to a deliberate mismatch for the opposing transmission bit. Given this method, the initial state represents a maximum of the power transfer from antenna to tag.
The power reflection coefficient on the one hand can be used to describe the power available at the chip, but on the other hand can also be used to represent the amplitude of the backscattered signal. Thus, a trade-off between power transmission to the chip and backscatter amplitude has to be considered, as we discussed in [14].

III. Experimentation

A. Antenna

To evaluate the antenna performance and characteristics, the designed antennas of the three tags were simulated using CST Microwave Studio. Additionally, the antennas included in the tags were rebuilt on a separate PCB without the RFID chip. The antennas were matched to a 50Ω 1:1 Balun connected to a 50Ω SMA connector. The data obtained using a Vector Network Analyzer (VNA) in comparison to the simulated results is shown in Fig. 4. The obtained deviations are expected to be due to a not perfect matching network using a L-network consisting of lumped elements. Furthermore, the results from the simulation are considering the exact dimensions and properties stated in the data sheets, whereas the measured antennas were all rebuilt using the same PCB and copper thickness.
All three antennas are resonant at a frequency, that lies between the defined North American and the European frequency bands. Thus, the complex antenna impedance Z_A is capacitive for the European band and inductive for the North American band. which has to be considered for the design of the impedance matching network. The AMS antenna shows the largest bandwidth, which considering the influence of the antenna impedance Z_A on the read range, results in a more constant maximum read range for the investigated frequency band.

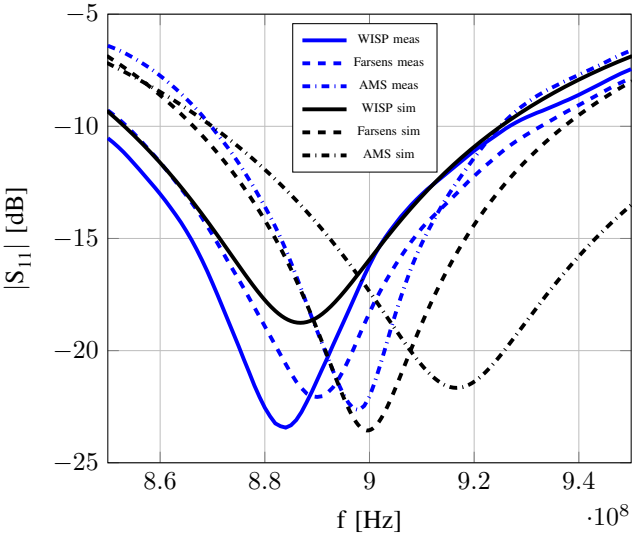

Fig. 4. S_{11} of the simulated and measured tag antennas

B. Matching Network

With the chip impedances Z_C stated in the data sheets of the compared tags and the tags' matching networks, the virtual chip impedance $Z_{C,Match}$ was calculated using a Smith chart. The computed values are shown in Tab. I. Given $Z_{C,Match}$ and the antenna impedance Z_A, the power reflection coefficient as a function of frequency $|s|^2(f)$ can be calculated. Using (1) to determine the read ranges for the different investigated tags one can obtain the peak read range which according to [12] is named the tag resonance. Due to the frequency dependence of the impedance matching network, the tag resonance does not necessarily coincide with the antenna resonance. Figure 5 shows the calculated tag read ranges for the three investigated tags, considering an equal threshold power $P_{th} = -10$dBm.

TABLE I
CHARACTERISTIC TAG IMPEDANCES IN Ω

	Wisp	Farsens	AMS
$Z_{A,\text{EU}}$	61.33 + 4.11j	47.49 -32.16j	34.54 -23.40j
$Z_{A,\text{res}}$	60.08	57.52	41.70
$Z_{A,\text{NA}}$	78.07 +50.62j	61.81 +12.41j	42.93 + 3.63j
Z_C	4 -30j	51-460j	123-303j
$Z_{C,\text{Match}}$	3.99-61.94j	30.13-44.02j	123.00-9.79j

C. RF energy harvesting

All three investigated transponders offer the possibility to measure the regulated voltage output by the RF energy harvesting circuit. This voltage, which is also considered the supply voltage for the chip is presented in Fig. 6. The measurement was conducted using a 10dBi circular polarized antenna, transmitting a continuous wave at 915MHz with a power of 10dBm. The tags were consecutively placed in the RF field at a distance of $d = 0.6m$. Figure 6 shows, that the regulated voltage achieved by the Farsens tag is about double the voltage obtained from the AMS tag. A major difference can be seen, in the regulated voltage curve measured at the V_{reg} port of the WISP. This behaviour underlines the operation properties of the boost-charge-pump IC. Depending on the current consumption of the circuitry on a certain chip, a different size of capacitor to store the harvested energy is needed. Typically the continuous power available at the tag is not enough to power a microcontroller, such as used in the WISP tag, thus duty cycling is used to allow operation.

D. Load modulation

According to the EPC C1G2 protocol, the tag can backscatter a response to the reader using either binary ASK or binary PSK modulation. Often ASK load modulation is considered a modulation of the resistance of the impedance seen by the antenna and PSK a modulation of the reactance. Neglecting

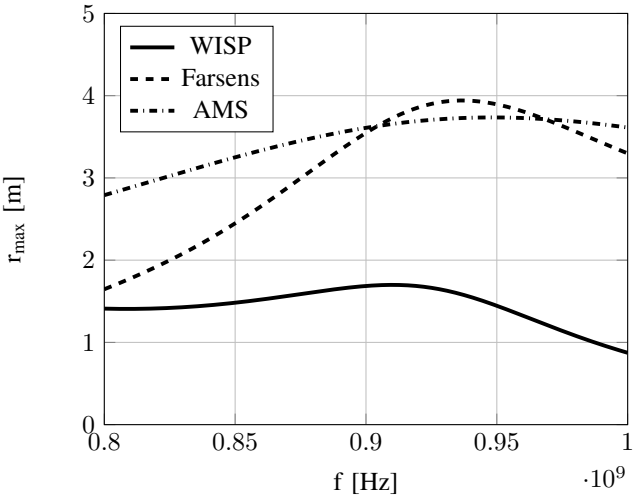

Fig. 5. Calculated tag read range for $P_{th} = -10$dBm

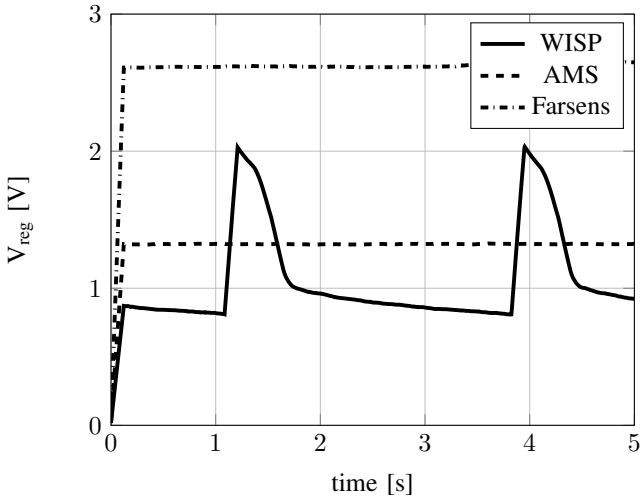

Fig. 6. Regulated voltage V_{reg} measured at the investigated tags

the imaginary part of the antenna impedance, this method will always result in a mixed modulation type. Furthermore, even if considering the imaginary part of the antenna, the frequency dependence of either of the parts will only allow a pure ASK or PSK modulation for a theoretically infinitely narrow frequency band.
The modulation types according to the data sheets for the WISP, Farsens and AMS are ASK, PSK and ASK respectively. The WISP is using a transistor to short the antenna terminals, as the second state of the transmission. This behavior results in no power harvesting during this period of time. For the other two tags, the second impedance state is not known and thus no investigation of the trade-off between the power harvested and the power of the back-scatter signal is possible during reader to tag transmission.

E. Tag read range

For the tag read range measurement, the tags were placed at a fixed distance from the circular polarized reader antenna with a gain of $G_t = 6$dBi. The tag direction was selected in a way, that the zero-axis of the half-wave dipole antennas does not affect the measurement (Fig. 7). For both the ETSI and the FCC frequency range the minimum transmit power P_{min} required for communication was detected using a discrete sweep of the transmit power P_t. The distance between the tag and the reader antenna was chosen to be $d = 0.7$m. For the minimum evaluated frequency this results in a distance of 2.02λ which does match the farfield condition required for the used method to calculate the tag read range. Given the chosen distance, and a maximum transmit power of 30dBm at the reader a communication to the WISP could not be established. Thus the following results only show the evaluation of the AMS and the Farsens tag. With the known parameters of the measurement system, the tag read range for a given $EIRP$, which was considered the maximum allowed in Europe

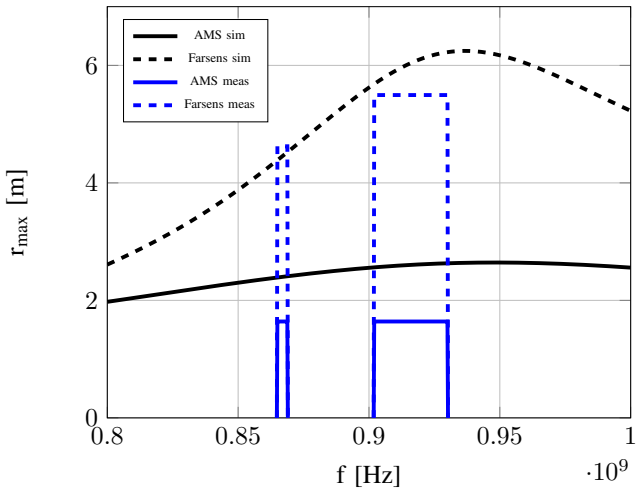

Fig. 7. Comparison of theoretical and measured tag read ranges

$EIRP = 3.28$W, can be calculated by

$$r = d\sqrt{\frac{EIRP}{P_t \cdot G_t \cdot L \cdot PLF}}, \tag{3}$$

where L denotes the cable loss which for the conducted measurement was $L = 3$dB. The reader used for the experimentation was a ThingMagic M6e connected to a circular polarized Alien Technology ALR-A0501 antenna. The communication and protocol was executed using the ThingMagic Mercury API. Figure 7 shows a comparison of the calculated and the theoretical read ranges of the Farsens and the AMS tag. The measurements obtained for the real-world scenario are in good agreement with the theoretical values. The wider bandwidth achieved with the AMS antenna also results in a more constant read range, considering the FCC and ETSI frequency bands. The measured read ranges clearly follow the trend presented by the theoretical values. Nevertheless, the calculated read range for the AMS tag could not be achieved during the tests, which could be due to a worse sensitivity of the energy harvesting unit or a decreased antenna gain on the measured tag. Considering these results and comparing them to the theoretical values obtained in Fig. 5, one can see, that the higher read range of the Farsens tag is resulting from its higher sensitivity. Hence, the antenna and matching network of the AMS tag are not handicapping in comparison to the Farsens tag. The influence of a different direction of the tag, with respect to the reader antenna, as well as the influence of a higher and moving population of such tags will be considered in future work.

IV. Conclusion

In this work, we evaluated the performance of the RF frontend, of 3 different commercially available passive computational RFID tags. It was shown, that due to a similar antenna design, this first part of the RF frontend exhibits a similar behaviour for all three of the investigated tags. Due to the impedance matching to a chip impedance far smaller than the antenna impedance, the WISP is outperformed by the Farsens and the AMS tag, which both show a similar behaviour considering the power matching. Finally, the read range measurement presented an overall measure of the real-word performance of the investigated tags. Thus, the Farsens tag, due to its high sensitivity can be read at distances of more than double the distance achieved by the AMS tag. A closer study of the energy harvesting and the load modulation in computational RFID tags will be conducted in the near future.

Acknowledgment

This work has been part-funded by the Basque Government under the project TEKINTZE (KK-2018/00104) and the Spanish Ministry of Science, Innovation and Universities (RTI2018-095499-B-C33).

References

[1] *Class 1 Generation 2 UHF Air Interface Protocol Standard Version 1.09*, EPCglobal Inc. Std. [Online]. Available: http://www.epcglobalinc.org/standards_technology/specifications.html
[2] R. Hansen, "Relationship between antennas as scatters and as radiators," *Proceedings of the IEEE*, vol. 77, pp. 659 – 662, 06 1989.
[3] A. P. Sample, D. J. Yeager, P. S. Powledge, A. V. Mamishev, J. R. Smith *et al.*, "Design of an RFID-based battery-free programmable sensing platform," *IEEE Transactions on Instrumentation and Measurement*, vol. 57, no. 11, p. 2608, 2008.
[4] "Wireless Identification and Sensing Platform WISP," Online, 2018. [Online]. Available: http://wisp5.wispsensor.net/
[5] Farsens, "EVAL01 Spider R," 2019. [Online]. Available: http://www.farsens.com/en/products/eval01-spider-r/
[6] AMS, "Demo kit for sl900a," 2018. [Online]. Available: https://ams.com/sl900a-demokit
[7] P. V. Nikitin and K. V. S. Rao, "Performance limitations of passive UHF RFID systems," *2006 IEEE Antennas and Propagation Society International Symposium*, pp. 1011–1014, 2006.
[8] P. V. Nikitin and K. S. Rao, "Antennas and propagation in UHF RFID systems," in *RFID, 2008 IEEE International Conference On*. IEEE, 2008, pp. 277–288.
[9] K. S. Rao, P. V. Nikitin, and S. F. Lam, "Impedance matching concepts in RFID transponder design," in *Automatic Identification Advanced Technologies, 2005. Fourth IEEE Workshop on*. IEEE, 2005, pp. 39–42.
[10] G. De Vita and G. Iannaccone, "Design criteria for the RF section of UHF and microwave passive RFID transponders," *IEEE Transactions on Microwave Theory and Techniques*, vol. 53, no. 9, pp. 2978–2990, 2005.
[11] K. Kurokawa, "Power waves and the scattering matrix," *IEEE Transactions on Microwave Theory and Techniques*, vol. 13, no. 2, pp. 194–202, 1965.
[12] P. V. Nikitin, K. S. Rao, S. F. Lam, V. Pillai, R. Martinez, and H. Heinrich, "Power reflection coefficient analysis for complex impedances in RFID tag design," *IEEE Transactions on Microwave Theory and Techniques*, vol. 53, no. 9, pp. 2721–2725, 2005.
[13] W. Serdijn, A. Mansano, and M. Stoopman, "Introduction to RF energy harvesting," in *Wearable Sensors*. Elsevier, 2014, pp. 299–322.
[14] F. Muralter, H. Landaluce, R. Del Rio, and A. Perallos, "Selecting impedance states in a passive computational RFID tag backscattering in PSK," *IEEE Microwave and Wireless Components Letters*, 2019, ACCEPTED.

3.2 A theoretical and experimental study of passive computational RFID tags

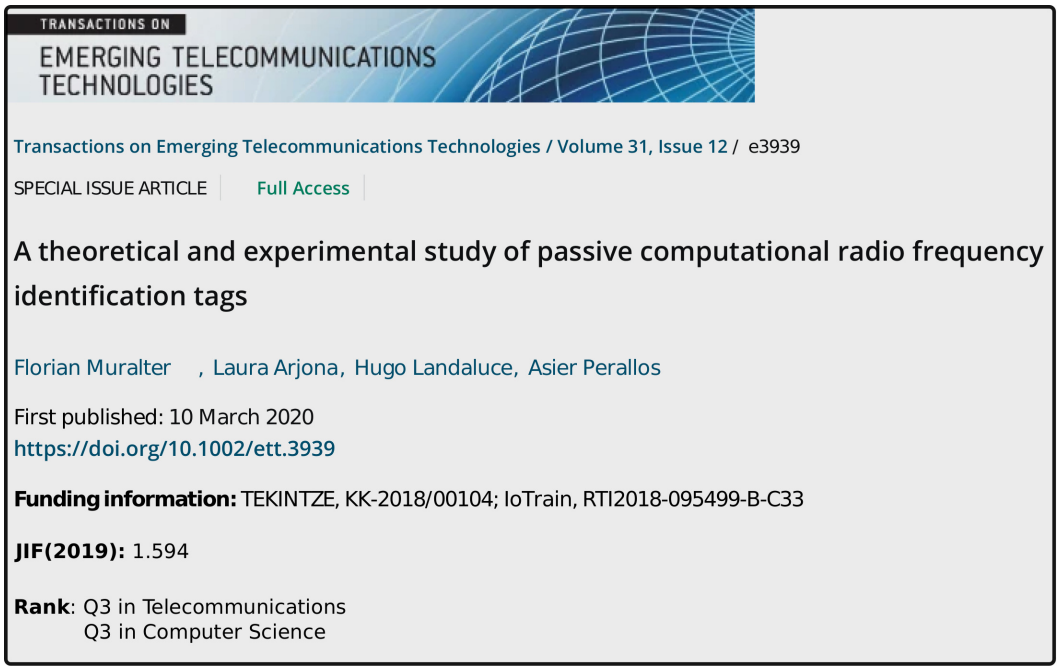

3.2.1 Preface

This article represents an extension of the previous manuscript. The additionally performed investigations were performed by the main author in the microwave laboratory of the DeustoTech Institute of Technology. All authors were involved in the preparation and revision of the published manuscript.

3.2.2 Article

SPECIAL ISSUE ARTICLE

A theoretical and experimental study of passive computational RFID tags

Florian Muralter[1] | **Laura Arjona**[2] | **Hugo Landaluce**[1] | **Asier Perallos**[1]

[1]DeustoTech, University of Deusto, Bilbao, Spain

[2]Paul G. Allen Center, University of Washington, Seattle, USA

Correspondence
Florian Muralter, DeustoTech, University of Deusto, Bilbao, Spain
Email: florian.muralter@deusto.es

Funding information
TEKINTZE (KK-2018/00104)
IoTrain (RTI2018-095499-B-C33)

The investigation and optimization of the RF frontend of radio frequency identification (RFID) tags represents a crucial topic when looking for an increased tag performance. This work studies the RF frontend of three state-of-the-art passive computational RFID tags: AMS SL900a Dev Kit, Farsens Spider Eval, WISP 5.1. Given a module-based approach, the antenna, the matching network, the RF energy harvesting and the load modulation are reviewed both theoretically and experimentally. The influence of a set of properties, corresponding to these modules, on the overall RFID tag performance is evaluated using a tag read range measurement.

KEYWORDS
computational radio frequency identification, power reflection, tags

1 | INTRODUCTION

Radio frequency identification (RFID) is an automatic identification technology mainly used in logistics and asset tracking. [1]. A typical RFID system consists of an interrogator (reader) and at least one transponder (tag). Such a tag incorporates an antenna and a chip, which executes the identification task. RFID tags operating in the ultra high frequency (UHF) band, can be grouped into three categories: (1) passive (battery-free), (2) semi-passive (battery-assisted) and (3) active (with battery). Thus, a passive RFID tag does not only receive the reader commands via the RF field, it also harvests the energy to operate from the incident electromagnetic wave. The technology used for responding to the message sent by the interrogator is based on the backscattering theorem [2]. Following each interrogator message, a continuous wave is transmitted. During this time period, the complex impedance between the terminals of the tag antenna is switched in a

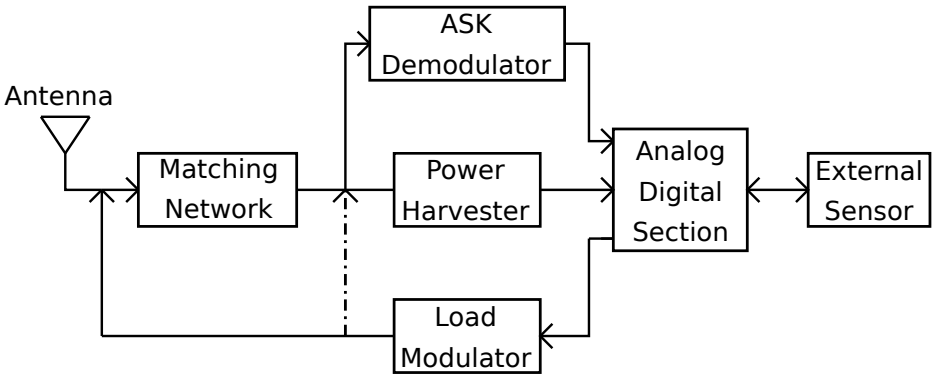

FIGURE 1 Modules of a passive computational RFID tag [6]

deterministic way, such that a load dependant re□ection of the signal is backscattered to the antenna of the reader [3]. In recent years, a new discipline within the area of UHF RFID has evolved. Passive computational RFID (CRFID) tags yield the possibility to execute simple computational tasks on a passively powered tag. Thus, they present a tool for researchers to closer investigate the implemented protocol and on the other hand offer the possibility of sensing in hardly accessible places, where the recharging or replacement of batteries represent dif□cult tasks [4].

This work presents a contemporary theoretical and experimental study of three state-of-the-art passive CRFID tags (Figure 2). Additionally, a couple of other proposed CRFID platforms are compared. Using a module-based methodology, the RF frontend of the investigated tags is studied.

Figure 1 shows a block diagram, presenting the different sections of a typical passive CRFID tag. The modules, which are part of the RF frontend - antenna, matching network, energy harvester, load modulator - are separately examined and their in□uence on the tag read range is investigated. The tag read range measurement is performed using a typical procedure as in [5] and compared to a CRFID speci□c approach using the measured regulated voltage of the tag. The presented study is intended to serve as a useful tool for researchers to more thoroughly understand the behavior of CRFID tags and thus, for developing new, improved concepts. Furthermore it presents a framework, combining several measurement methodologies to obtain a broad impression of the performance characteristics of CRFID systems.

This paper represents an extension of [6]. Existing measurements have been revised and improved. Further experimentation and results have been added to provide a more thorough understanding of the investigated performance characteristics. The manuscript is structured as follows: In Section 2 an analysis of the state-of-the art is presented. Sections 3 and 4 represent the theoretical and experimental analysis, respectively. In the □nal section 5 some conclusions and a resumé are presented.

2 | STATE-OF-THE-ART

In recent years a number of passive CRFID solutions have been presented. The platforms mainly differ in their □exibility, being either □xed passive RFID sensor tags, prototyping tags for adding different sensors or open-source research platforms with the possibility to additionally adapt communication parameters. For research purposes the commercial sensor tags can be neglected, as they don't offer any □exibility regarding their adaptability. Thus, the following section represents a review of □ve different passive CRFID solutions (Figure 2).

- WISP 5.1: The Wireless Identi□cation and Sensing Platform (WISP) is a passive open-source CRFID tag, □rst

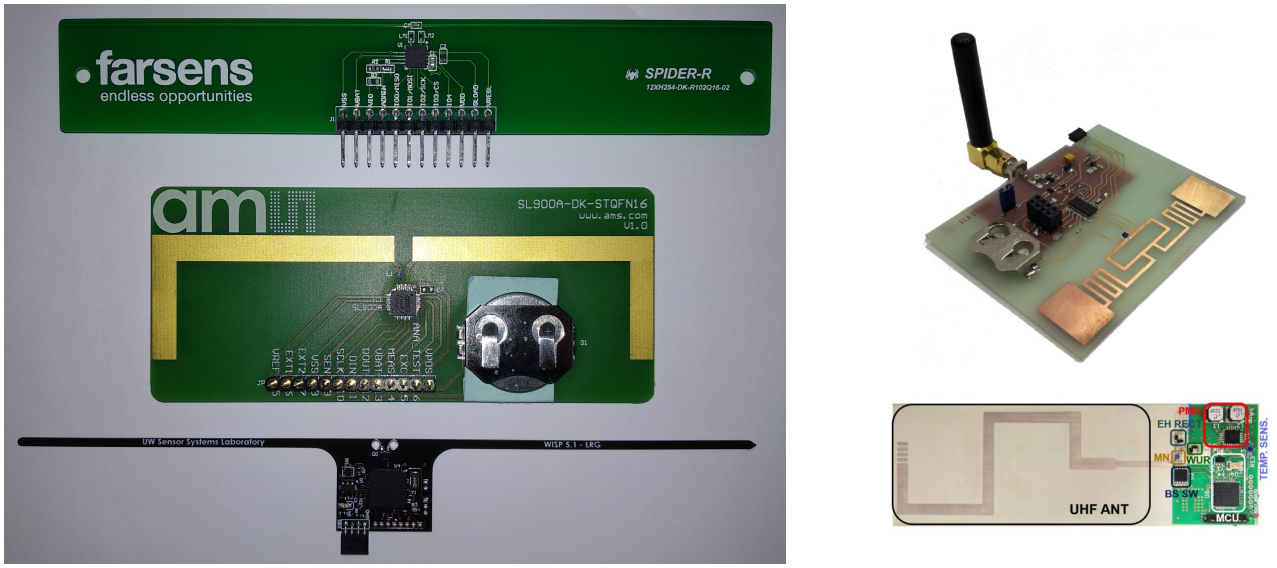

(a) Farsens Spider (top), AMS SL900A (mid), WISP 5.1 (bottom)

(b) Ramses (top) [12], Fabbri (bottom) [11]

FIGURE 2 Investigated passive computational RFID tags: Experimental and theoretical study (left); additional state-of-the-art analysis (right) [6]

presented in [4] and investigated in its updated version 5.1 [7]. The WISP's EPC Class 1 Gen 2 (EPCC1G2) [8] protocol is implemented on the used MSP430FR5969 microcontroller, which allows an adaptation to improve and test different protocol variations. The tag incorporates an accelerometer and yields the possibility to communicate with additionally added sensors via Serial Peripheral Interface (SPI) and (Inter-Integrated Circuit) I2C.

- Farsens Spider: The EVAL01-Spider-R by Farsens is a development board for the Rocky100 UHF RFID chip by Farsens [9]. This tag is mainly designed to offer a flexible platform to investigate the usage of different additional sensors. Many communication parameters and operation characteristics can be adapted using the EPCC1G2 commands or the SPI.
- AMS SL900A Demo Kit: This device represents an evaluation tool for the implemented SL900A smart EPCC1G2 sensor tag IC [10]. Similar to the Farsens tag, this platform is built to offer an investigation platform based on the SL900A Chip.
- RAMSES: The RAMSES is a RFID sensor platform based on the Monza X-2K Dura chip. This chip , connected to a dipole antenna, performs the RFID communication according to the EPCC1G2. A second separate section performs the energy harvesting for the sensoric and computational needs from a second separate antenna.
- Fabbri: The tag presented in [11] represents one of the latest advances in the field of passive RFID. This research platform was designed as an improvement of the WISP 5.1.

Table 1 shows a comparison of the performance characteristics of the presented tags. Reviewing these characteristics, one can see, that the type of antenna used for the tag is similar for all investigated platforms. The main differences occur in the read range, as well as in the way the RFID communication is implemented. The SL900A and the Spider use the company's own RFID chips, incorporating energy harvesting and backscatter communication, on the WISP and the Fabbri the communication protocol is implemented on a microcontroller. Given the RAMSES, a commercial RFID chip performs this task.

Given the presented platforms only three of them were obtainable and thus, the following theoretical and experi-

Tag	Farsens Spider	AMS SL900A	WISP 5.1	RAMSES	Fabbri
Band	ETSI, FCC	ETSI, FCC	FCC	ETSI, FCC	ETSI
Range	5m	1.5m	4m	10m	9.7m
Sensitivity	-14dBm	-7dBm	not specified	-17dBm	-16dBm
Size	13.7x2.1cm	10.2x4cm	14.8x2cm	8x8cm	9.5x3.1cm
Communication	Rocky100	SL900A	MSP430FR5969	X-2K Dura	MCU
Antenna	Dipole	bent Dipole	Dipole	meandered Dipole	Monopole

TABLE 1 Performance characteristics of state-of-the-art passive CRFID tags

mental study will consist of (1) the WISP 5.1 (2) the Farsens Spider Eval and (3) the AMS SL900A Dev.

3 | THEORETICAL STUDY

According to [13] the tag's read range is the most significant tag characteristic and thus, the most important optimization criterion. Its limiting factors are the reader sensitivity as well as the power level of the incident wave at the tag. Due to the high sensitivity of modern RFID readers, the first factor can be neglected for this investigation [14]. Considering the second factor, the tag read range in a free space environment can be estimated using Friis equation [15].

$$r = \frac{\lambda}{4\pi}\sqrt{\frac{P_t \cdot G_t \cdot PLF \cdot G_r \cdot \left(1 - |s|^2\right)}{P_{th}}} \tag{1}$$

with

$$|s|^2 = \left|\frac{Z_C - Z_A^*}{Z_C + Z_A}\right|^2 \tag{2}$$

where

- P_t - transmitted power
- G_t - gain of transmit antenna
- PLF - polarization loss factor
- G_r - gain of receiving antenna
- λ - wavelength
- $|s|^2$ - power reflection coefficient
- r - distance between reader and tag antenna
- Z_A - complex antenna impedance
- Z_C - complex chip impedance
- P_{th} - power threshold (chip)

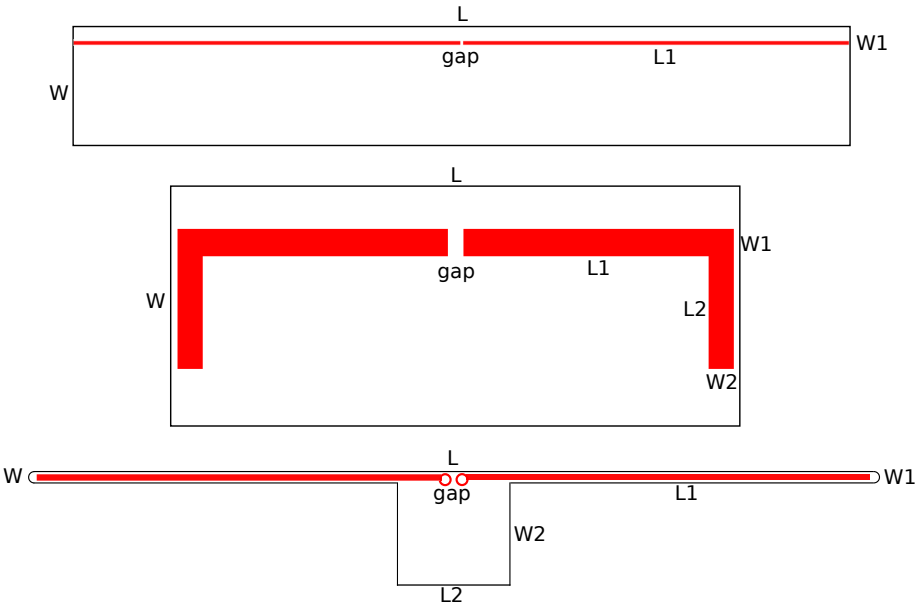

FIGURE 3 Antenna designs with characterization of the dimension variables

Tag	L	W	L1	W1	L2	W2	gap
Farsens Spider	137.1	21.3	77.9	0.5	-	-	0.5
AMS SL900A	102.1	40	48	5.2	25	4.6	3.8
WISP 5.1	147.5	1.6	146.8	1	18	18	4

TABLE 2 Measured antenna dimensions

3.1 | Antenna

The tag antenna represents the first part of the RFID tag interacting with the incoming electromagnetic wave. Considering the antenna design of the investigated tags, all represent versions of half-wave dipoles. This type of antenna is the most common example used in RFID, as it is easy to design and adapt to fulfill the needed requirements. The parameters, which are part of (1) and directly influenced by the design of the antenna are the gain of the receiving antenna G_r and the polarization loss factor *PLF*. Given a half-wave dipole, the gain is considered to be $G_r = 1.64$ and slowly varying with frequency. As this type of antenna represents a linear polarized antenna and most of the reader antennas have a circular polarization, $PLF = 0.5$ has to be taken into account. The reflection coefficient $|s|^2$ is one of the main parameters influencing the read range of a given tag. The antenna impedance represents the source impedance from which the reflection coefficient is calculated. Hence the variation of the antenna impedance has a strong impact on the resulting maximum read range of the tag.

To allow a thorough investigation of the performance of the antenna, the antenna dimensions as well as the dimensions of the Printed Circuit Board (PCB) they are fabricated on have been measured and are shown in Figure 3 and Table 2.

TABLE 3 Antenna Impedances Z_A and Chip Impedances Z_C at $f_c = 915$MHz

Tag	$Z_A[\Omega]$	$Z_C[\Omega]$
Farsens Spider	63.2-2.9j	51-469j
AMS SL900A	27.1-26.2j	31-300j
WISP 5.1	68.8-4.9j	13-65j

3.2 | Matching Network

A matching network is incorporated in a CRFID tag to allow a maximum power transfer from the tag antenna to the RFID chip, thus, optimizing the re□ection coef□cient $|s|^2$ present in (1). The two impedances to be matched, are the antenna impedance Z_A and the chip impedance Z_C. Table 3 shows the values of the mentioned parameters. The antenna impedance at the center frequency of the FCC UHF band ($f_c = 915$MHz) has been extracted from the tag antenna measurement, performed within the experimental study. The chip impedance Z_C for the Farsens tag is stated in the corresponding datasheet [9]. For the AMS tag, the impedance stated in the separately published RF characteristics document [16] was considered. The WISP's chip impedance is not stated in none of the published works, thus, a chip impedance measurement using the method proposed in [17] was performed at a power level of $P_{in} = -10dBm$.

Using the two impedances to be matched, a matching network can be designed. Two common solutions are the use of a lumped element matching network and the design of a microstrip matching network. Even though both options offer a cost ef□cient solution, the lumped element network adds the possibility to adapt the design after having built the actual PCB, where using a microstrip matching network would mean building a new PCB [5]. All investigated tags use a lumped element matching network to allow for a maximum power transfer. Figure 4a shows the schematics of the implemented matching networks, where Figure 4b shows their visual representation in a Smithchart. The simplest design is used for the SL900A tag, where a single inductor is used to compensate the highly capacitive imaginary part of the chip impedance. This approach does not yield the possibility to consider a difference between the real parts of the antenna and the chip impedance. As the resistance of the WISP antenna is smaller, the proposed L-network represents an easy to design cost-effective solution to provide a good narrowband matching network. The matching network design on the Farsens Spider distributes the inductance to the two branches of the network. This method yields a symmetric layout typically used in balanced systems and thus, considering the differential nature of signal generated by the dipole antenna.

3.3 | RF Energy Harvesting

In order to operate, the used RFID chip draws a certain current and needs a known voltage to wake up. The power needed by the chip is supplied by the RF energy harvesting unit. This device performs the task of rectifying the incoming RF signal and boosting it to surpass the threshold voltage. Furthermore, this unit incorporates a voltage regulator to avoid the destruction of the device by supplying a too large voltage. Depending on the current needed for operation, the different devices use different storage capacitors insuring suf□cient power for a whole cycle of communication.
Considering the three investigated tags, the power harvesting unit is not accessible, except for the WISP 5.1, where it consists of a Greinacher Voltage Doubler, a low dropout Boost-Charge-Pump-IC and a voltage regulator. The parameter present in (1) in□uenced by the energy harvester is the power threshold P_{th}. This parameter corresponds to the minimum power needed at the input terminal of the energy harvester to allow a suf□cient harvesting. With a sensitivity of $P_{th} = -14$dBm, the Farsens Rocky100 chip outperforms the Ams SL900A by 7dB. Additionally, the input impedance

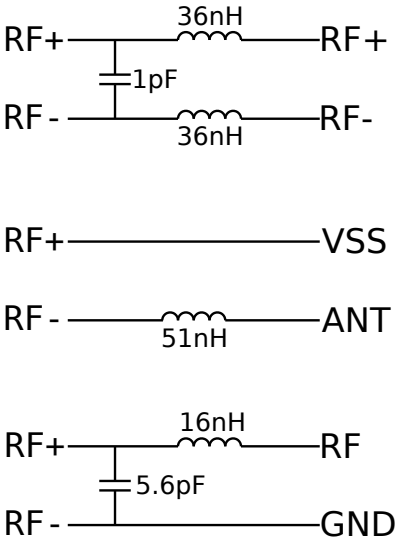

(a) Schematics of the incorporated lumped element matching networks: Spider (top), SL900A (mid), WISP 5.1 (bottom)

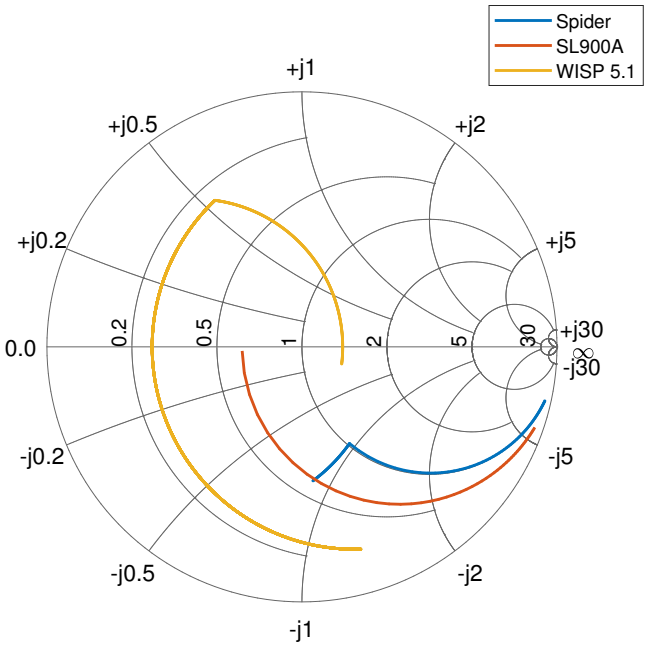

(b) Smithchart representations of the matching networks at $f = 915\text{MHz}$ and $Z_0 = 50\Omega$

FIGURE 4 Impedance matching networks incorporated in the investigated tags

of the energy harvester, represent the main contribution to the chip impedance Z_C and thus, has a strong impact on the re□ection coef□cient $|s|^2$.

3.4 | Load Modulation

Load modulation represents the modulation scheme for backscatter RFID communications. The impedance seen by the antenna terminals is switched between determined states, such that the amplitude as well as the phase of the backscattered signal are changed. A proper design of the different impedance states can yield various constellations. The current EPCC1G2 protocol is based on a 1-bit backscatter communication, typically using a heterodyne reader structure, which allows the usage of either phase-shift-keying (PSK) or amplitude-shift-keying (ASK). The choice of the modulation format depends on several aspects, but according to [18], using PSK results in an increased performance. With PSK communication [14] it is possible to achieve a constant power transfer between the antenna and the chip, as the impedance states can be selected in a way, that they yield the same power re□ection coef□cient $|s|^2$.
For an RFID system backscattering ASK, the most common method to choose the impedance states is to create a near perfect conjugate match for the main state, and switch to a deliberate mismatch for the opposing transmission bit. Given this method, the initial state represents a maximum of the power transfer from antenna to tag.
The power re□ection coef□cient can be used to describe the power available at the chip. It can also be used to represent the amplitude of the backscattered signal. Hence, a trade-off between power transmission to the chip and backscatter amplitude has to be considered, as we have discussed in [14].

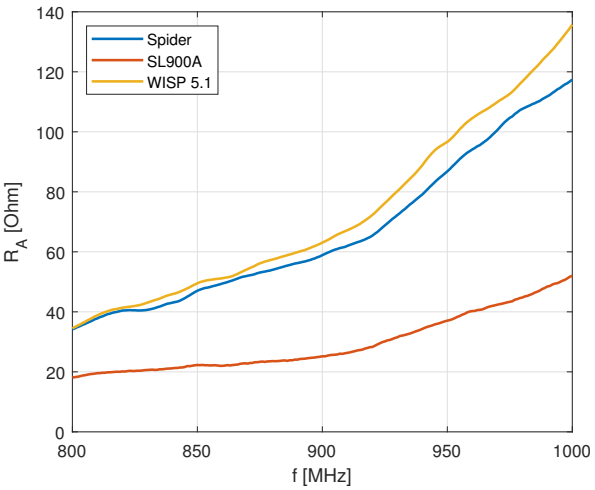

(a) Measured antenna resistance R_A

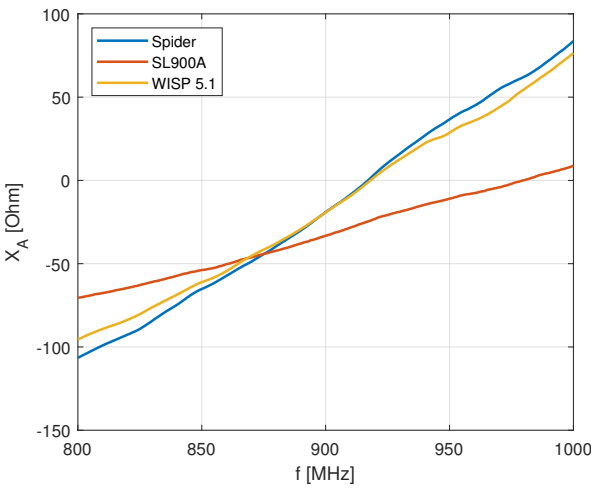

(b) Measured antenna reactance X_A

FIGURE 5 On-tag measurement of the incorporated antenna designs' impedances

4 | EXPERIMENTAL STUDY

The previously discussed theoretical considerations have been studied experimentally to provide a comparison with the theoretically obtained performance characteristics.

4.1 | Antenna

To evaluate the antenna performance and characteristics, the planar antennas placed on the chip's substrate have been measured using the S-parameter method [19]. A custom jig (port extension) has been fabricated to allow a measurement of the balanced symmetrical antennas. The port extension function of the vector network analyzer (VNA) was then used to take into account the losses and phase delay of the jig [20]. An open correction was performed. Figure 5a shows the differential input resistance R_A of the measured antennas, where Figure 5b shows their reactance X_A. The two straight dipole antennas of the WISP and the Spider show a very similar trend regarding their impedance, where the wider and bent dipole of the SL900A gives a lower resistance as well as a lower gradient of the imaginary part as a function of frequency. These presented values are to be considered during the design process of the matching network.

4.2 | Matching Network

Using the measured S-parameters of the antennas and considering a constant chip impedance Z_C over the whole investigated frequency range, the re□ection coef□cient has been simulated in Advanced Design System (ADS). Parasitics of the PCB, as well as in□uencing reactances and resistances of the printed traces, were not considered. Figures 6a and 6b show the antenna's S_{11} and the tag's S_{11}. It can be seen, that the resonant frequency of the antenna structure does not necessarily correspond to the resonant frequency of the tag, which corresponds to the explanations in [21].

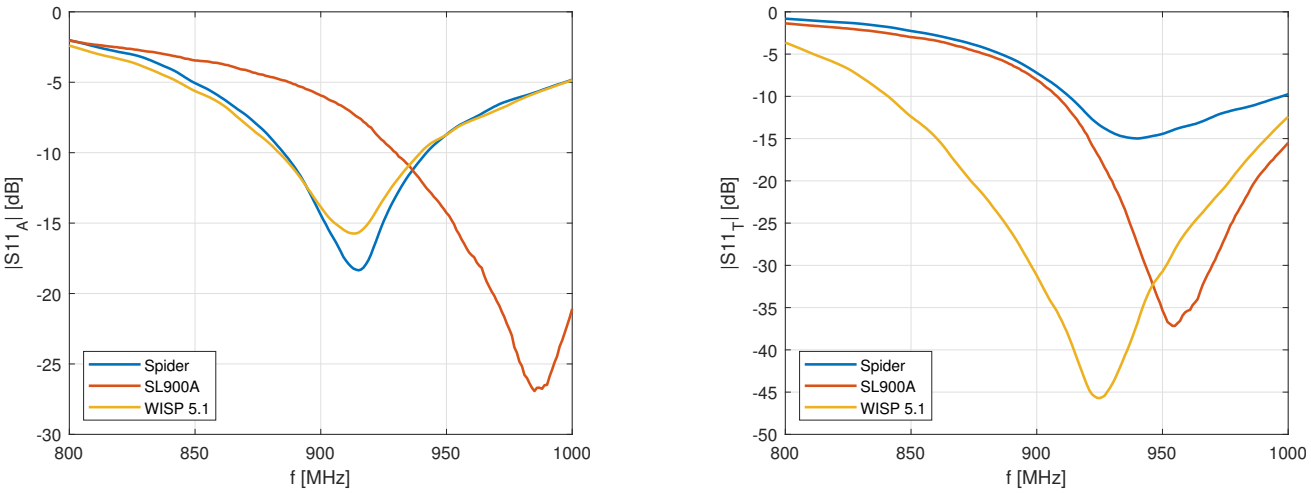

(a) Measured antenna S_{11}

(b) Simulated S_{11} of the tag

FIGURE 6 Re□ection Coef□cients S_{11} of the antennas and the tags

4.3 | RF Energy Harvesting

All three investigated transponders offer the possibility to measure the regulated voltage output produced by the RF energy harvesting circuit. This voltage, which is also considered the supply voltage for the other parts, is presented in Figure 7a. An RF signal generator was used to emit a continuous wave at the center frequencies of the European (ETSI) and the North American (FCC) UHF bands. As the maximum output power of the signal generator is limited to 20 dBm, the signal was ampli□ed using a Skyworks SKY01267 power ampli□er. The achieved output was measured using a spectrum analyzer to obtain accurate values of the input power at the antenna. A 6dBi circular polarized ALR-A0501 antenna was used. The tags were consecutively placed in the RF □eld at a distance of $d = 0.6m$ (Figure 7b). Figure 7a shows, that the regulated voltage achieved by the Farsens tag reaches saturation at about 16 dBm for the ETSI band whereas for the AMS tag no saturation is visible within the emitted power range. The intersection of the measured voltages with the visualization of the power-on voltage threshold for either of the tags, does not necessarily correspond to the read range values measured using a RFID reader as RFID tags' read ranges differ depending on the EPCC1G2 characteristics. [22]

Due to the fact that a constant V_{reg} could, considering the WISP, only be obtained at the highest allowed input power, this tag is not represented in Figure 7a. Nevertheless, the WISP remains active at lower radiated powers or larger distances. The tag uses a particular duty cycle creating peaks long enough to allow a communication cycle. This decreases the possible read rate but expands the maximum read range, being now limited by the EPCC1G2's maximum interrogator on-time.

4.4 | Load Modulation

According to the EPCC1G2 protocol, the tag can backscatter a response to the reader using either binary ASK or binary PSK modulation. Often ASK load modulation is considered a modulation of the resistance of the impedance seen by the antenna and PSK a modulation of the reactance. Neglecting the imaginary part of the antenna impedance, PSK will always result in a mixed modulation type. Furthermore, even if considering the imaginary part of the antenna, the frequency dependence of either of the parts will only allow a pure ASK or PSK modulation for an in□nitely narrow

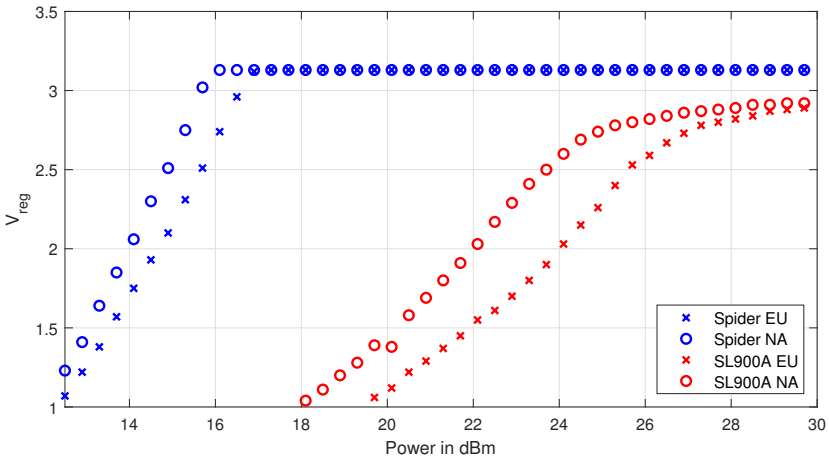

(a) Regulated voltage V_{reg} as a function of input power measured at $f_{c,EU} = 866.5$MHz and $f_{c,NA} = 915$MHz

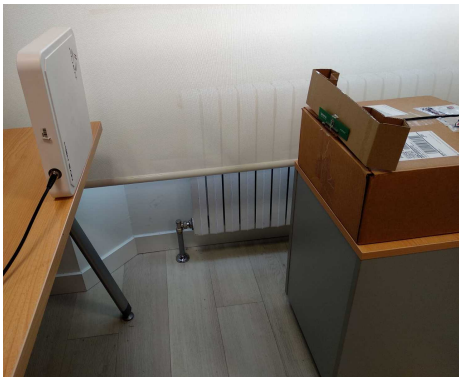

(b) Setup for the V_{reg} and read range measurement

FIGURE 7 Setup and results of regulated voltage V_{reg} measurement

frequency band.

The modulation types according to the data sheets for the WISP, Farsens and AMS are ASK, PSK and ASK respectively. The WISP is using a transistor to short circuit the antenna terminals, as the second state of the transmission. This behavior results in no power harvesting during this period of time. For the other two tags, the second impedance state is not known and thus no investigation of the trade-off between the power harvested and the power of the backscatter signal is possible during reader to tag transmission.

4.5 | Read Range

The tag read range measurement was performed using the methodology described in [23]. The tags were placed at a fixed distance from the circular polarized reader antenna with a gain of $G_t = 6$dBi. The tag direction was selected in a way, that the zero-axis of the half-wave dipole antennas did not affect the measurement. For both the ETSI and the FCC frequency range the minimum transmit power P_{min} required for communication was detected using a discrete sweep of the transmit power P_t with a stepsize of 0.5dB. The distance between the tag and the reader antenna was chosen to be $d = 0.6$m. With the known parameters of the measurement system, the tag read range for a given *EIRP*, which was considered the maximum allowed in Europe $EIRP = 3.28$W, can be calculated by

$$r = d\sqrt{\frac{EIRP}{P_t \cdot G_t \cdot L \cdot PLF}}, \tag{3}$$

where L denotes the cable loss, which for the conducted measurement was $L = 3$dB. The reader used for the experimentation was a ThingMagic M6e connected to a circular polarized Alien Technology ALR-A0501 antenna. The communication was established using the Universal Reader Assistant with the preset EPCC1G2 protocol parameters. Figure 8a shows a comparison of the calculated and the theoretical read ranges of the Farsens and the AMS tag. The measurements obtained for the real-world scenario clearly follow the trend presented by the theoretical values. The SL900A tag is outperformed by the Spider in the whole investigated frequency range, showing a lower read range maximum. Considering the calculated values, the Farsens tag shows a read range resonance at $f = 930$MHz. The

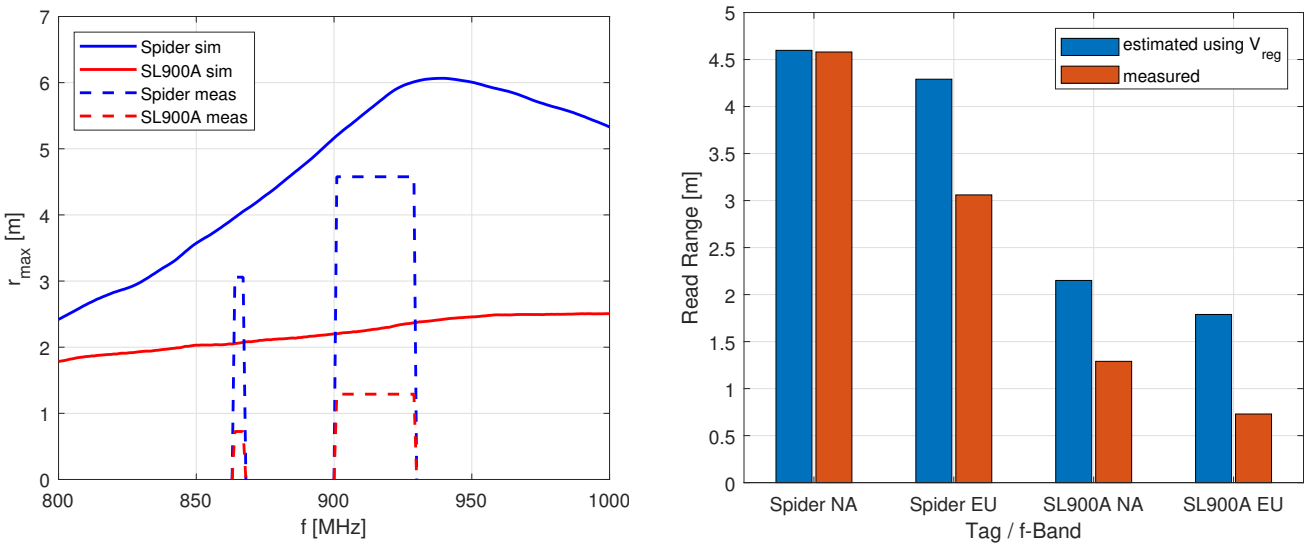

(a) Theoretical and experimental read range

(b) Read range measurement method comparison

FIGURE 8 Re□ection Coef□cients S_{11} of the antennas and the tags

smaller bandwidth of this peak represents a less constant read range regarding the European and North American frequency bands. The difference between measurement and theoretical estimation that can be observed is expected to be introduced by the multipath losses given the laboratory measurement and by the tag re□ection coef□cient model neglecting fabrication and additional line traces.

Additionally the read range of the investigated tags has been estimated using the measured regulated voltages from Figure 7a. Given this value and the minimum voltage needed for operation of the RFID chips, a second read range estimate can be calculated using (3). The Spider and the SL900A, according to their datasheets start working at a regulated voltage of $V_{reg} = 1.4$V and $V_{reg} = 1.3$V respectively. The different measured read ranges are illustrated in □gure 8b. A signi□cant difference in the read range can be identi□ed, which is expected to be due to the fact that during tag identi□cation, only a short time window is available to harvest the energy needed, while for the regulated voltage measurement a constant signal source was used.

5 | CONCLUSION

In this work, the RF Frontend of three passive CRFID platforms has been studied and evaluated. The proposed module-based approach considers all parameters present in the commonly used Friis equation for calculating the tag read range in a free space scenario and connects each one to the corresponding module.

The measured tag read ranges are in good agreement with the theoretical tag read ranges. A consideration of certain fabrication parameters and thus, a better model for tag's impedance could yield a further improvement of the method and will be investigated in the close future.

ACKNOWLEDGEMENTS

This work has been part-funded by the Basque Government under the project TEKINTZE (KK-2018/00104) and IoTrain (RTI2018-095499-B-C33).

REFERENCES

[1] Finkenzeller K. RFID-Handbuch: Grundlagen und praktische Anwendungen von Transpondern, kontaktlosen Chipkarten und NFC. Carl Hanser Verlag GmbH Co KG; 2015.

[2] Hansen RC. Relationship between antennas as scatters and as radiators. Proceedings of the IEEE 1989 06;77:659 – 662.

[3] Fuschini F, Piersanti C, Paolazzi F, Falciasecca G. Analytical approach to the backscattering from UHF RFID transponder. IEEE Antennas and Wireless Propagation Letters 2008;7:33–35.

[4] Sample AP, Yeager DJ, Powledge PS, Mamishev AV, Smith JR, et al. Design of an RFID-based battery-free programmable sensing platform. IEEE Transactions on Instrumentation and Measurement 2008;57(11):2608.

[5] Rao KS, Nikitin PV, Lam SF. Impedance matching concepts in RFID transponder design. In: Fourth IEEE Workshop on Automatic Identi□cation Advanced Technologies (AutoID'05) IEEE; 2005. p. 39–42.

[6] Muralter F, Arjona L, Landaluce H, Perallos A. A theoretical and experimental study of passive computational RFID tags. In: 2019 4th International Conference on Smart and Sustainable Technologies (SpliTech) IEEE; 2019. p. 1–5.

[7] Wireless Identi□cation and Sensing Platform WISP; 2018. http://wisp5.wispsensor.net/, accessed: 2019-11-11.

[8] Class 1 Generation 2 UHF Air Interface Protocol Standard Version 1.09;. https://www.gs1.org/standards/epc-rfid/uhf-air-interface-protocol, accessed: 2019-11-11.

[9] Farsens, EVAL01 Spider R; 2019. http://www.farsens.com/en/products/eval01-spider-r/, accessed: 2019-11-11.

[10] AMS, Demo Kit for SL900A; 2018. https://ams.com/sl900a-demokit, accessed: 2019-11-11.

[11] Fabbri D, Berthet-Bondet E, Masotti D, Costanzo A, Dardari D, Romani A. Long Range Battery-Less UHF-RFID Platform for Sensor Applications. In: 2019 IEEE International Conference on RFID Technology and Applications (RFID-TA) IEEE; 2019. p. 80–85.

[12] De Donno D, Catarinucci L, Tarricone L. RAMSES: RFID augmented module for smart environmental sensing. IEEE Transactions on Instrumentation and Measurement 2014;63(7):1701–1708.

[13] Nikitin PV, Rao KVS. Performance limitations of passive UHF RFID systems. 2006 IEEE Antennas and Propagation Society International Symposium 2006;p. 1011–1014.

[14] Muralter F, Landaluce H, Del-Rio-Ruiz R, Perallos A. Selecting impedance states in a passive computational RFID tag backscattering in PSK. IEEE Microwave and Wireless Components Letters 2019;29(10):680–682.

[15] Friis HT. A note on a simple transmission formula. Proceedings of the IRE 1946;34(5):254–256.

[16] AMS, SL900A RF Characteristics; 2014. https://ams.com/documents/20143/36005/SL900A_AN000200_1-00.pdf/40d9991e-3779-b581-b30e-8a69f1c442c4, accessed: 2019-11-11.

[17] Nikitin PV, Rao KS, Martinez R, Lam SF. Sensitivity and impedance measurements of UHF RFID chips. IEEE Transactions on Microwave Theory and Techniques 2009;57(5):1297–1302.

[18] De Vita G, Iannaccone G. Design criteria for the RF section of UHF and microwave passive RFID transponders. IEEE Transactions on Microwave Theory and Techniques 2005;53(9):2978–2990.

[19] Meys R, Janssens F. Measuring the impedance of balanced antennas by an S-parameter method. IEEE Antennas and Propagation Magazine 1998;40(6):62–65.

[20] Qing X, Goh CK, Chen ZN. Measurement of UHF RFID tag antenna impedance. In: 2009 IEEE International Workshop on Antenna Technology IEEE; 2009. p. 1–4.

[21] Rao KS, Nikitin PV, Lam SF. Antenna design for UHF RFID tags: A review and a practical application. IEEE Transactions on antennas and propagation 2005;53(12):3870–3876.

[22] Nikitin PV, Rao K. Effect of Gen2 protocol parameters on RFID tag performance. In: 2009 IEEE International Conference on RFID IEEE; 2009. p. 117–122.

[23] Nikitin PV, Rao KS. Antennas and propagation in UHF RFID systems. In: RFID, 2008 IEEE International Conference On IEEE; 2008. p. 277–288.

3.3 UHF RFID chip impedance and sensitivity measurement using a transmission line transformer

Conferences > 15th Annual Conference on RFID

A theoretical and experimental study of passive computational RFID tags

Publisher: IEEE

Florian Muralter ; Laura Arjona ; Hugo Landaluce ; Asier Perallos **All Authors**

Published in: 2021 15th Annual Conference on RFID (IEEE RFID 2021)

Status: Accepted

Date of Conference: 27-29 April 2021

3.3.1 Preface

The following paper was prepared in cooperation between DeustoTech and the Technical University Munich (TUM) during the 6-month research stay of this thesis' author in Munich, Germany. The design and fabrication of the test fixture was carried out by Michael Hani and Florian Muralter at the Associate Professorship for Microwave Engineering of the TUM. All authors were involved in the manuscript's preparation and revision process.

3.3.2 Article

UHF RFID chip impedance and sensitivity measurement using a transmission line transformer

Florian Muralter[1,2], Michael Hani[2], Hugo Landaluce[1], Asier Perallos[1], Erwin Biebl[2]
[1]DeustoTech, University of Deusto, Bilbao, Spain
[2]Associate Professorship for Microwave Engineering, Technical University Munich, Munich, Germany

***Abstract*—This article describes an alternative procedure for measuring the impedance of an ultra high frequency (UHF) radio frequency identification (RFID) chip and finding its turnon-point. The proposed method is based on measuring the balanced impedance of the RFID chip using a standard vector network analyzer (VNA) and a custom fabricated printed circuit board (PCB) test fixture. The test fixture uses a transmission line transformer to (1) provide a balanced signal to the ports of the RFID chip and (2) achieve a pre-matching to avoid the inaccuracies resulting from measuring high Q components with a VNA. No additional RFID reader is needed, as the turnon-point is extracted from the measured voltage reflection coefficient as a function of frequency and input power. A matching network is designed using a Smith chart approach to prove the applicability of the method by measuring the resulting reflection coefficient. A comparison with the typically used single-ended technique is provided.**

***Index Terms*—power reflection, impedance matching, radio frequency identification (RFID)**

I. Introduction

Ultra high frequency (UHF) radio frequency identification (RFID) is an automated identification technology operating in the industrial, scientific and medical (ISM) UHF band [1]. A typical UHF RFID system consists of a minimum of one reader (interrogator) and at least one tag (transponder). These RFID tags can be subdivided into passive (batteryless), semi-passive and active (with battery). A passive tag draws all of the power needed for operation from the incident electromagnetic waves. The following backscatter communication is achieved by reflecting a distinct part of the incident radio frequency (RF) field, changing the complex impedance of the RFID chip based on the antenna scattering theorem [2]. Given the need of a maximum power transfer between the tag's antenna and the RFID chip to guarantee operation at a maximum possible distance from the reader, the impedance matching procedure represents one of the most important tasks in UHF RFID tag design [3]. Hence, the knowledge of the impedance of the chip and the antenna is indispensable. Especially more power consuming concepts in RFID (e.g. wireless RFID sensor networks [4]) and recent technological advances such as the exploitation of the harmonics of UHF RFID chips [5] rely on these measurement procedures.

This article presents an alternative and reliable method for the measurement of the impedance and the turnon-point of UHF RFID chips. The proposed method uses a custom fabricated printed circuit board (PCB) test fixture consisting of an sub-miniature A (SMA) connector and a transmission line transformer which, at the same time, serves as a balance-unbalanced converter (BALUN) and a pre-matching network. The applicability to impedance matching UHF RFID chips is proven by designing, implementing and measuring a 50 Ω lumped element matching network.

II. Related Work

The measurement of the complex impedance of the tag antenna, as well as the RFID chip represent an important and difficult part of the performance optimization of RFID tags [6]. Furthermore, the knowledge of the sensitivity or turnon-point is indispensable for maximizing its read range. Given these parameters, the following section presents a compact review of the commonly used methods.

A. Chip Impedance Measurement

As most of the typically used antenna structures are dipole type antennas, several methods to obtain a differential measurement of the antenna impedance have been proposed (e.g., [3], [7]). However, most of the recent publications on this topic propose a single-ended approach for measuring the impedance of the RFID chip [8]-[14]. Most of these methods use a standard vector network analyzer (VNA) to calculate the chip impedance Z_C from the obtained reflection coefficient Γ as

$$Z_C = Z_0 \frac{1+\Gamma}{1-\Gamma}, \tag{1}$$

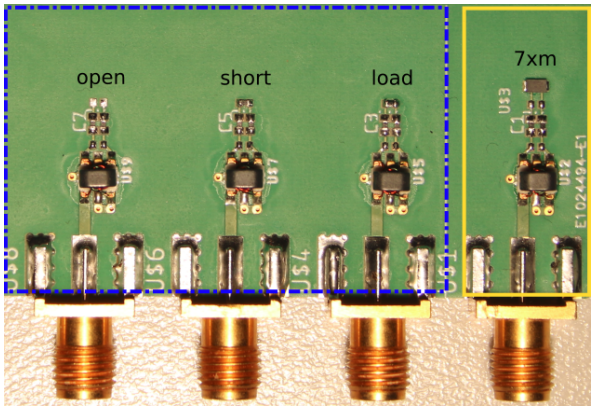

Fig. 1. PCB test fixture and calibration kit using a transmission line transformer.

Publication	Voltage Reference	Pre-Matching	Equipment	Fixture
[9]	Single-Ended	no	VNA, Reader	SMA connector
[10], [11]	Single-Ended	yes	VNA, Reader, power meter, 2 Slug Tuner	SMA connector + PCB Fixture
[12]	Single-Ended	no	Oscilloscope, Reader, Coupler	SMA connector + PCB Fixture
[14]	Single-Ended	no	Oscilloscope, Reader, Coupler	SMA connector + PCB Fixture
[13]	Single-Ended	no	VNA, Reader, RF probe	—
[15]	Single-Ended	no	VNA	LRL fixture
[16]	Differential	no	VNA	custom fabricated jig
[This work]	Differential	yes	VNA	transmission line transformer fixture

TABLE I
COMPARISON OF THE STATE-OF-THE-ART UHF RFID CHIP IMPEDANCE MEASUREMENT TECHNIQUES

with Z_0 denoting the reference impedance. Nikitin et al. in [9] proposed to measure the impedance of UHF RFID chips by mounting them directly to a SMA connector.

This yields a very simple approach neglecting the effect of the RFID chip being a high Q component. In [17] the problems of measuring high-Q, low-ESR components are described in detail. These drawbacks are considered in the measurement methodology presented in [10], by using a double slug tuner to perform a pre-matching as previously described in [18]. This procedure allows a smaller voltage standing wave ratio (VSWR) but highly increases the price of the test fixture. Table I shows a comparison of the published methods on UHF RFID chip impedance measurement techniques, revealing the lack of a differential pre-matched test fixture.

B. Chip Sensitivity Measurement

The RFID chip's sensitivity is typically measured using the same test fixture as for the impedance measurement (e.g., [9], [11]). A reader-like device is used to send a wake-up sequence to the tag to evaluate the minimum power P_{min} for the tag to start operating. Given the chip's voltage reflection coefficient Γ and the minimum operating power P_{min}, the sensitivity P_{th} can then be calculated as

$$P_{th} = P_{min}\left(1 - |\Gamma|^2\right). \tag{2}$$

Considering this procedure, the accuracy of the sensitivity measurement depends on the accuracy of the measured reflection coefficient.
Kronberger et al. in [19] showed that the sensitivity can also be extracted from a feature detected within the function of the resistance over power. A significant decrease of the resistance occurs at the power level, where the chip starts to draw power. This procedure avoids the need of an additional RFID reader to detect the power threshold.

III. METHODOLOGY

The following section provides a step-wise explanation of the proposed measurement technique.

A. Chip Impedance Measurement

The proposed test fixture (Fig. 1) was fabricated according to the schematic shown in Fig. 2-(Balanced). A Macom MABA-010125-TC1113 [20] transmission line transformer was connected to a SMA port to transform the single-ended signal present at the ports of a vector network analyzer (VNA)

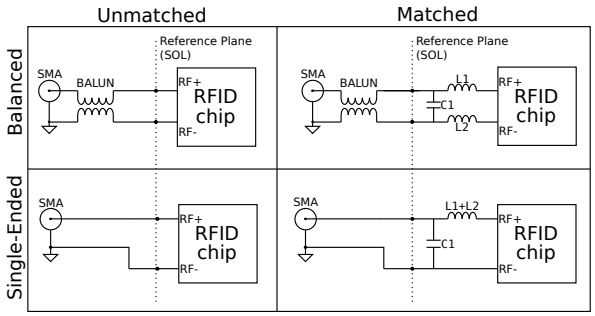

Fig. 2. Equivalent circuits of the different test fixtures with and without matching networks

to a differential signal, as drawn from the ports of a balanced antenna. Additionally to the BALUN characteristic of the chosen transmission line transformer, the device represents a mainly inductive component in the signal path. This behaviour compensates part of the negative reactance of the RFID chip, thus, reducing the Q factor of the device connected to the SMA port and achieving a pre-matching as proposed in [10], but without the need of an expensive slug or stub tuner. Fig. 3 shows a simulation of the impedance seen at the terminals of the SMA port, for a single-ended measurement in comparison to the proposed balanced approach. As a representative chip impedance for simulation, a parallel RC-network 1600 Ω and 1 pF was chosen. For the simulation, the S-parameter file of the BALUN provided by MACOM was used. Fig. 3 shows that the reactance is about one tenth when using the proposed design. This behaviour decreases the Q factor to less than one third and allows a more accurate reflection coefficient measurement [17]. To calibrate the impedance measurement directly to the input ports of the RFID chip, a short-open-load (SOL) calibration kit, using two 100 Ω resistors in parallel as a load was designed. For the measurement of Γ, the test fixture was directly connected to a R&S ZVA40 network analyzer. A power calibration was performed at the measurement port of the VNA. The resulting impedance was calculated using (1)

B. Chip Sensitivity Measurement

The extraction of the chip sensitivity is performed using the reflection coefficient data measured using the presented test fixture. According to [19], a significant change of the resistance is visible at the power threshold of the RFID chip. The power level corresponding to this feature will be further

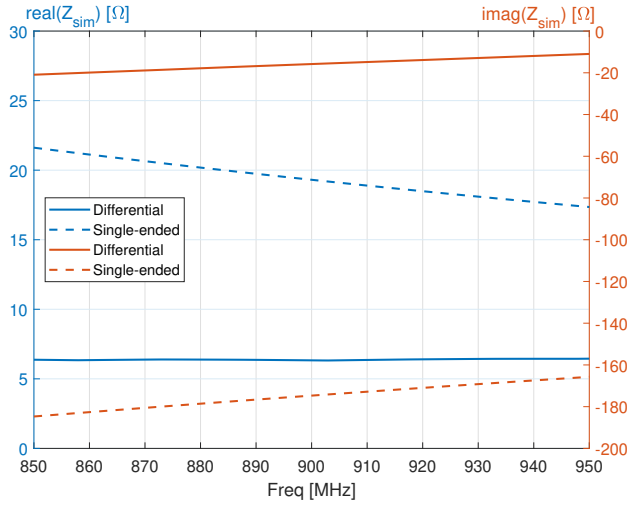

Fig. 3. Simulated impedance at the SMA port terminals for the different test fixtures

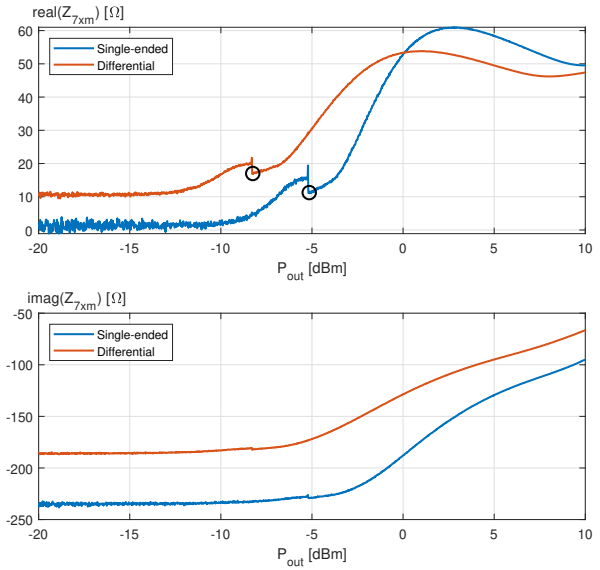

Fig. 4. Measured impedance of the MURATA 7xm chip as a function of the output powerof the VNA; black circles highlight the turnon-point.

called the turnon-point. The quasi continuous curve at power levels below the turnon-point refers to the region where the energy harvesting is insufficient for powering the chip's circuitry. Referring to [9], the impedance at the power level just above the turnon-point represents the impedance a matching network should be designed for. Given the measurement of Γ as a function of frequency and power, the input power value corresponding to the abrupt change in the reflection coefficient was then extracted using the maximum of the first derivative. The values obtained at 868 MHz are shown in Table II and are further used to design suitable matching networks.

IV. Results

The following section describes the results obtained using the proposed measurement methodology. The measurements were performed using 3 commercial off-the-shelf UHF RFID chips (Murata 7xm, NXP G2xm, Farsens Rocky100). A lumped element matching network as shown in Fig. 2 was designed using the impedance values stated in Table II and attached to the SOL calibration reference plane to prove the validity of the measurements.

Fig. 4 shows the real and imaginary parts of the chip impedance as a function of P_{out} for the Murata 7xm chip.

	investigated RFID chips		
	7xm	G2xm	Rocky100
$Z_{C,DI}$	(17.03-182.07j)Ω	(24.56-160.36j)Ω	(30.56-328j)Ω
L1+L2 (DI)	39nH	33nH	66nH
C1 (DI)	4.7pF	3.3pF	2.2pF
$Z_{C,SE}$	(11.21-229.14j)Ω		
L1+L2 (SE)	46nH		
C1 (SE)	6.8pF		
$Z_{C,DS}$	N/A	(18.6 - 171.2j)Ω	(64 - 469j)Ω

TABLE II
Measured impedance values at (f = 868MHz, turnon-point) and corresponding lumped element matching network values, where DI-Differential, SE-Single Ended and DS-Datasheet

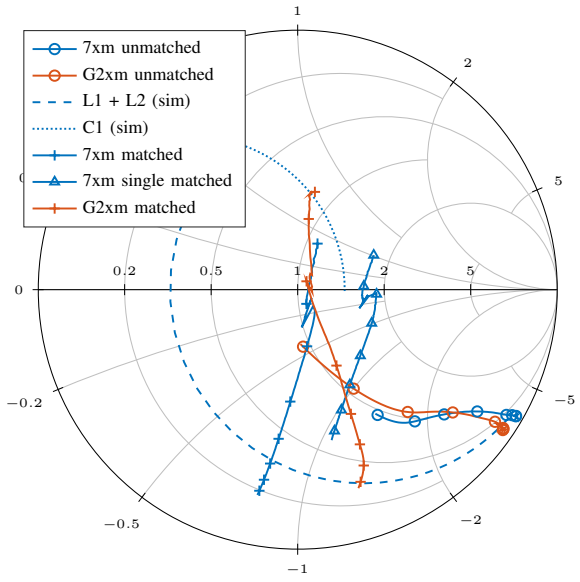

Fig. 5. Smith chart showing Γ of the unmatched and matched chip assemblies as a function of power and visualizing the design process of the lumped element matching network at the turnon-point and f = 868 MHz

A power sweep ranging from −20 dBm to 10 dBm with a step size of 0.01 dBm has been used. It can be seen that the measurements for the same chip yield different results. The visible difference of about 40 Ω for the reactance would mean that a completely different inductance is needed to compensate the chip's capacitance when designing a matching network. Furthermore the different reflection coefficients obtained from the measurement result in a different sensitivity P_{th} when calculated using (2).

Fig. 5 shows the design process of the matching network in

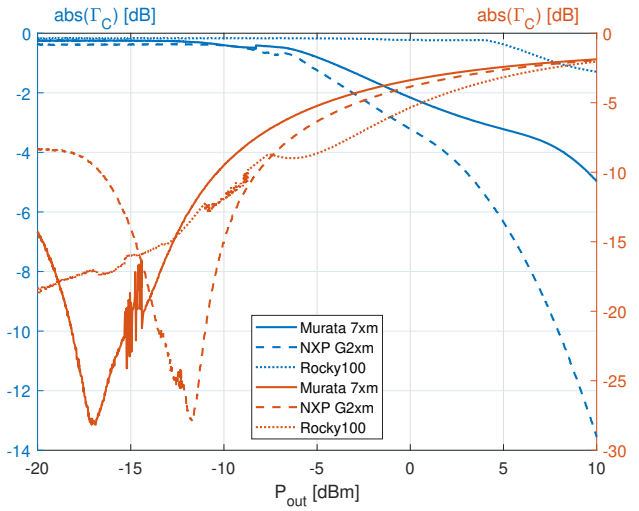

Fig. 6. Magnitude of Γ of the unmatched (blue) and matched (red) chip assemblies as a function of VNA output power P_{out} at $f = 868\,\mathrm{MHz}$

the Smith chart. The obtained impedances at the turnon-point have been transformed towards the matching point using the lumped component values stated in Tab. II. The measurement of the resulting matched chip assembly lies well within the discrete component's tolerances stated in the corresponding datasheets. The same procedure has been evaluated using the single-ended measurement of the Murata 7xm chip. For this case, the designed matching network did not result in an improved matching condition at the desired frequency-power point, thus, indicating an impedance measurement error. To prove the validity of the measurement using the proposed approach, the matching network design using the balanced measurement was attached to the SOL calibration plane of the single-ended test fixture. The result is also visualized in Fig. 5 and further underlines the obtained impedance values. Fig. 6 shows the measured power reflection coefficients as a function of input power for the three different investigated chips. The data corresponding to the unmatched assemblies shows a large reflection coefficient of $\Gamma > -1$ for all chips at power levels below 5 dBm. It is clearly visible that the matched chip assemblies, using the matching network designed based on the impedances measured via the proposed approach show a good matching condition ($\Gamma < -10$) close to the turnon-point. The slightly worse reflection coefficient of the Rocky100 chip is expected to be due to the larger spacing between lumped elements at larger inductances. To achieve the desired inductance of 66 nH, two 33 nH inductors were soldered in series. These real components further introduce parasitics and losses resulting in this slight discrepancy.

V. Conclusion

The method presented within this article is a simple, yet reliable alternative to the commonly used RFID chip measurement procedures. The described method only uses a standard VNA and a custom fabricated test fixture. The benefit of using a transmission line transformer as a BALUN and prematching circuit for obtaining an accurate chip impedance was validated comparing it to the typically used single-ended technique. Furthermore, the need of an additional RFID reader is omitted by the extraction of the turnon-point from the reflection coefficient measurement.

References

[1] K. Finkenzeller, *RFID-Handbuch: Grundlagen und praktische Anwendungen von Transpondern, kontaktlosen Chipkarten und NFC*. Carl Hanser Verlag GmbH Co KG, 2015.

[2] R. Hansen, "Relationships between antennas as scatterers and as radiators," *Proceedings of the IEEE*, vol. 77, no. 5, pp. 659–662, 1989.

[3] G. Marrocco, "The art of UHF RFID antenna design: Impedance-matching and size-reduction techniques," *IEEE antennas and propagation magazine*, vol. 50, no. 1, pp. 66–79, 2008.

[4] H. Landaluce, L. Arjona, A. Perallos, F. Falcone, I. Angulo, and F. Muralter, "A review of iot sensing applications and challenges using rfid and wireless sensor networks," *Sensors*, vol. 20, no. 9, p. 2495, 2020.

[5] G. A. Vera, Y. Duroc, and S. Tedjini, "Third harmonic exploitation in passive uhf rfid," *IEEE Transactions on Microwave Theory and Techniques*, vol. 63, no. 9, pp. 2991–3004, 2015.

[6] K. S. Rao, P. V. Nikitin, and S. F. Lam, "Antenna design for UHF RFID tags: A review and a practical application," *IEEE Transactions on antennas and propagation*, vol. 53, no. 12, pp. 3870–3876, 2005.

[7] X. Qing, C. K. Goh, and Z. N. Chen, "Impedance characterization of RFID tag antennas and application in tag co-design," *IEEE Transactions on Microwave Theory and Techniques*, vol. 57, no. 5, pp. 1268–1274, 2009.

[8] G. A. Vera, Y. Duroc, and S. Tedjini, "RFID test platform: Nonlinear characterization," *IEEE Transactions on Instrumentation and Measurement*, vol. 63, no. 9, pp. 2299–2305, 2014.

[9] P. V. Nikitin, K. S. Rao, R. Martinez, and S. F. Lam, "Sensitivity and impedance measurements of uhf rfid chips," *IEEE Transactions on Microwave Theory and Techniques*, vol. 57, no. 5, pp. 1297–1302, 2009.

[10] L. W. Mayer and A. L. Scholtz, "Sensitivity and impedance measurements on UHF RFID transponder chips," in *Proc. 2nd Int. EURASIP Workshop RFID Technol.*, 2008, pp. 1–10.

[11] J. Grosinger, C. Mecklenbrauker, and A. L. Scholtz, "UHF RFID transponder chip and antenna impedance measurements," in *Proc. of the Third International EURASIP Workshop RFID Technology, La Manga del Mar Menor (Spain)*, 2010, pp. 43–46.

[12] J. Yang and J. Yeo, "Chip impedance evaluation method for UHF RFID transponder ICs over absorbed input power," *ETRI journal*, vol. 32, no. 6, pp. 969–971, 2010.

[13] B. Couraud, T. Deleruyelle, E. Kussener, and R. Vauché, "Real-time impedance characterization method for RFID-type backscatter communication devices," *IEEE Transactions on Instrumentation and Measurement*, vol. 67, no. 2, pp. 288–295, 2017.

[14] E. Bergeret, P. Seurre, R. Saba, and D. Michelon, "UHF RFID chip measurement," in *2016 IEEE International Conference on RFID (RFID)*. IEEE, 2016, pp. 1–7.

[15] A. Ghiotto, T. Vuong, and K. Wu, "Chip and antenna impedance measurement for the design of passive uhf rfid tag," in *The 40th European Microwave Conference*. IEEE, 2010, pp. 1086–1089.

[16] C. Stoumpos, D. Anagnostou, and M. T. Chryssomallis, "Experimental characterization of the impedance of balanced uhf rfid tag antennas," *Microwave and Optical Technology Letters*, vol. 59, no. 12, pp. 3127–3134, 2017.

[17] Agilent. How To Accurately Evaluate Low ESR, High Q RF Chip Devices; Application Note 1369-6. [Online]. Available: http://literature.cdn.keysight.com/litweb/pdf/5989-0258EN.pdf

[18] U. Pisani, A. Ferrero, and G. L. Madonna, "Experimental characterization of nonlinear active microwave devices," *Review Of Radio Science*, pp. 3–22, 2001.

[19] R. Kronberger, A. Geissler, and B. Friedmann, "New methods to determine the impedance of UHF RFID chips," in *2010 IEEE International Conference on RFID (IEEE RFID 2010)*. IEEE, 2010, pp. 260–265.

[20] MACOM. MABA-010125-TC1113, RF 1:1 Transmission Line Transformer, 4.5 -3000 MHz. [Online]. Available: https://cdn.macom.com/datasheets/MABA-010125-TC1113.pdf

3.4 Harmonic Voltage Reflection Analysis of UHF RFID chips

Journals & Magazines > IEEE Transactions on Instrume... > Volume: 70

Harmonic Voltage Reflection Analysis of UHF RFID Chips

Publisher: IEEE

Florian Muralter ; Michael Hani ; Hugo Landaluce ; Asier Perallos ; Erwin M...

Published in: IEEE Transactions on Instrumentation and Measurement (Volume: 70)

Article Sequence Number: 8002107 **INSPEC Accession Number:** 20294780

Date of Publication: 10 December 2020 **DOI:** 10.1109/TIM.2020.3043942

JIF(2019): 3.658 **Rank**: Q1 in Electrical Engineering Q1 in Engineering

3.4.1 Preface

The following paper was prepared in cooperation between the DeustoTech Institute of Technology and the Technical University Munich (TUM) during the 6-month research stay of this thesis' author in Munich, Germany. Additional measurement equipment needed for the experimentation setup, was provided by Rohde & Schwarz GmbH & Co KG and the SPINNER GmbH. The measurements were carried out by Michael Hani and Florian Muralter at the Associate Professorship for Microwave Engineering of the TUM. The development of the signal processing framework was performed by Florian Muralter. The project was supervised by Asier Perallos and Erwin Biebl. All authors were involved in the manuscript's preparation and revision process.

3.4.2 Article

Harmonic Voltage Reflection Analysis of UHF RFID chips

Florian Muralter*, Michael Hani, Hugo Landaluce,
Asier Perallos, Erwin Biebl

***Abstract*—In recent years, the exploitation of the nonlinear behaviour of ultra high frequency (UHF) radio frequency identification (RFID) chips has gained popularity. This manuscript presents a measurement platform for the harmonic characterization of UHF RFID chips. The measurement of the incident and reflected wave at the RFID chip terminals is performed using a digital sampling oscilloscope. A novel signal processing methodology is presented to extract time-domain reflection coefficient equivalents from a digital sampling oscilloscope measurement at the different load modulation states. Using a simultaneous measurement of the reflection coefficient with a vector network analyzer the obtained measurement results were validated. Furthermore, a comparison to using real-time sampling and a power spectral density analysis is presented.**

***Index Terms*—power reflection, nonlinear analysis, radio frequency identification (RFID)**

I. Introduction

Ultra high frequency (UHF) radio frequency identification (RFID) represents an automated, contactless identification technology mainly used in logistics and asset tracking [1]. In recent years, technical advances in the area of RFID (e.g. computational RFID, RFID sensors) and the evolution of the Internet of Things (IoT) have pushed the boundaries of this technology.

A standard RFID system consists of at least one interrogator (reader) and a minimum of one transponder (tag). Such a tag, representing the device to be identified, can be either active (with battery), semi-passive (battery-assisted) or passive (batteryless). Typical passive UHF RFID tags consist of an antenna, a matching network and the RFID chip. This chip performs the back-scatter communication by modulating the load impedance seen by the antenna terminals based on the antenna scattering theorem [2]. The energy needed for the operation of the internal logic is harvested from the incident electromagnetic wave. Due to the energy harvester topology, consisting of Schottky diodes, this circuitry represents a nonlinear behaviour and thus, poses problems when trying to measure linear parameters such as the linear voltage reflection coefficient Γ. The basics to measuring impedance and sensitivity as presented in e.g., [3]-[5] all rely on extracting the linear reflection coefficient at the fundamental frequency. These methods are expected to yield sufficiently accurate results at low power levels, but are expected to show a larger deviation from the real reflected power at higher power levels [6]. Fig. 1 shows an illustration of the incident and reflected waves at the RFID chip, highlighting its nonlinear nature.

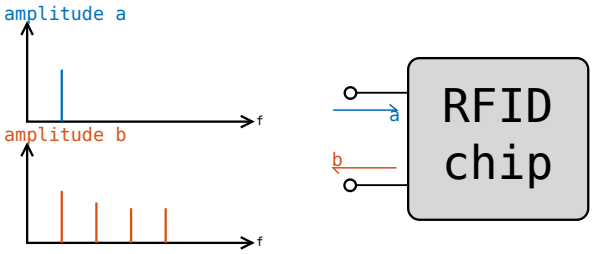

Fig. 1. Illustration of harmonic back-scattering in UHF RFID chips.

The nonlinear characterization of UHF RFID tags and chips has first been considered by J. Essel in [7] and A.G. Vera in [6], [8] and [9]. Table I presents a comparison of the mentioned measurement methodology for UHF RFID chips. The measurement platform presented in [6] allows for a time-domain measurement of the reflected signal. With the consecutive power spectral density (PSD) analysis, an estimate of the reflected power is obtained. From this data, it is possible to extract the power reflected at the different harmonics. This methodology has opened up a new area of interest, which has evolved in several new methods on how to exploit the reflected nonlinear content. In [10], [11], [12] a number of possible exploitation strategies are presented. The currently existing methods using the harmonic nature of the back-scattered UHF RFID signal range from (1) harmonic power harvesting [13], [14], (2) harmonic UHF RFID ranging [15] to (3) harmonic UHF RFID sensing [16], [17]. This evolution of methods has also increased the need of accurate and reliable methods for measuring nonlinear RFID chip parameters.

The proposed measurement platform presents a novel approach to obtaining reflection coefficients from time series data measured with a digital sampling oscilloscope (DSO). This procedure reduces the real-time bandwidth requirement of the method presented in [6] by using the DSO in sampling mode and a novel data processing strategy. The measurement of both the reflected and incident voltage signals allows for the calculation of a time-domain reflection coefficient equivalent. The simultaneous measurement of the reflection coefficients with a vector network analyzer (VNA) is used to validate the presented methodology.

The presented manuscript is structured as follows: In Section

Manuscript received __, __.

F. Muralter is with DeustoTech (University of Deusto) and Technical University Munich (e-mail: florian.muralter@deusto.es).

M. Hani and E. Biebl are with the Technical University of Munich (Associate Professorship for Microwave Engineering)

H. Landaluce and A. Perallos are with DeustoTech (University of Deusto)

Publication	Equipment	Technique	Measurement Domain	Extracted Parameters
[6]	VSG, 2 Antennas, DSO, Anechoic chamber	PSD Analysis	Time Domain	Reflected Signal Characteristics
[7]	VSG, Power Meter, Source Tuner, IV Meter	Source Pull	Frequency Domain (Fundamental)	VI-Characteristics Impedance at fundamental
[8]	VSG, VNA, 2 Couplers, 2 Impedance tuners, DSO	PSD Analysis	Time Domain	Reflected Signal Characteristics (over the air)
This work	2 VSGs, Coupler, DSO (VNA)	Curve Fitting	Time & Frequency Domain	Harmonic Reflection Coefficients Reflected Signal Characteristics

TABLE I
COMPARISON OF THE STATE-OF-THE-ART NONLINEAR CHARACTERIZATION METHODS FOR UHF RFID CHIPS.

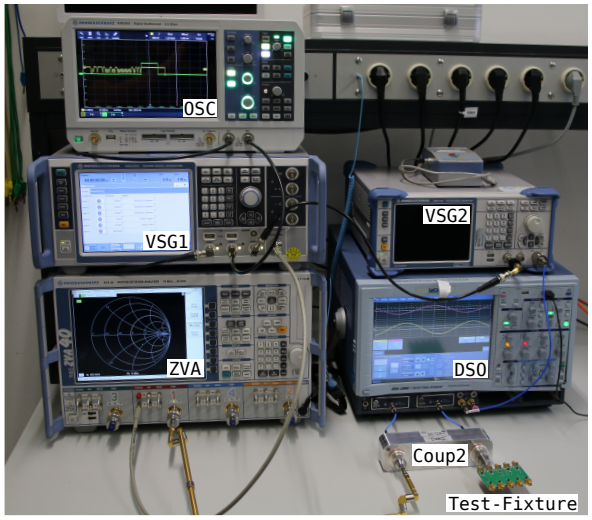

Fig. 2. Measurement setup of the proposed measurement platform

II, the Measurement Platform and the corresponding data acquisition methodology are explained; Section III offers a description of the signal processing steps used for processing the DSO data; In section IV, results for commercially available UHF RFID chips are shown and compared to state-of-the-art measurement procedures; Section V presents the conclusions drawn from the presented work.

II. MEASUREMENT PLATFORM

The following section presents the proposed measurement setup allowing for a simultaneous measurement of the incident and reflected waves in both the time and the frequency domain using a DSO and a VNA, respectively. The measurement is possible during all states of the communication, as the RFID signal is generated by a vector signal generator (VSG), which generates the baseband data as programmed in a Python script. The EPC Class 1 Generation 2 command selected for the interrogation of the RFID chip under test was a Query command. The corresponding bit sequence [1000 0101 1010 1110] requests a random number 16 (RN16) message with a data rate of 80 kS/s without tone and encoded in FM0. Fig 3 shows a signal flow block diagram of the proposed measurement platform and Fig. 2 shows a picture of the measurement setup. The proposed system consists of:

(1) As VSG 1, a Rohde&Schwarz SMW200A vector signal generator with an incorporated baseband generator to allow for the creation of RFID specific signals was used. A standard Query message was programmed according to the EPC Class 1 Generation 2 standard. The custom user outputs are used to output trigger signals, such that all measurements can be performed simultaneously.
(2) VSG 2 (Rohde&Schwarz SMBV100B) is a vector signal generator which is set to the transmission frequency of VSG 1 but uses a constant power level of 0 dBm. This continuous wave source is used as the trigger signal for the DSO. The RF output is modulated using the I-Modulation input, such that the trigger signal is only present at the DSO during the response of the RFID chip.
(3) A Rohde&Schwarz ZVA40 vector network analyzer was used for the frequency domain measurements. The reflection coefficient measurement at the chosen port is triggered by a trigger signal created on VSG 1. To allow for a measurment of the back-scatter communication a measurement time larger than the tag response was used. A time series of reflection coefficients was measured with a measurement bandwidth of 1 MHz to identify the different states of the load modulation.
(4) A LeCroy WaveExpert digital sampling oscilloscope with two separate input channels was used in sampling mode. The transmitted and reflected voltage signals split by Coupler 2 were fed to the inputs of the DSO. The continuous wave trigger signal is provided by VSG 2.
(5) A Spinner bidirectional 3 dB coupler was used to separate the incident and reflected waves for the measurment at the DSO.
(6) The test fixture used for the proposed measurement platform consists of a transmission line transformer which works simultaneously as a balanced-unbalanced converter and a pre-matching network. Additionally a short-open-load (SOL) calibration kit was designed on the same printed circuit board (PCB) to allow for a shift of the reference plane towards the terminals of the measured RFID chip.
(7) The oscilloscope marked as OSC in Fig. 2 was used to visualize the timing of the different signals during measurement to prove the correct operation.
(8) The whole measurement platform is controlled by a computer using a Python script, which allows the measurement at any given frequency and power point within the hardware limits of the used equipment.

Fig. 4 shows the used timing strategy, visualizing the use of the different trigger signals to perform measurements only

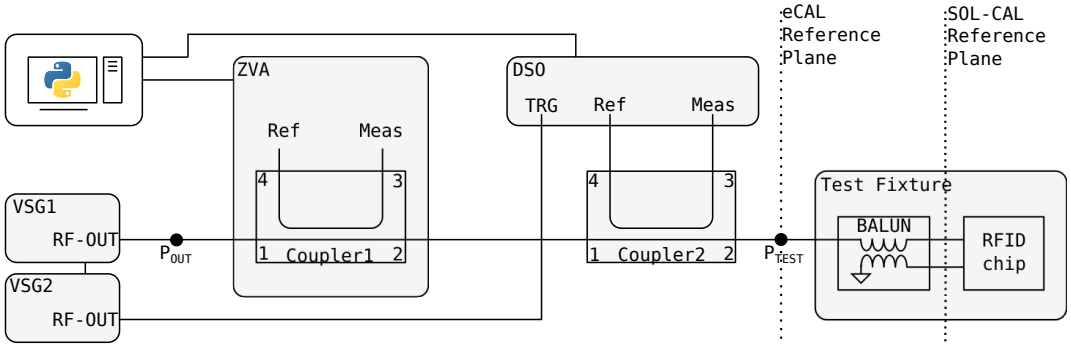

Fig. 3. Structure and signal flow chart of the proposed measurement platform.

during the time period of back-scatter communication.

A. VNA measurement

With the VNA, a measurement of the complex reflection coefficient was performed. Using the eCAL kit, a calibration to the subminiature A (SMA) port of the test fixture is achieved. With the deployed SOL calibration standards a further transformation of the reference plane to the terminals of the RFID chip is possible, which, if applicable, was performed in MATLAB considering the measured SOL calibration standards as ideal. A time series measurement of Γ is initiated using the trigger output of VSG 1. The measurement duration is set to a duration of 140 us, such that the time period of the response of the RFID chip is covered. Additionally, to consider the losses of the couplers and the cables that connect the test fixture, the S parameter $S_{through}$, representing the losses between P_{Out} and P_{Test}, as depicted in Fig. 3, has been measured and can be used to calculate the power at the SMA port of the test fixture P_{Test}

$$P_{Test} = P_{Out}|S_{through}|^2. \tag{1}$$

Considering the error model obtained from the measurement of the SOL calibration standards, the power at the terminals of the RFID chip P_{Chip} can be obtained by

$$P_{Chip} = P_{Test}|e_{10}|^2, \tag{2}$$

where e_{10} denotes the forward transmission coefficient of the error model as shown in Fig. 5. The influence of e_{11} on the power present at the chip terminals was neglected as $|e_{11}| \ll |e_{10}|$.

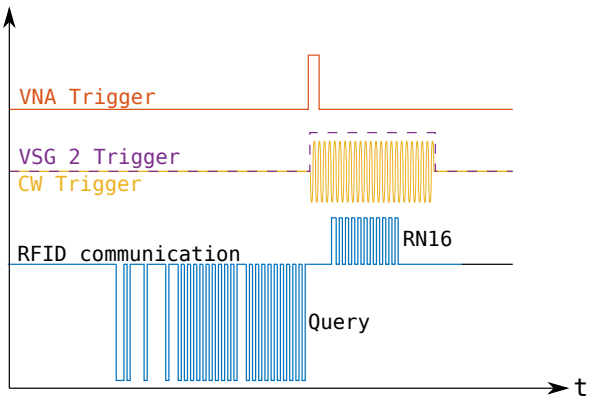

Fig. 4. Measurement timing and trigger signals

B. DSO measurement

A sampling oscilloscope uses a periodic trigger signal to measure one sample with a deliberate time delay per period to consecutively reconstruct the periodic input signal [18]. The mentioned continuous wave trigger signal is fed to the trigger input only during the time of back-scatter tag communication. As the step generator of the DSO uses a pulse rate of 1 MHz, close to 300 samples are acquired per RN16 response. Consecutive query commands and their corresponding RN16 responses are thus used to acquire the total amount of 5 kS. The acquisition parameters were set in a way, that the 5000 samples are acquired using a time-base of 2 ns, hence, measuring roughly two periods of the fundamental wave. Both coupled paths of coupler 2 are measured at the DSO allowing an aquisition of both the transmitted and reflected waves. The reflected signal, if a communication is established, jumps between two states caused by the changing mismatch. As only one sample is considered in each CW trigger period, the resulting signal switches between the two states at random time steps, yielding a sequence $M[n]$ as shown in Fig. 6-(Raw Data).

$$M[n] = \begin{cases} \sum_k^N A_{0,k}\Re\{\exp\left(j\omega_f kn + \phi_{0,k}\right)\} & \text{if Bit0} \\ \sum_k^N A_{1,k}\Re\{\exp\left(j\omega_f kn + \phi_{1,k}\right)\} & \text{if Bit1} \end{cases} \tag{3}$$

with A and ϕ denoting amplitude and phase respectively, the subscripts 0 and 1 corresponding to Bit0 and Bit1 and the indices k and n standing for the harmonic and sample index, respectively. N represents the highest harmonic index measurable, given the used equipment (VNA, DSO, couplers,

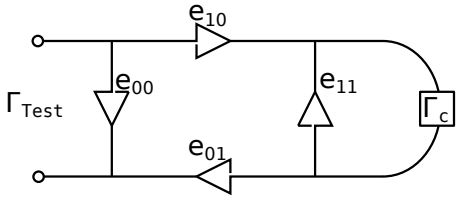

Fig. 5. SOL calibration error model

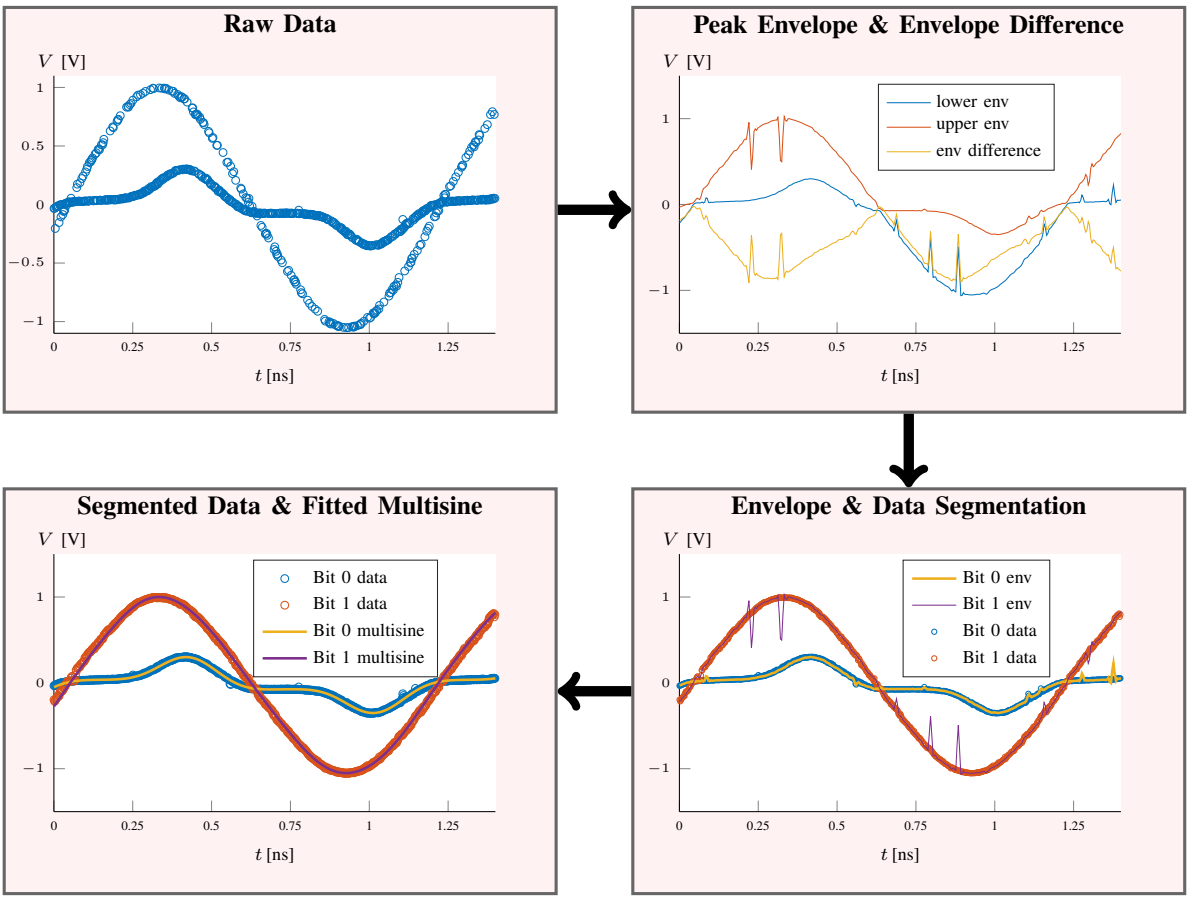

Fig. 6. Flow chart visualizing the DSO signal processing steps

test fixture). To separate the reflected waves components corresponding to the different load modulation states the signal processing described in section III was used.

III. DSO Signal Processing

The following section explains the signal processing steps performed to identify the samples of the time series data corresponding to each of the load modulation states and thus, segment the obtained DSO signal. Consecutively, to obtain a voltage reflection coefficient equivalent and to transform the reference plane from the terminals of the DSO to the ports of the RFID chip, the obtained time-domain signals have to be evaluated at the harmonic frequencies and put in relation to the reference signal. All of the DSO signal processing was performed using MATLAB. Fig. 6 shows a flow chart of the different signals obtained during the following signal processing steps:

(1) The first step towards performing a segmentation of the time-domain signal, was to calculate its peak envelope. Therefore, the MATLAB function *envelope*, which determines the upper and lower envelope using spline interpolation over local maxima separated by at least N samples [19] was used. The number of samples N was set to $N = 20$ to minimize the number of spikes pointing towards the other envelope, but yet not achieve a strong time shift due to the moving average characteristic. As can be seen in Fig. 6-(Peak Envelope & Envelope Difference), the upper end lower envelope represent the different states at about each half-cycle.

(2) To distinguish the intersections of the two present waveforms, the difference of the envelopes (lower-upper) was calculated and a peak detection performed. To avoid the detection of non relevant peaks and by knowing the wavelength of the signal, a minimum peak distance was set.

(3) The extracted peaks were used to segment the envelopes and create curves corresponding to the different impedance states. For each consecutive segment, the other envelope (lower/upper) was used.

(4) The samples closer to each of the created curves were then selected as corresponding to the selected state. Around the intersection particular samples might be considered part of both waveforms. However, this behaviour does not influence the further processing.

(5) To get rid of the missing values, at time steps where the other waveform was present, the *fillmissing* function, set to *linear interpolation* was used.

(6) Given the input frequency of the measurement, *lsqcurvefit* was used to fit a multi-sine signal to the segmented

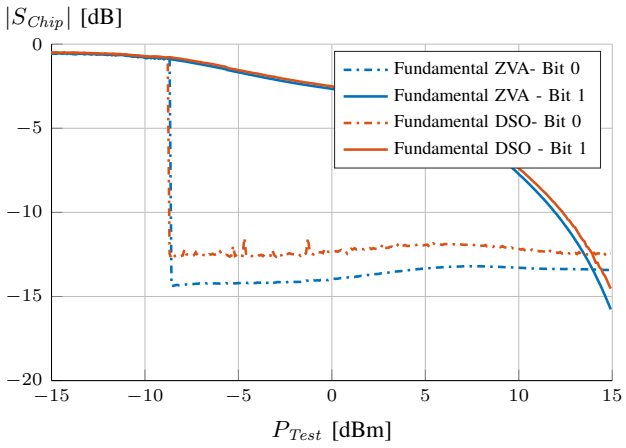

Fig. 7. Comparison of the power reflection coefficients obtained from the DSO and the VNA measurement at 868 MHz (Monza R6)

data, and thus obtain the amplitudes $A_{0,k}, A_{1,k}$ and phase $\phi_{0,k}, \phi_{1,k}$ of the reflected wave of both back-scattered load modulation states.

The described procedure yields a discrete frequency domain representation of the reflected wave for each load modulation state:

$$Bit_i[k] = A_{i,k} \exp\left(j\omega_f k + \phi_{i,k}\right) \tag{4}$$

with $i = 0, 1$ representing the first and second bit of the binary communication. Additionally using the frequency domain representation of the incident signal Ref evaluated at the harmonic frequencies, the reflection coefficient S_{DSO} based on the time-domain measurement for each state can be obtained as

$$S_{DSO,i}[k] = \frac{Bit_i[k]}{Ref[k]}. \tag{5}$$

As no overtones are present in the signal output by the VSG, all reflection coefficients were calculated using the incident wave at the fundamental frequency as the amplitude and phase reference. The resulting voltage reflection coefficient at the ports of the DSO can then transformed to the desired reference planes. To obtain the reflection coefficient at the SMA port of the test fixture $S_{Test,DSO}$, Coupler 2 and its connecting cables have to be de-embedded using the following formula.

$$S_{Test,DSO,i} = S_{DSO,i} \cdot \frac{S_{32,coup} \cdot S_{41,coup}}{S_{21,coup}}, \tag{6}$$

where the S parameters with port numbers denote the S parameters of coupler 2. This method is performed for the scavenging state as well as the reflecting state to obtain both complex reflection coefficients at integer multiples of the fundamental frequency. Due to the used coupler 2, the proposed method allows a characterization up to the third harmonic, but can be easily expanded as most DSO's and VNA's offer a wider bandwidth. The reflection coefficient can further be transformed to the reference plane directly at the terminals of the RFID chip by using the 3-term error model obtained using the fabricated SOL-calibration standards and sketched in Fig. 5.

	Impinj Monza R6 [20]	NXP G2XM [21]
P_{th}-datasheet	-20 dBm	-15 dBm
P_{th}-DSO	-17.82 dBm	-13.89 dBm
P_{th}-VNA	-17.55 dBm	-13.05 dBm
Z-datasheet	(14.13-129.43)Ω	—
Z-DSO	(16.5-126.5) Ω	(27.1-147.2) Ω
Z-VNA	(18.8-130.3) Ω	(35.0-154.1) Ω

TABLE II
SENSITIVITY AND IMPEDANCE OF THE INVESTIGATED RFID CHIPS AT 868 MHz

IV. RESULTS

The following section shows measurement results for two different commercially available UHF RFID chips: (1) NXP G2XM [21] and (2) Impinj Monza R6 [20].
The voltage reflection coefficient was measured simultaneously with the VNA and deduced from the DSO measurement, as described in sections II and III. Fig. 7 shows a comparison of the reflection coefficients at the fundamental frequency as a function of the power at the RFID chip terminals. It can be seen, that the scavenging states, as expected, show a strong dependence on the input power. The measurements of both different measurement techniques show a good agreement for the scavenging state and a slight discrepancy in the reflective state. This behaviour is expected to be due to a slightly different matching condition present at the ports of the VNA compared to the ports of the DSO.

The chip sensitivity P_{th} is clearly visible and similar in both measurements. Using

$$P_{th} = P_{On} \cdot (1 - |S_{Chip}|^2), \tag{7}$$

the corresponding values for the sensitivity are $P_{th,VNA} = -17.55\,\mathrm{dBm}$ and $P_{th,DSO} = -17.82\,\mathrm{dBm}$, which are in good agreement. P_{On} denotes the turn-on power, which corresponds to the minimum power, where two different modulation states are visible. The difference between the datasheet value [20] and the values measured is expected to be due to a different query command sent to interrogate the tag and a 50 Ω source

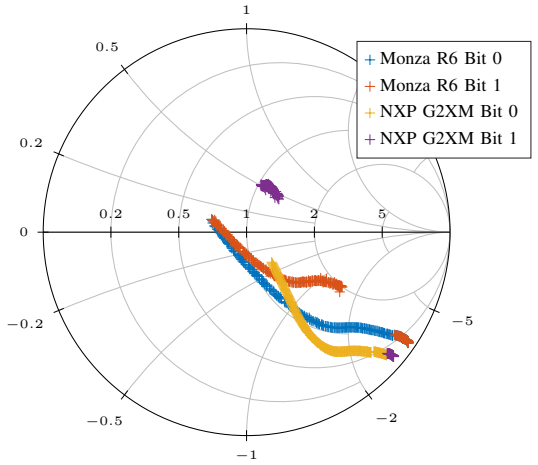

Fig. 8. Smith chart visualizing the reflection coefficients of the investigated chips as a function of input power at 868 MHz

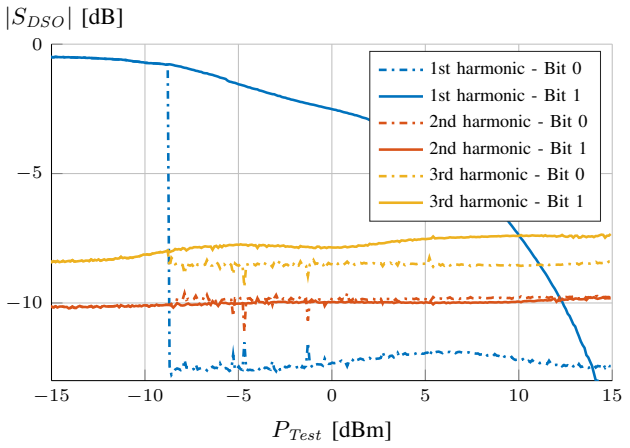

Fig. 9. Power reflection coefficients at the first three harmonic frequencies; $f_0 = 868\,\text{MHz}$ (Monza R6)

impedance directly at the RFID chip terminals as stated in [21]. According to [22], EPC C1G2 protocol parameters influence the sensitivity of the communicating RFID chip. The obtained sensitivities and impedances at the power threshold are listed in Table II. The shown similarity in the obtained reflection coefficient furthermore proves, that calculating the reflection coefficient from the DSO measurement provides sufficient accuracy and thus, can be used solely in future measurement setups.

In Fig. 8, the reflection coefficients of both investigated RFID chips are visualized in a Smith chart. Using this representation, a major difference between the two chips becomes visible. The second state of the NXP chip shows far less power dependence compared to the Impinj chip. This behaviour results in a better separation of the impedance states, but also influences the energy harvesting during the back-scatter communication.

The reflection coefficient equivalents were calculated from the DSO measurement at all evaluated harmonics and visualized in Fig. 9. It can be seen, that the message back-scattered towards the reader is also present in the overtones. At the overtones the power reflection coefficient, for both load modulation states show a relatively constant behavior as a function of power compared to the fundamental frequency.

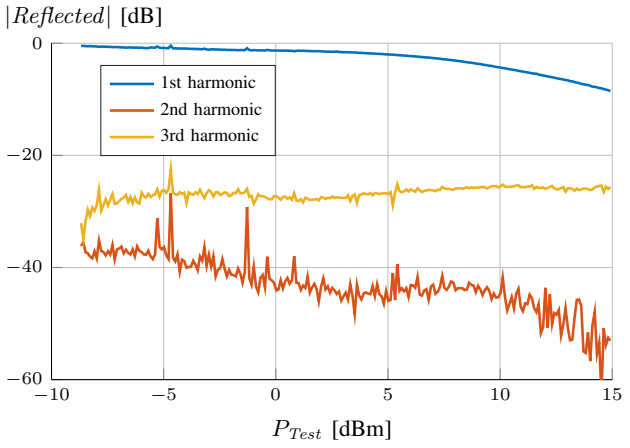

Fig. 10. Harmonic reflected power as a function of input power at $f_0 = 868\,\text{MHz}$ (Monza R6)

From the obtained reflection coefficients, the back-scattered signal strength can be calculated. This measure can also be obtained using a power spectral density (PSD) analysis, as proposed in [6] and thus, allows a comparison of the measurement methodologies. Fig. 10 shows the back-scattered signal strength calculated from the obtain reflection coefficients at the fundamental frequency, as well as at the evaluated harmonics. The signal strength of the third harmonic is predominant throughout the power sweep.

V. Conclusion

The presented measurement platform allows for a measurement of both the incident and reflected waveforms at the terminals of a UHF RFID chip using a DSO. With the proposed signal processing methodology, a time-domain reflection equivalent can be computed. Additionally, a standard reflection coefficient measurement using a VNA can be performed. This measure has been used to validate the DSO measurement and the consecutive signal processing steps. Using the proposed measurement setup, a full characterization of the nonlinear behavior of UHF RFID chips can be performed, allowing also the calculation of typical linear RFID chip parameters, such as the sensitivity and the impedance at the fundamental frequency. Based on the results proving the validity of the DSO measurement, the platform - without the VNA - represents a simplified, yet accurate tool for investigating novel technologies in the area of harmonic exploitation in UHF RFID.

Acknowledgment

This work has been part-funded by the Basque Government under the project IoTrain (RTI2018-095499-B-C33). The authors would also like to thank Rohde & Schwarz GmbH & Co KG as well as the SPINNER GmbH for providing us the measurement equipment used in the proposed measurement platform.

References

[1] K. Finkenzeller, *RFID-Handbuch: Grundlagen und praktische Anwendungen von Transpondern, kontaktlosen Chipkarten und NFC*. Carl Hanser Verlag GmbH Co KG, 2015.

[2] R. Hansen, "Relationships between antennas as scatterers and as radiators," *Proceedings of the IEEE*, vol. 77, no. 5, pp. 659–662, 1989.

[3] L. W. Mayer and A. L. Scholtz, "Sensitivity and impedance measurements on UHF RFID transponder chips," in *Proc. 2nd Int. EURASIP Workshop RFID Technol.*, 2008, pp. 1–10.

[4] P. V. Nikitin, K. S. Rao, R. Martinez, and S. F. Lam, "Sensitivity and impedance measurements of UHF RFID chips," *IEEE Transactions on Microwave Theory and Techniques*, vol. 57, no. 5, pp. 1297–1302, 2009.

[5] J. Grosinger, C. Mecklenbrauker, and A. L. Scholtz, "UHF RFID transponder chip and antenna impedance measurements," in *Proc. of the Third International EURASIP Workshop RFID Technology, La Manga del Mar Menor (Spain)*, 2010, pp. 43–46.

[6] G. A. Vera, Y. Duroc, and S. Tedjini, "RFID test platform: Nonlinear characterization," *IEEE Transactions on Instrumentation and Measurement*, vol. 63, no. 9, pp. 2299–2305, 2014.

[7] J. Essel, D. Brenk, J. Heidrich, R. Weigel, and D. Kissinger, "Large-signal measurements and nonlinear characterization of an analog frontend for passive UHF CMOS RFID transponders," *IEEE transactions on microwave theory and techniques*, vol. 61, no. 2, pp. 948–959, 2012.

[8] G. A. Vera, Y. Duroc, and S. Tedjini, "Analysis of harmonics in UHF RFID signals," *IEEE transactions on microwave theory and techniques*, vol. 61, no. 6, pp. 2481–2490, 2013.
[9] ——, "Analysis and exploitation of harmonics in wireless power transfer (H-WPT): passive UHF RFID case," *Wireless Power Transfer*, vol. 1, no. 2, pp. 65–74, 2014.
[10] ——, "Third harmonic exploitation in passive UHF RFID," *IEEE Transactions on Microwave Theory and Techniques*, vol. 63, no. 9, pp. 2991–3004, 2015.
[11] S. Tedjini, G. Andia-Vera, M. Zurita, R. C. Freire, and Y. Duroc, "Augmented RFID tags," in *2016 IEEE Topical Conference on Wireless Sensors and Sensor Networks (WiSNet)*. IEEE, 2016, pp. 67–70.
[12] G. A. Vera, D. Allane, Y. Duroc, and S. Tedjini, "Exploitation of harmonic signals generated by the UHF RFID chips: New promises for the radio frequency identification technology," in *2017 XXXIInd General Assembly and Scientific Symposium of the International Union of Radio Science (URSI GASS)*. IEEE, 2017, pp. 1–4.
[13] G. A. Vera, S. D. Nawale, Y. Duroc, and S. Tedjini, "Read range enhancement by harmonic energy harvesting in passive UHF RFID," *IEEE Microwave and Wireless Components Letters*, vol. 25, no. 9, pp. 627–629, 2015.
[14] D. Allane, G. A. Vera, Y. Duroc, R. Touhami, and S. Tedjini, "Harmonic power harvesting system for passive RFID sensor tags," *IEEE Transactions on microwave theory and techniques*, vol. 64, no. 7, pp. 2347–2356, 2016.
[15] X. Hui and E. C. Kan, "Harmonic UHF RFID Ranging with 50-Micron Accuracy and 1-kHz Sampling Rate," in *2019 IEEE International Conference on RFID (RFID)*. IEEE, 2019, pp. 1–8.
[16] Y. Ma, X. Hui, and E. C. Kan, "Harmonic-WISP: A passive broadband harmonic RFID platform," in *2016 IEEE MTT-S International Microwave Symposium (IMS)*. IEEE, 2016, pp. 1–4.
[17] A. Lazaro, R. Villarino, and D. Girbau, "A passive harmonic tag for humidity sensing," *International Journal of Antennas and Propagation*, vol. 2014, 2014.
[18] Tektronix, "Oscilloscope Fundamentals," https://engineering.case.edu/lab/circuitslab/sites/engineering.case.edu.lab.circuitslab/files/docs/Oscilloscope_Fundamentals_-_Tektronix.pdf, accessed: 2020-08-13.
[19] "Matlab envelope function description," https://de.mathworks.com/help/signal/ref/envelope.html, accessed: 2020-08-13.
[20] "Impinj Monza R6 datasheet," https://support.impinj.com/hc/en-us/articles/202765328-Monza-R6-Product-Brief-Datasheet, accessed: 2020-08-13.
[21] "NXP G2XM datasheet," https://www.nxp.com/docs/en/data-sheet/SL3ICS1002_1202.pdf, accessed: 2020-08-13.
[22] P. V. Nikitin and K. Rao, "Effect of Gen2 protocol parameters on RFID tag performance," in *2009 IEEE International Conference on RFID*. IEEE, 2009, pp. 117–122.

3.5 Selecting impedance states in a passive computational RFID tag backscattering in PSK

Journals & Magazines > IEEE Microwave and Wireless C... > Volume: 29 Issue: 10

Selecting Impedance States in a Passive Computational RFID Tag Backscattering in PSK

Publisher: IEEE

Florian Muralter ; Hugo Landaluce ; Ruben Del-Rio-Ruiz ; Asier Perallos **All Authors**

Published in: IEEE Microwave and Wireless Components Letters (Volume: 29 , Issue: 10, Oct. 2019)

Page(s): 680 - 682

Date of Publication: 28 August 2019

INSPEC Accession Number: 19115387

DOI: 10.1109/LMWC.2019.2935303

JIF(2019): 2.310

Rank: Q2 in Electrical Engineering
Q1 in Engineering

3.5.1 Preface

The work presented in this article was carried out by the thesis' author in the microwave laboratory of the DeustoTech Institute of Technology, under the supervision of Hugo Landaluce. Ruben Del-Rio-Ruiz supported the measurements performed, where Asier Perallos supervised the whole project. All authors were included in the article's preparation and revision process.

3.5.2 Article

Selecting impedance states in a passive computational RFID tag backscattering in PSK

Florian Muralter, Hugo Landaluce, Ruben Del-Rio-Ruiz, Asier Perallos

***Abstract*—A methodology to carefully select the impedance states of a backscatter PSK load modulator in a passive computational UHF RFID tag is presented. Considering the most significant tag read range limitations reader sensitivity, power transmission and Bit Error Rate, the proposed selection results in a constant power transmission to the energy harvester and thus in an increase of the average power at the input of the energy harvester during tag-to-reader communication. A graphical tool to select the modulator impedance states using a Smith chart is proposed.**

***Index Terms*—passive modulated backscatter, computational radio frequency identification (CRFID), tags, power reflection.**

I. Introduction

PASSIVE, computational ultra-high-frequency (UHF) radio frequency identification (RFID) tags are battery-free transponders with limited computational power, used to execute simple tasks. The power needed for operation is harvested from the incident RF field radiated by the RFID reader. This RF signal also represents the carrier of the downlink (reader to tag) and the uplink (tag to reader) communication. The uplink most commonly deploys backscatter load modulation, which is based on the antenna scattering theorem [1]. Thus, the impedance seen by the terminals of the tag's antenna is switched between two states to achieve either binary amplitude shift keying (ASK) or binary phase shift keying (PSK) load modulation. One of the most relevant tag characteristics - the tag read range - strongly depends on the power transmission to the implemented RFID chip, which is restricted by the impedance match between antenna and chip. Considering this, [2] suggests to rather use PSK modulation for the uplink communication, as it offers the possibility to achieve the same power transmitted to the chip for all implemented impedance states.

This work presents a tool to determine the additional modulator impedance states needed for backscattering a PSK modulated signal. Previous publications have considered this problem, but either chosen constellation states with a maximum backscatter amplitude (possible only in semipassive tags) [3], or used a mixed "PSK" modulation format, which decreases the inter-symbol-difference [4] and does not allow a constant input power at the harvester for a fixed tag to reader distance. The proposed method considers a given antenna design and a given energy harvester (main contribution to the chip impedance Z_C), adapting the modulator to their impedances. We present a graphical representation of the read range limitations and propose a method for the modulator impedance selection which increases the average power available for harvesting during the tag-to-reader communication.

F. Muralter, H. Landaluce, R. del Rio, A. Perallos are with the DeustoTech, University of Deusto, Bilbao, Bizkaia, 48007 Spain e-mail: florian.muralter@deusto.es

Manuscript received February 27, 2019; revised July 12, 2019.

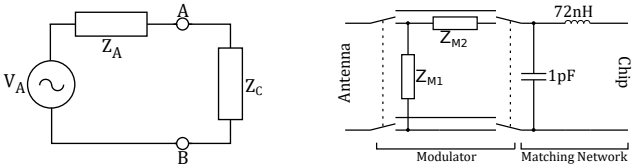

(a) Equivalent model of tag (b) Modulator and Matching

Fig. 1: Equivalent model of a sample RFID tag in the receiving mode with additional modulator and matching network.

II. Methodology

A. Power Reflection Coefficient Analysis

Considering the equivalent circuit for the tag in its receiving mode, shown in Fig. 1a, the power wave reflection coefficient according to [5] is defined as:

$$s = \frac{Z_C - Z_A^*}{Z_C + Z_A} \tag{1}$$

This measure plotted on a Smith chart, normalized to the resistance of the antenna R_A at a given frequency, corresponds to the vector drawn between the origin of the Smith chart and the mapped normalized impedance [6]

$$r + jy = \frac{R_C}{R_A} + j\frac{X_C + X_A}{R_A}. \tag{2}$$

The squared magnitude of the power wave reflection coefficient s yields the power reflection coefficient $|s|^2$. Thus, the contour of a circle with radius $|s|^2$ centered at the origin of the Smith chart, stands for a line of equal power reflection.

B. Tag Read Range

The tag read range is considered one of the most significant tag characteristics [2], [7]. This limitation of RFID tags, is mainly influenced by the following three RFID system properties:

- Power transmission: considering all power limiting factors between the reader and the tag's chip
- Reader sensitivity: a measure for the sensitivity of the reader to the incoming back-scattered tag signal
- Bit Error Rate (BER): describes the effect of symbol proximity due to channel alterations

1) Power Transmission: Given a minimum power P_{th}, needed for the chip to start operating and given the antenna characteristics, the maximum achievable read range r_{max} considering a free space environment can be calculated by

$$r_{max} = \frac{\lambda}{4\pi}\sqrt{\frac{P_t \cdot G_t \cdot G_r \cdot (1-|s|^2)}{P_{th}}}, \tag{3}$$

with P_t denoting the transmitted reader power, G_t the gain of the transmitting antenna and G_r the gain of the tag antenna [6]. All parameters in (3) can be considered slowly varying with frequency, except for the power reflection coefficient $|s|^2$, which presents the largest contribution to tag resonance [8]. Therefore, given a read range distance r_{max} to be achieved during tag optimization, one can use (4) to obtain the maximum power reflection coefficient for receiving the threshold power P_{th} at the chip.

$$|s|_u^2 = 1 - \left(\frac{4\pi r_{max}}{\lambda}\right)^2 \frac{P_{th}}{P_t \cdot G_t \cdot G_r} \tag{4}$$

A circle drawn on the Smith chart, with the calculated power reflection coefficient $|s|_u^2$ as the radius thus represents the maximum tag read range. For any mapped impedance point inside this circle enough energy can be harvested by the tag to start operating (see Fig. 2).

2) Reader Sensitivity: Another factor limiting the read range of a tag is the sensitivity of the RFID reader [6]. The power of the back-scattered signal received at the reader P_r can be described by,

$$P_r = \sigma P_t G_t^2 \left(\frac{\lambda}{4\pi r}\right)^2 \tag{5}$$

with σ representing the Radar Cross Section (RCS) of the tag

$$\sigma = \frac{(\lambda G_r R_A)^2}{\pi |Z_A + Z_C|^2}. \tag{6}$$

Substituting the power reflection coefficient into (6) into (5), the minimum power reflection coefficient $|s|^2$ to receive a backscatter signal amplitude higher than the reader sensitivity P_r can be computed as

$$|s|_l^2 = \frac{16\pi^3 r^2}{\lambda^4} \cdot \frac{P_r}{P_t \left(G_t G_r\right)^2} \cdot \frac{|Z_C - Z_A^*|^2}{R_A^2}. \tag{7}$$

The resulting power reflection coefficient is plotted in Fig. 2 as the inner radius and thus represents a lower bound. As stated by [6], $|s|^2$ will, at typical operating conditions, not be the read range limiting factor.

3) Inter-Symbol Difference: Considering impedance states which are in agreement with the two above conditions, the BER represents an additional measure that has an impact on the read range. According to [4] a minimization of the BER corresponds to a maximization of the distance between two power wave reflection coefficients, which for a pure PSK modulation represents a maximization of the distance between their angles ϕ_i.

$$\max\{\text{BER}\} \overset{Mod=PSK}{\hat{=}} \max\{|\phi_1 - \phi_2|\} \tag{8}$$

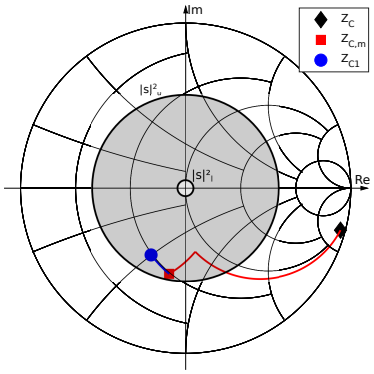

Fig. 2: Lower and upper power reflection limits mapped onto the Smith chart normalized to $R_A = 62\Omega$.

4) Visualization: Given the maximum power reflection to keep the tag operating $|s|_u^2$ and the minimum power reflection to keep the back-scatter signal amplitude above the reader sensitivity $|s|_l^2$, the Smith chart can be normalized, such that the unit circle represents this maximum value. Thus, all impedance states within the resulting Smith chart in Fig. 3 will create enough power up to the predefined tag-reader distance r_{max}.

III. Selection of Impedance States

In binary PSK the carrier wave is switched between two phase states, which are commonly chosen to be separated by π. Considering (8), this reflects to the maximum phase difference for two possible symbols. To achieve a power reflection coefficient $|s|^2$ that allows the tag to operate, an impedance transformer (matching network) is used. For the presented case study, a L-network with a series inductance of $L_m = 72$nH and a shunt capacitance of $C_m = 1$pF was used (see Fig. 1b). The matched chip impedance Z_{C_m}, which lies within the ring spanned by the bounding conditions $|s|_u^2$ and $|s|_l^2$ (see Fig. 2) can then be modulated. For a chosen passive, commercial, computational RFID tag [9] with the characteristics shown in Table I, $Z_{C1} = (30.39 - j43.48)\Omega$, the corresponding power reflection coefficient calculated using (4) is $|s|^2 = 0.23$.

Using the Smith chart to determine the second state of the load modulator, the matched chip impedance Z_{C1} can be mirrored on the origin of the Smith chart, resulting in an impedance state Z_{C2}, phase shifted by π with the same power reflection coefficient and thus the same power delivered to the chip at both states of the tag-to-reader communication. Mathematically this can be easily achieved by adding π to the argument of the complex impedance. For M-PSK modulation,

TABLE I: Tag Characteristics at $fc = 915$MHz [9]

G_r	P_{th}	Z_A	r_{max}	Z_C
1.64	-14dBm	$(62 + j13)\Omega$	5m	$(51 + j460)\Omega$

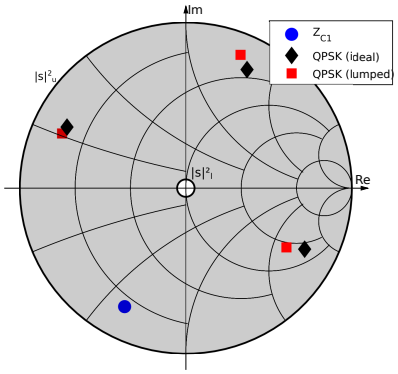

Fig. 3: Smith chart normalized to $|s|_u^2 = 0.5633$ showing the calculated constellation, and the one using lumped elements.

only the phase angle to determine the additional states has to be adapted:

$$arg(Z_{Ck}) = arg\,(Z_{C1}) + \frac{2\pi(k-1)}{M} \tag{9}$$

with $k = 1...M$ to yield a e.g. 4-PSK (M=4), 8-QPSK (M=8) constellation.

To determine the values of the lumped elements to be used, a graphical approach using the Smith chart, or a mathematical solution similar to an impedance matching process are possible. The calculated lumped elements (Table II) are placed as a L-network (Fig. 1b), where the circuit in Fig. 1b is inserted at the ports A, B of Fig. 1a. The corresponding Smith chart, illustrating the solutions for binary PSK and 4-PSK, is shown in Fig. 3.

Taken into account, that for all implemented modulator impedance states, the power reflection coefficient will be equal, the power transmitted to the input of the energy harvester will be equal during all states of operation (see Fig. 4). Thus, a "0"-bit and a "1"-bit corresponding to the modulator impedance states Z_{C1} and Z_{C2} respectively, will result in the same $|s|^2$. Considering a duty cycle of 60 to 75% as for a communication according to [10], an increase of the average harvestable power during uplink communication is achieved. Hence, the back-scatter signal amplitude, as expected for PSK modulation, is constant during the tag-to-reader communication.

The proposed method considers the chip impedance at P_{th} and thus, does not take into account non-linearities of the chip impedance with respect to the input power. Future work should investigate the influence of a varying chip impedance on the read range and on the resulting constellation.

TABLE II: Calculated normalized impedance states and their corresponding lumped elements Z_{M1}, Z_{M2} using a L-network

Modulation	Bit	I/Q	Z_{M1}	Z_{M2}
BPSK/QPSK	0	-0.0988 - 0.5171i	-	-
BPSK	1	0.0988 + 0.5171i	6.8nH	0.5pF
QPSK	01	-0.5171 + 0.0988i	3pF	18nH
QPSK	10	0.0988 + 0.5171i	6.8nH	0.5pF
QPSK	11	0.5171 - 0.0988i	1pF	15.8nH

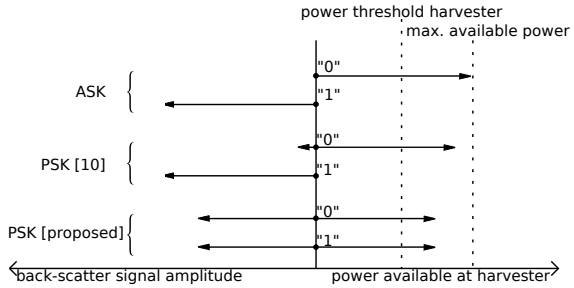

Fig. 4: Comparison of existing and proposed load modulation performance

IV. Conclusion

The careful selection of load impedances in passive computational RFID tags is a critical task, as it strongly affects the performance of the tag. PSK modulation in the uplink communication offers a possibility to achieve a power transmission to the energy harvester, which is not influenced by the state of the transmission. The offered solution generates a higher average power presented to the chip. In the special case of additionally supplying a sensor this can yield a significant increase of the tag read range. We showed that for a given antenna design and energy harvester, the modulating impedances were chosen guaranteeing operation at the requested distance.

Acknowledgment

This work has been part-funded under the projects TEKINTZE (KK-2018/00104) and RTI2018-095499-B-C33.

References

[1] R. Hansen, "Relationship between antennas as scatters and as radiators," *Proceedings of the IEEE*, vol. 77, pp. 659 – 662, 06 1989.

[2] G. De Vita and G. Iannaccone, "Design criteria for the RF section of UHF and microwave passive RFID transponders," *IEEE Transactions on Microwave Theory and Techniques*, vol. 53, no. 9, pp. 2978–2990, 2005.

[3] S. J. Thomas, E. Wheeler, J. Teizer, and M. S. Reynolds, "Quadrature amplitude modulated backscatter in passive and semipassive uhf rfid systems," *IEEE Transactions on Microwave Theory and Techniques*, vol. 60, no. 4, pp. 1175–1182, 2012.

[4] A. Bletsas, A. G. Dimitriou, and J. N. Sahalos, "Improving backscatter radio tag efficiency," *IEEE Transactions on Microwave Theory and Techniques*, vol. 58, no. 6, pp. 1502–1509, 2010.

[5] K. Kurokawa, "Power waves and the scattering matrix," *IEEE Transactions on Microwave Theory and Techniques*, vol. 13, no. 2, pp. 194–202, 1965.

[6] P. V. Nikitin, K. S. Rao, S. F. Lam, V. Pillai, R. Martinez, and H. Heinrich, "Power reflection coefficient analysis for complex impedances in RFID tag design," *IEEE Transactions on Microwave Theory and Techniques*, vol. 53, no. 9, pp. 2721–2725, 2005.

[7] P. V. Nikitin and K. V. S. Rao, "Performance limitations of passive UHF RFID systems," *2006 IEEE Antennas and Propagation Society International Symposium*, pp. 1011–1014, 2006.

[8] K. S. Rao, P. V. Nikitin, and S. F. Lam, "Impedance matching concepts in RFID transponder design," in *Automatic Identification Advanced Technologies, 2005. Fourth IEEE Workshop on*. IEEE, 2005, pp. 39–42.

[9] Farsens, "EVAL01 Spider R," 2019. [Online]. Available: http://www.farsens.com/en/products/eval01-spider-r/

[10] *Class 1 Generation 2 UHF Air Interface Protocol Standard Version 1.09*, EPCglobal Inc. Std. [Online]. Available: http://www.epcglobalinc.org/standards_technology/specifications.html

3.6 A Fully Customizable RFID Research Platform with Exchangeable Modules

Journals & Magazines > IEEE Sensors Journal > Early Access

A Fully Customizable RFID Research Platform with Exchangeable Modules

Publisher: IEEE

Florian Muralter ; Laura Arjona ; Hugo Landaluce ; Asier Perallos **All Authors**

Published in: IEEE Sensors Journal (Early Access)

Page(s): 1 - 1

DOI: 10.1109/JSEN.2021.3073421

Date of Publication: 15 April 2021

Publisher: IEEE

JIF(2019): 3.073

Rank: Q2 in Electrical Engineering
Q1 in Engineering

3.6.1 Preface

The design and implementation process of the passive, modular, computational UHF RFID research platform presented in the corresponding article was performed by the author of this thesis in the laboratory of the DeustoTech Institute of Technology and at the Associate Professorship for Microwave Engineering of the Technical University Munich. The measurement's were carried out Laura Arjona, Florian Muralter and Hugo Landaluce. Asier Perallos supervised the whole process. All authors were included in the article's preparation and revision procedure.

3.6.2 Article

A Fully Customizable RFID Research Platform with Exchangeable Modules

Florian Muralter*, Laura Arjona, Hugo Landaluce, Asier Perallos

***Abstract*—This manuscript presents the design and implementation of a passive, modular, computational ultra high frequency (UHF) radio frequency identification (RFID) research platform. The proposed platform consists of a software defined radio (SDR) reader and a modular UHF RFID tag. Such a tag can be subdivided into a number of modules (e.g., Modulator, Rectifier, etc.), which have been separated and optimized for easy connectability using sub-miniature A (SMA) connectors and standard jumper wires. Experimental results of module specific parameters show the accessibility of each section and prove the platform's value for designing novel UHF RFID solutions.**

***Index Terms*—power reflection, nonlinear analysis, radio frequency identification (RFID)**

I. Introduction

Ultra high frequency (UHF) radio frequency identification (RFID) represents an automated identification technology mainly used in logistics and asset tracking. The direct adaptability of RFID to the demands of supply chains, goods tracking and monitoring, traceability of patients, or the management of medication for elderly people are a number of applications that have, in recent years, increased the popularity of this technology. [1]

A standard UHF RFID system, as shown in Fig. 1, consists of at least one interrogator (reader) and a minimum of one transponder (tag). Such platforms communicate in the industrial, scientific and medical (ISM) band around 900 MHz using the EPC Class 1 Generation 2 (EPC-C1G2) communication standard. Depending on the region of operation, the frequency bands and regulations differ (e.g., EU...865-868 MHz; NA...902-928 MHz) [2]. UHF RFID tags can be grouped depending on the technology incorporated:

- RFID identification only: The simplest version of an RFID tag is solely used to uniquely identify objects equipped with an RFID tag.
- RFID sensing: These RFID tags incorporate sensors to measure e.g., the temperature, humidity, etc., storing the acquired values in the internal memory of the RFID chip, to be consecutively read by the reader using an EPC-C1G2 read command.
- Computational RFID: Computational RFID tags use low power microcontrollers to perform simple computational tasks. In some research platforms, the EPC-C1G2 logic is also implemented in the microcontroller (e.g., [3], [4]).

Manuscript received __, __.
This work has been part-funded by the Basque Government under the project IoTrain (RTI2018-095499-B-C33).

F. Muralter (e-mail: florian.muralter@deusto.es), L. Arjona, H. Landaluce and A. Perallos are with DeustoTech - University of Deusto.

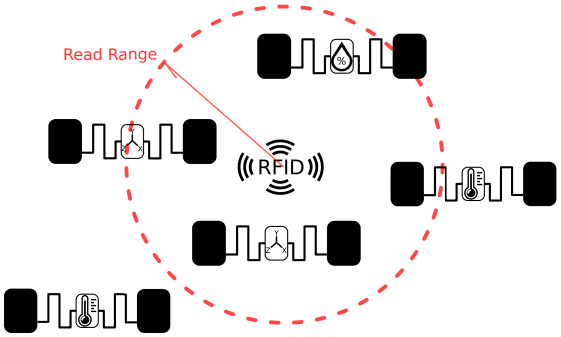

Fig. 1. Illustration of an RFID based Wireless Sensor Network (WSN).

Tags can also be grouped considering their power source [5]:

- *passive* RFID tags typically consist of an antenna and the RFID chip. The tag-to-reader communication is achieved by backscattering a certain part of the incident electromagnetic wave using load modulation at the antenna terminals. The energy needed for the RFID chip to operate is harvested from the incident electromagnetic wave. (e.g., NXP Ucode 8 [6], Impinj M700 Series [7])
- *semi-passive* RFID tags also use backscattering to communicate with the interrogator but are provided with an external (e.g., battery) power source as the power supply. Most of these chips can be used passively, but an external power source can be connected to extend their read range. (e.g., Impinj Monza-8k [8], Farsens Rocky100 [9])
- *active* RFID tags use a power supply to provide sufficient energy to the RFID chip and incorporate an active transmitter to respond to the messages received from the reader. (e.g., Nordic Semiconductor nRF52832 [10])

A typical passive UHF RFID tag consists of several modules performing certain tasks. Fig. 3 (Tag) shows a block chart visualizing the signal flow in such a tag with an additional external sensor. Each of the mentioned modules presents a distinct area of research, indispensable for the improvement and progress in UHF RFID. Given the growing importance of RFID sensing and computational RFID, the requirement of being able to investigate and design each section separately, to meet the specific needs of the desired application, both on the reader as well as on the tag side, becomes more evident. This article presents the design and implementation of a passive, modular, computational UHF RFID research platform with sensing capabilities. The proposed platform consists of a software defined radio (SDR) modular UHF RFID reader and

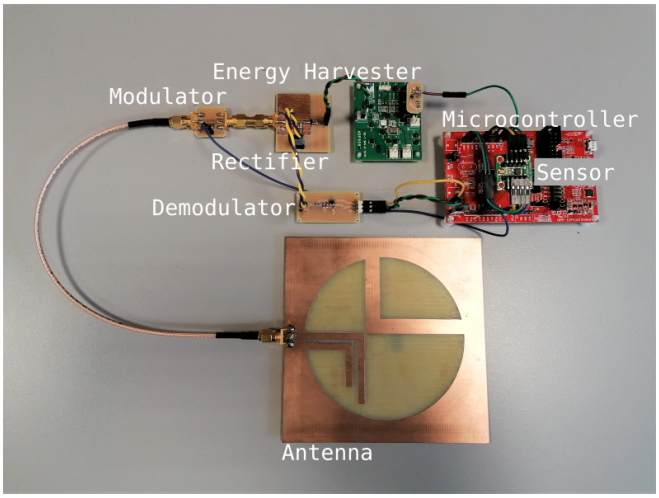

Fig. 2. Modular, passive, computational UHF RFID research platform.

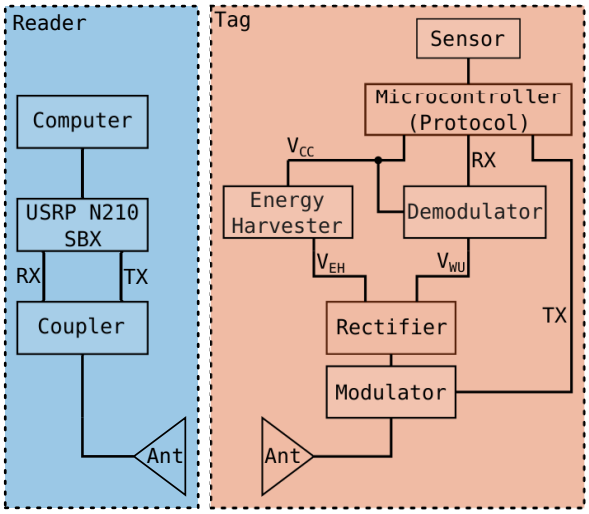

Fig. 3. Architecture of the presented modular UHF RFID research platform.

the corresponding modular, passive, computational UHF RFID tag. The easy interconnection of the different tag modules using jumper wires and subminiature A (SMA) connectors provides the opportunity of investigating and evaluating the performance of each section separately. The execution of the EPC-C1G2 logic by the deployed microcontroller unit (MCU), in addition to the SDR reader, offers the additional possibility to investigate and implement novel approaches considering the RFID communication protocol. Thanks to this architecture, the researcher does only have to consider designing the module of the investigations and can use all other modules unaltered. The presented experimental results provide insight on the accessibility of the described modules and performance details of the presented platform. Finally, a comparison of specially designed modules is shown to prove the value of the platform for developing novel UHF RFID solutions.

II. Related Work

The following section investigates, reviews, and discusses the state-of-the-art of both SDR reader implementations and passive, computational UHF RFID tags.

A. UHF SDR RFID reader

Commercially available readers present optimized interrogator designs operating according to the implemented standard. Nevertheless, they lack flexibility when considering them for research [11]. The possibility to change certain parameters of the EPC-C1G2 or to adapt the protocol yields an important task when designing novel RFID solutions. Thus, SDR UHF RFID readers represent a flexible alternative.

UHF SDR readers have evolved during the last decade. The first steps towards interrogators incorporating the full protocol, were RFID listeners. Both De Donno in [12] and Buettner in [11] presented RFID monitors based on an Ettus Research Universal Software Radio Peripheral (USRP). These devices use a standard commercial reader for communicating with the RFID tags, whereas the SDR platform is used to capture and decode the transmit and receive signals of both the interrogator and the transponder. Based on the RFID listener presented in [13] a full SDR implementation of a EPC-C1G2 reader was proposed in [11], [14]. This platform uses a USRP 1 connected to a host computer to send and receive the interrogator specific commands. The RF frontend of the RFX900 daughterboard is used with a separate RX and TX antenna. The implementation of the protocol is done using the open-source GNU radio software architecture. In [15] a fully-coherent EPC-C1G2 SDR reader based on [11] was presented. This open-source available implementation is designed to work with commercial UHF RFID tags responding with FM0 encoding and a backscatter link frequency (BLF) of 40 kHz, corresponding to a tag data rate of 40 kBits/s. This design uses a single transceiver board on a USRP 2 connected to separate RX and TX antennas, thus not allowing to investigate a typical scenario of one RX/TX antenna, as commonly used in commercial UHF RFID readers.

B. Passive computational UHF RFID tag

Passive computational and passive sensor UHF RFID tags represent a recent addition to the field of UHF RFID. While a number of commercially available UHF RFID tags with sensors or additional interfaces for sensors (e.g., AMS SL900A [16], Farsens Rocky100 [9], Impinj Monza 8K-Dura [8]) have been released, the number of research platforms allowing more flexibility considering the communication protocol is still limited. However, approaches using integrated circuit (IC) UHF RFID chips to perform the communication task according to the EPC-C1G2 standard, but being altered to host computing and sensing capabilities, have been presented. RAMSES, the RFID Augmented Module for Smart Environmental Sensing [17] and SPARTACUS, the Self-Powered Augmented RFID Tag for Autonomous Computing and Ubiquitous Sensing [18], [19] represent such platforms, benefiting from the low power thresholds achieved by commercially available UHF RFID chips, but adding the size constraint of a second antenna needed for energy harvesting. Furthermore, considering all mentioned platforms and chips, none of them yields the possibility to adapt the protocol layer. The Wireless Identification

TABLE I
COMPARISON OF STATE-OF-THE-ART PASSIVE COMPUTATIONAL/SENSOR UHF RFID PLATFORMS

Platform/Publication	Sensitivity	Read Range	Number of Antennas	EPC in MCU	Detachable	Commercial
WISP [3]	$-9.5\,\mathrm{dBm}$	$4.3\,\mathrm{m}$	1	Yes	No	No
AMS SL900A [16]	$-15\,\mathrm{dBm}$	$11.9\,\mathrm{m}^*$	1	No	No	Yes
Farsens Rocky100 [9]	$-14\,\mathrm{dBm}$	$16.2\,\mathrm{m}^*$	1	No	No	Yes
Impinj Monza X-8k Dura [8]	$-19.1\,\mathrm{dBm}$	$19.1\,\mathrm{m}^*$	1	No	No	Yes
RAMSES [17]	$-17\,\mathrm{dBm}$	$22\,\mathrm{m}$	2	No	No	No
SPARTACUS [18], [19]	$-9.5\,\mathrm{dBm}$	$3\,\mathrm{m}$	2	No	No	No
Fabbri et al. [4]	$-16\,\mathrm{dBm}$	$7\,\mathrm{m}$	1	Yes	No	No
This work	$-8\,\mathrm{dBm}$	$5.3\,\mathrm{m}^+$	1	Yes	Yes	No

and Sensing Platform (WISP) presented in [3] was the first released passive, programmable, open-source UHF RFID research platform incorporating sensing capabilities, incorporating the EPC-C1G2 communication protocol in the MCU. This architecture has, during the last decade, been improved and expanded by its developers as well as by other researchers. The latest version is the WISP 5.1, whose hardware and firmware details are available in [20]. A platform with extended read range and a monopole antenna, but based on the architecture and implementation of the WISP has been published in [4]. Furthermore, the WISP has recently been adapted to offer an undergraduate learning tool, equipped with a light sensor [21]. Table I shows a comparison of the available architectures considering important platform specific parameters and details. The read ranges marked with an asterisk have been calculated using

$$r = \frac{\lambda}{4\pi}\sqrt{\frac{EIRP \cdot G_{\mathrm{T}}}{P_{\mathrm{TH}}}}, \tag{1}$$

where λ denotes the wavelength, $EIRP$ the maximum allowed Effective Isotropic Radiated Power, G_{T} the antenna gain of the tag and P_{TH} the threshold power. The parameters used are $f_c = 915\,\mathrm{MHz}$, $EIRP = 4\,\mathrm{W}$ and $G_{\mathrm{T}} = 2\,\mathrm{dBi}$. The read range stated for the proposed platform, marked with a superscript plus, have been extrapolated considering the before mentioned parameters, to provide better comparability as the SDR reader only provides a maximum power output $P_{\mathrm{OUT}} = 20\,\mathrm{dBm}$.

Considering these investigated SDR based UHF RFID reader architectures and the reviewed passive, computational UHF RFID tags, no platform consisting of a compatible reader and tag architecture with higher tag data rates of $BLF \geq 160\,\mathrm{kHz}$ as used in passive computational tags has yet been presented. This allows for a full customization of the communication protocol, including a complete interchange of the multi-access strategy, not being limited to the EPC C1G2. Furthermore, none of the current architectures yields the possibility to detach the modules, allowing for the investigation of a single section without having to adapt the complete platform. The changes can be summarized as:

III. MODULAR UHF RFID PLATFORM

This section presents a detailed explanation of the proposed modular UHF RFID research platform, regarding both the SDR UHF reader and the passive, modular, computational UHF RFID tag.

TABLE II
EPC-C1G2 PARAMETERS AND LUMPED COMPONENT VALUES USED IN THE PROPOSED PLATFORM.

Parameter	Value	Component	Value
Delimiter	12.5 us	CM	6.8 pF
TARI	12.5 us	LM	8.2 nH
Divide Ratio	8	$CD1$	3.3 pF
Tag Encoding	FM0	$CD2$	4.7 pF
BLF	160 kHz	$CB1 = CB2$	10 pF
Pilot Tone	No	C_EH	10 pF
		C_WU	33 pF
		R_WU1=R_WU2	1 MΩ
		C_WU1	0.1 uF
		R_{SYS1}	1 MΩ
		R_{SYS2}	9 MΩ
		R_{PGOOD1}	3.9 MΩ
		R_{PGOOD2}	6.1 MΩ

A. UHF SDR RFID reader

The reader design presented in this work uses an Ettus Research USRP N210 with an SBX daughterboard. The communication to the USRP is established from a computer with Ubuntu 18.04 as the operating system via a gigabit network cable. GNURadio 3.7.11 is used, where out-of-tree modules are programmed in C++ and the interconnection of the modules is achieved using a Python script. The firmware implementation is based on the open-source platform presented in [15], but has been altered to provide further flexibility in the communication with computational RFID tags.

- To provide the possibility of using a single TX and RX antenna as typically used in commercial RFID readers and to also be able to connect a tag directly to the interrogator via an SMA connector, a Mini-Circuits ZFDC-15-10-S+ coupler was added as shown in Fig. 3 (Reader).
- The design originally implemented for identification only, was expanded to incorporate the full *Read* cycle according to the EPC C1G2 communication protocol in order to obtain the measurements from CRFID sensors. Thus, the reader-tag communication sequence of *ReqRN-Handle-Read-Data* has been implemented.
- To enable a communication with the proposed modular tag, the reader implementation was adapted to work with a BLF of 160 kHz.

An Alien Technology ALR-A0501 6 dBi circular polarized antenna [22] was used as the reader antenna.

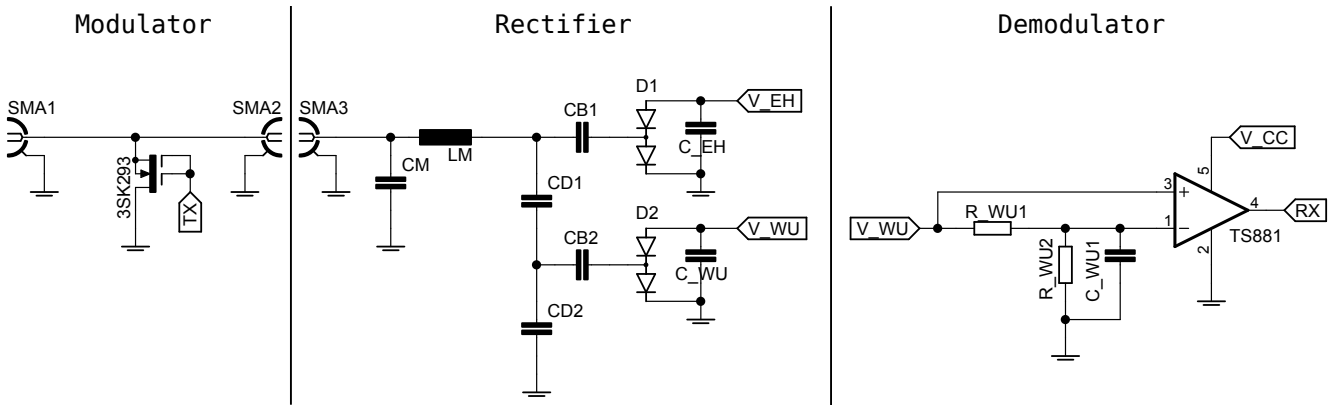

Fig. 4. Schematic of the modules fabricated on custom PCBs (Modulator, Rectifier, Demodulator).

B. Modular passive computational UHF RFID tag

The modular transponder presented in this work (see Fig. 2) is built using the architecture shown in Fig. 3 (Tag). The proposed module and platform designs have been investigated, separated and adapted to yield an easily adaptable platform allowing the accessibility of each module. The antenna design used in Fig. 2 is based on [23]. For the energy harvester (EH), the MCU and the sensor, commercially available evaluation boards were used. The Analog Devices ADP5090 was chosen as the EH because of its low start-up power of 16 μW. To make it compatible with the available firmware for the WISP 5.1 [20], the MSP430FR5969 microcontroller was chosen. Nevertheless, the firmware had to be adapted to allow operation with the evaluation board, as most of the pin configurations used on the WISP are not wired on the evaluation board. The low power accelerometer evaluation board EVAL-ADXL362Z [24] was chosen as a sensor and directly connected to the headers of the evaluation board of the MCU. The modulator, rectifier and demodulator designs were built on custom fabricated printed circuit boards (PCBs) as follows:

1) Modulator: The load modulator used for this platform consists of a microstrip line designed with an impedance of 50 Ω and a dual gate N-channel MOSFET (Toshiba 3SK293) connected with its drain terminal to the middle of the microstrip line and the source terminal to ground (see Fig. 4). The first and second gate are used as the input and, thus, connected to the TX pin of the MCU.

2) Rectifier: The rectifier PCB produced as part of the proposed modular tag is based on the design presented in [4]. This section incorporates an L-type matching network consisting of an RF inductor $LM = 8\,\text{nH}$ and a $CM = 6.8\,\text{pF}$ capacitor. The matching network is considered part of the rectifier, as the rectifier stages represent the main contribution to the impedance of the RFID tag. The following capacitive power divider ($CD1 = 3.3\,\text{pF}$, $CD2 = 4.7\,\text{pF}$) separates the part of the input signal used for the energy harvesting and the part used for the wake-up radio. $CB1 = CB2 = 10\,\text{pF}$ capacitors are further used to block any DC current before entering the rectification stages based on Skyworks SMS7630 series pairs Schottky diodes, which are specially designed for low power, high frequency application.

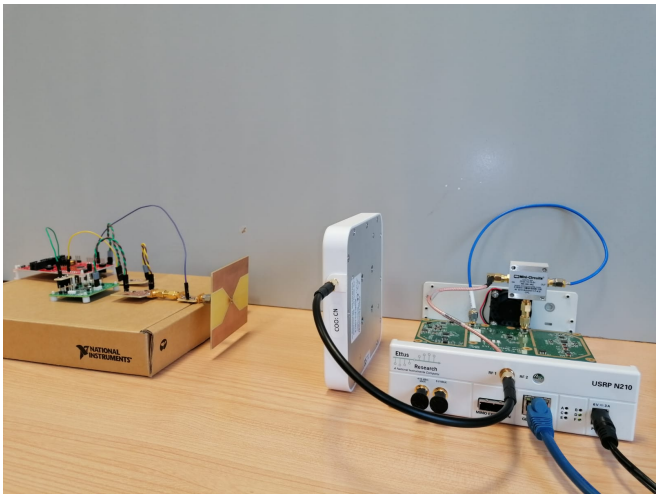

Fig. 5. Setup used for the measurement of the tag read range.

3) Demodulator: The actual decoding and demodulation of the signal is performed by the MCU. The analog circuitry shown in Fig. 4-Demodulator is designed to obtain a logic digital signal at the RX pin of the microcontroller. The rectified voltage signal V_{WU} at the input of the demodulator section already represents a baseband signal, having subtracted the carrier wave during the rectification step. An STMicroelectronics TS881 is then provided with V_{WU} at the positive input and a low pass filtered and halfened (resistive divider) signal at the negative input. The output signal of the demodulator module then represents a logic signal with V_{CC} as the logic high voltage.

IV. Performance Evaluation

The following section presents experimental results obtained using the proposed modular platform. Different approaches have been implemented for some of the modules to show the ability to modify each section separately without altering the remaining modules and to prove the value of the platform for designing novel UHF RFID solutions. The measurement

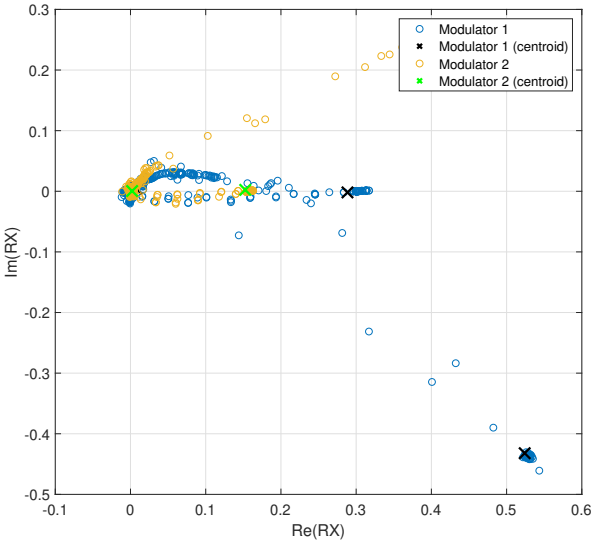

Fig. 6. Constellation of the 2 different investigated modulator designs.

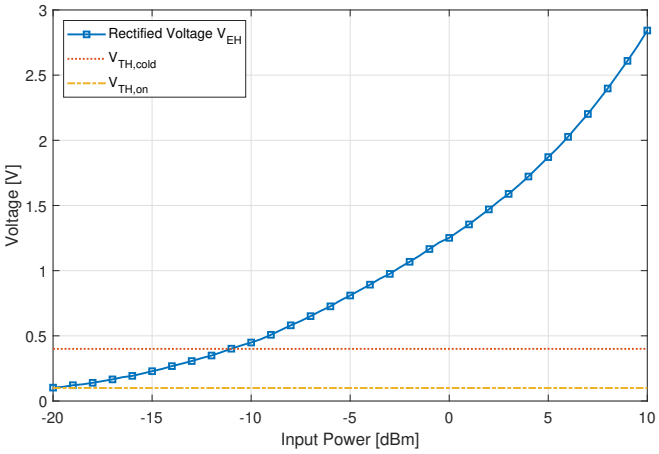

Fig. 7. Output voltage of the rectifier section as a function of input power at the SMA port.

setup used for the performance evaluation is shown in Fig. 5. The platform agrees with the architecture presented in Fig. 3 and the tag antenna was fabricated according to the design proposed in [25].

A. Modulator

Two different modulators have been designed and measured. The common approach of using a MOSFET to short the RF signal to ground, as used in the WISP was investigated using two different dual-gate N-channel MOSFETs. Modulator 1 was built using a Toshiba 3SK293 MOSFET, where Modulator 2 uses an NXP BF1105R MOSFET. Both setups were used with the TX signal connected to both gates, as this approach yielded the largest change of the reflection coefficient. Fig. 6 shows the received constellations of the designed modulators visualized using the RX signal digitalized on the USRP. The received signal's DC component has been subtracted, the channel of Bit 1 estimated and its conjugate multiplied to the signal representation to achieve the mapping of Bit 1 onto the real axis. Thus, the two states present on the real axis correspond to the two tag states (absorbing state; reflecting state), whereas the third visible cluster represents the modulated state of the reflected reader signal. The mentioned clusters were then estimated using a k-means algorithm in MATLAB 2018b to facilitate the localization of the centroids. It can be seen that the constellations not only yield a different angle, but also result in a different amplitude, which also influences the sensitivity of the tag, as this measure represents the modulation depth.

B. Rectifier

Fig. 7 shows the open circuit output voltage of the rectifier V_{EH} as a function of the input power at the SMA connector. A continuous wave signal was applied using an RF signal generator. The voltage thresholds of the energy harvester have been added to the figure to visualize the power needed for first activation and for operation after the cold start-up of the EH. The minimum needed voltages according to the EH datasheet [26] are typically $V_{\mathrm{TH,cold}} = 380\,\mathrm{mV}$ for the cold start-up case and $V_{\mathrm{TH,on}} = 100\,\mathrm{mV}$ after having passed first activation. These values would represent tag power sensitivities of $P_{\mathrm{TH,cold}} = -11\,\mathrm{dBm}$ for first activation and $P_{\mathrm{TH,on}} = -20\,\mathrm{dBm}$ after cold start-up corresponding to read ranges of 7.43 m and 20.87 m, respectively. These theoretical read ranges r were calculated using (1). For the calculation, $G_{\mathrm{T}} = 2\,\mathrm{dBi}$ as typical for a dipole antenna and $EIRP = 4\,\mathrm{W}$ as the maximum allowed in the FCC region $f_{\mathrm{c}} = 915\,\mathrm{MHz}$, was considered. Given the charge-pump architecture of the following EH section, these theoretical values would correspond to an infinitely long continuous wave allowance before starting communication.

C. Energy Harvester

The ADP5090 evaluation board is equipped with various test points. Given the minimum operating voltage $V_{\mathrm{minop,MCU}} = 1.8\,\mathrm{V}$, the system operation voltage $V_{\mathrm{SYS,op}}$ and the $V_{\mathrm{PGOOD,th}}$ threshold of the EH section can be set using resistive dividers. The corresponding resistor ratios R_{SYS} and R_{PGOOD} have been deducted from the formulas stated in the corresponding datasheet [26]

$$R_{\mathrm{SYS}} = \frac{2}{3}\frac{V_{\mathrm{SYS,op}}}{V_{\mathrm{REF}}} - 1, \tag{2}$$

$$R_{\mathrm{PGOOD}} = \frac{V_{\mathrm{PGOOD,th}}}{V_{\mathrm{REF}}} - 1, \tag{3}$$

where $V_{\mathrm{SYS,op}}$ and $V_{\mathrm{PGOOD,th}}$ denote the desired voltage levels and the voltage reference is typically $V_{\mathrm{REF}} = 1.21\,\mathrm{V}$. The chosen values for the corresponding resistors, given the suggestion of a $10\,\mathrm{M\Omega}$ resistive divider are stated in Table II. Considering these selected resistors the calculated corresponding voltage levels are $V_{\mathrm{SYS}} = 2.02\,\mathrm{V}$ and $V_{\mathrm{SYS}} = 1.85\,\mathrm{V}$. The resulting voltages at the EH V_{IN}, V_{SYS} and V_{CC} were measured using a digital oscilloscope. Fig. 8 shows the measured voltages as a function of time, during reader interrogation. Considering V_{IN}, the start of the reader interrogation is visible

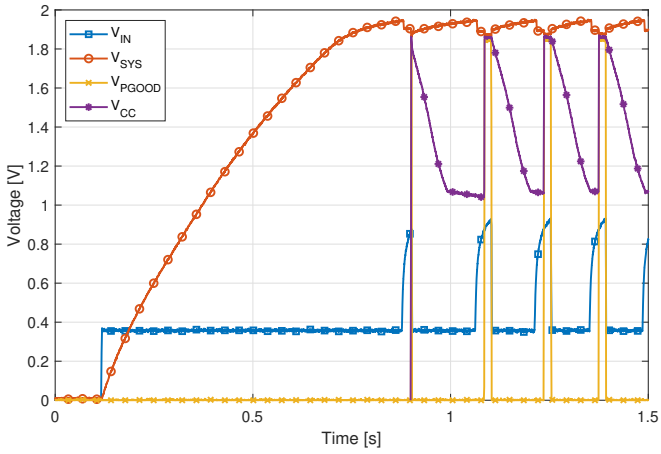

Fig. 8. Voltage signals at the EH module.

as the first step from 0 V to slightly above 0.4 V. The time following this step is then needed for the harvester to boost the voltage to a level above the programmed threshold of the P_{GOOD} pin. This period can be identified by the increasing V_{SYS}. Once V_{SYS} surpasses $V_{\mathrm{PGOOD,th}}$ the voltage V_{PGOOD} is used to switch on the system load. Like this, the port of the EH connected to the load is kept in a high impedance state until enough power is available. Each V_{CC} high state thus represents the time where the tag is able to respond.

D. Protocol

As both the reader and the tag are re-programmable, this platform also allows to adapt the protocol layer. The approach presented in [27] was used to provide a comparison of two different communication strategies to receive data from the tag using a *Read* command. This alteration of the EPC-C1G2 protocol uses one single identification phase (*Query-RN16-ACK-EPC*) for a defined number of consecutive Read commands. The EPC-C1G2 *Handle* received at the reader is stored and used for sending these consecutive *Read* commands, thus, achieving a higher read data rate. Fig. 9 shows the communication using the two different strategies, with the

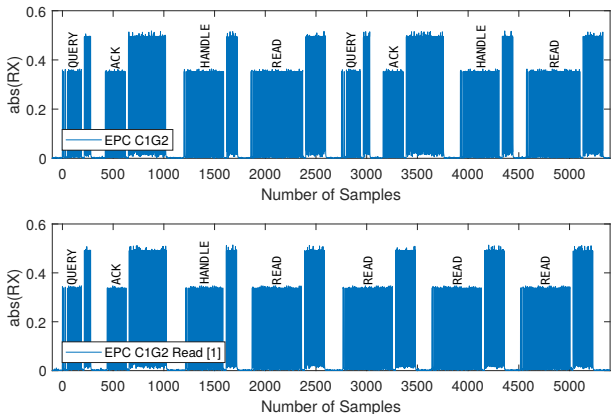

Fig. 9. Signalling of a multiple data read sequence executed using the EPC-C1G2 and a modified version presented in [27].

command sequence indicated. It can be seen that the first four reader-tag-reader message exchanges until the reception of the first data sequence, represent identical commands in both strategies. However, after the first identification phase the approach visualized in the bottom graph is sending consecutive *Read* commands requesting a new data sequence from the corresponding tag each time a reader message is sent. Given a single tag in the surrounding of the reader, the visualized communication sequence, shows that using [27], 4 data reads have been established in the same time as 2 reads using the typically deployed EPC-C1G2 approach.

E. Limitations

Besides the benefits achieved by creating a passive, computational UHF RFID platform with easily exchangable modules, the platform's read range is limited due to the maximum transmit power $P_{\mathrm{max}} = 20\,\mathrm{dBm}$ of the USRP N210 with an SBX daughterboard. Furthermore, providing easy accessibility and connectability by using jumper wires and SMA connectors on the tag side yields a circuitry, which is not optimized for a maximized read range.

V. Conclusion

In this article we presented a passive, modular, computational UHF RFID research platform, consisting of an SDR UHF RFID reader and a modular, passive, computational UHF RFID tag. The proposed architecture allows the researcher to investigate each tag module of a typical UHF RFID chip separately and without modifying the other sections. Thus, the proposed design yields improved flexibility when investigating novel RFID solutions. The experimental results prove the capabilities of the platform considering the measurement of module specific parameters for the incorporated sections.

References

[1] H. Landaluce, L. Arjona, A. Perallos, F. Falcone, I. Angulo, and F. Muralter, "A Review of IoT Sensing Applications and Challenges Using RFID and Wireless Sensor Networks," *Sensors*, vol. 20, no. 9, p. 2495, 2020.

[2] K. Finkenzeller, *RFID Handbook: Fundamentals and Applications in Contactless Smart Cards, Radio Frequency Identification and Near-Field Communication*. John Wiley & Sons, 2010.

[3] A. P. Sample, D. J. Yeager, P. S. Powledge, A. V. Mamishev, and J. R. Smith, "Design of an RFID-based battery-free programmable sensing platform," *IEEE Transactions on Instrumentation and Measurement*, vol. 57, no. 11, pp. 2608–2615, 2008.

[4] Fabbri, Davide and Berthet-Bondet, Eliot and Masotti, Diego and Costanzo, Alessandra and Dardari, Davide and Romani, Aldo, "Long range battery-less uhf-rfid platform for sensor applications," in *2019 IEEE International Conference on RFID Technology and Applications (RFID-TA)*. IEEE, 2019, pp. 80–85.

[5] F. Muralter, L. Arjona, H. Landaluce, and A. Perallos, "A theoretical and experimental study of passive computational RFID tags," in *2019 4th International Conference on Smart and Sustainable Technologies (SpliTech)*. IEEE, 2019, pp. 1–5.

[6] "NXP Ucode 8 Datasheet," https://www.nxp.com/docs/en/data-sheet/SL3S1205-15-DS.pdf, Accessed: 2020-11-30.

[7] "Impinj M700 Series Datasheet," https://support.impinj.com/hc/article_attachments/360016110979/Impinj_M730_and_M750_Tag_Chip_Datasheet_20200902_R4.pdf, Accessed: 2020-11-30.

[8] "Impinj Monza X-8k Dura Datasheet," https://support.impinj.com/hc/article_attachments/360016110999/Impinj_Monza_X-8K_Dura_Tag_Chip_Datasheet_R8_1_20200721.pdf, Accessed: 2020-11-30.

[9] "Farsens Rocky 100; RFID tag ICs for IoT solution development," http://www.farsens.com/en/products/rocky100/, Accessed: 2020-11-30.
[10] "Nordic Semiconductor nRF52832 Product Specification v1.4," https://infocenter.nordicsemi.com/pdf/nRF52832_PS_v1.4.pdf, Accessed: 2021-02-01.
[11] M. Buettner and D. Wetherall, "A software radio-based UHF RFID reader for PHY/MAC experimentation," in *2011 IEEE International Conference on RFID*. IEEE, 2011, pp. 134–141.
[12] D. De Donno, F. Ricciato, L. Catarinucci, and L. Tarricone, "Design and applications of a software-defined listener for UHF RFID systems," in *2011 IEEE MTT-S International Microwave Symposium*. IEEE, 2011, pp. 1–4.
[13] M. Buettner and D. Wetherall, "A" Gen 2" RFID monitor based on the USRP," *ACM SIGCOMM Computer Communication Review*, vol. 40, no. 3, pp. 41–47, 2010.
[14] M. Buettner and D. Wetherall, "A Flexible Software Radio Transceiver for UHF RFID Experimentation: UW TR: UW-CSE-09-10-02," 2011.
[15] N. Kargas, F. Mavromatis, and A. Bletsas, "Fully-coherent reader with commodity SDR for Gen2 FM0 and computational RFID," *IEEE Wireless Communications Letters*, vol. 4, no. 6, pp. 617–620, 2015.
[16] "AMS SL900A EPC Gen2 Sensor Tag," https://ams.com/sl900a, Accessed: 2020-11-30.
[17] D. De Donno, L. Catarinucci, and L. Tarricone, "RAMSES: RFID augmented module for smart environmental sensing," *IEEE Transactions on Instrumentation and Measurement*, vol. 63, no. 7, pp. 1701–1708, 2014.
[18] R. Colella, L. Tarricone, and L. Catarinucci, "SPARTACUS: Self-powered augmented RFID tag for autonomous computing and ubiquitous sensing," *IEEE Transactions on Antennas and Propagation*, vol. 63, no. 5, pp. 2272–2281, 2015.
[19] R. Colella, L. Catarinucci, and L. Tarricone, "Improved battery-less augmented RFID tag: Application on ambient sensing and control," *IEEE Sensors Journal*, vol. 16, no. 10, pp. 3484–3485, 2016.
[20] "WISP 5 firmware repository," https://github.com/wisp/wisp5, Accessed: 2020-11-30.
[21] S. J. Thomas, "RFID for everyone: Design of an easily-accessible, experimental UHF RFID platform," in *2019 IEEE International Conference on RFID (RFID)*. IEEE, 2019, pp. 1–6.
[22] "Alien Technology ALR-A0501 Datasheet," https://www.alientechnology.com/download/alr-a0501-documents/?wpdmdl=7954&ind=QUxSLUEwNTAxIEFudGVubmEgMjAxNy0wMi0yOC5wZGY, Accessed: 2021-01-20.
[23] R. Cao and S.-C. Yu, "Wideband compact CPW-fed circularly polarized antenna for universal UHF RFID reader," *IEEE Transactions on Antennas and Propagation*, vol. 63, no. 9, pp. 4148–4151, 2015.
[24] "Analog Devices ADXL362 Datasheet," http://www.analog.com/media/en/technical-documentation/data-sheets/ADXL362.pdf, Accessed: 2020-11-30.
[25] L. Andrade-Fonseca, A. C. Lisboa, R. Adriano, and E. J. Silva, "Optimized limited size printed bowtie antenna for uhf rfid readers," *Journal of Microwaves, Optoelectronics and Electromagnetic Applications*, vol. 16, no. 4, pp. 922–931, 2017.
[26] "Analog Devices; ADP5090 Datasheet," https://www.analog.com/en/products/adp5090.html, Accessed: 2020-11-30.
[27] G. Souto, F. Muralter, L. Arjona, H. Landaluce, and A. Perallos, "Protocol for Streaming Data from an RFID Sensor Network," *Sensors*, vol. 19, no. 14, p. 3148, 2019.

3.7 A passive computational UHF RFID platform using vector backscatter modulation

Journals & Magazines > IEEE Sensors Journal

A passive computational UHF RFID platform using vector backscatter modulation

Publisher: IEEE

Florian Muralter ; Laura Arjona ; Hugo Landaluce ; Asier Perallos **All Authors**

Submitted to: IEEE Sensors Journal

Status: Under Review

Date of Submission: 13 April 2021

JIF(2019): 3.073

Rank: Q2 in Electrical Engineering
Q1 in Engineering

3.7.1 Preface

The work presented in this manuscript was performed by the author of this thesis, at the DeustoTech Institute of Technology under the supervision of Hugo Landaluce. The corresponding measurements were carried out jointly by Laura Arjona, Hugo Landaluce and Florian Muralter. Asier Perallos supervised the whole project. All authors were involved in the preparation and review process of the manuscript.

3.7.2 Article

A passive computational UHF RFID platform using vector backscatter modulation

Florian Muralter*, Laura Arjona, Hugo Landaluce, Asier Perallos

***Abstract*—This article presents the design and implementation of a passive, computational ultra high frequency (UHF) radio frequency identification (RFID) platform using vector backscatter modulation on the uplink (tag-to-reader). The proposed RFID system consists of a software defined radio (SDR) reader and the corresponding passive, computational tag. The communication protocol is firmware-implemented, thus offering high flexibility in configuring its functionalities. A dual-gate MOSFET is used to implement the vector backscatter modulator. Experimental results prove the feasibility of the platform and show the benefits of using vector backscatter communication in comparison to using the standard binary phase-shift keying (BPSK). For the investigated 128-bit tag-to-reader message based on the EPC Class 1 Generation 2 communication protocol, the sequence length was shortened by a factor of 1.91.**

***Index Terms*—backscatter communication, radio frequency identification (RFID), wireless sensor networks (WSN)**

I. Introduction

Passive, computational, ultra high frequency (UHF) radio frequency identification (RFID) represents a subarea of the initially pure automated identification technology RFID. A typical UHF RFID system consists of a minimum of one reader (interrogator) and at least one tag (transponder) communicating in the industrial, scientific and medical (ISM) UHF band [1]. A passive tag is powered solely by the incident electromagnetic waves emitted by the reader. The tag-to-reader communication is achieved by backscattering a distinct part of this incident radio frequency (RF) field based on the antenna scattering theorem [2]. By changing the impedance seen at the antenna/connector port, the reflection coefficient is changed, and thus, the magnitude and phase of the backscattered electromagnetic wave can be controlled [3]. The EPC Class 1 Generation 2 (EPC-C1G2) standard [4] considers two different types of modulation schemes: binary phase-shift keying (binary PSK) and binary amplitude-shift keying (binary ASK) for the tag-to-reader (uplink) communication. Given the increased complexity of UHF RFID systems incorporating sensing and computational capabilities, the amount of data to be backscattered has been altered. Thus, there is an growing interest in increasing the data rate of such platforms. Vector backscatter modulation presents a promising opportunity to achieve this task [5].

This article presents the design and implementation of a passive, computational UHF RFID research platform using vector backscatter modulation. The proposed RFID system consists of a Software Defined Radio (SDR) reader implemented on an Ettus Research USRP N210 and an RFID tag incorporating a vector backscatter modulator based on a dual-gate N-channel MOSFET.

Manuscript received __, __.

This work has been part-funded by the Basque Government under the project IoTrain (RTI2018-095499-B-C33).

F. Muralter, L. Arjona, H. Landaluce and A. Perallos are with DeustoTech (University of Deusto) .

II. Related Work

With RFID being enabler to the Internet of Things (IoT) [6], sensor and computational RFID have gained further importance. Thus, the uplink backscatter communication has in recent years seen the addition of vector backscatter modulation. In [7] a theoretical study of higher order coded backscatter modulation was performed, concluding that the gained spectral efficiency of moving from 2-QAM (Quadrature Amplitude Modulation) to 4-QAM also comes with an increased power loss. Thomas et al. in [5] proposed a quadrature backscatter modulator, later extended to 16-QAM [5], thus, further investigating the relevance of vector backscatter modulation in UHF RFID. Simulation and measurements of the modulator are presented for a semi-passive implementation only. Additionally, several quadrature backscatter modulators have been proposed in combination with the NeuroDisc brain-computer interface [8], [9], [10].

However, to the best of our knowledge, all proposed architectures have only been used in semi-passive systems. Furthermore, neither have they been implemented to respond to an interrogator message, nor have they been using a communication protocol.

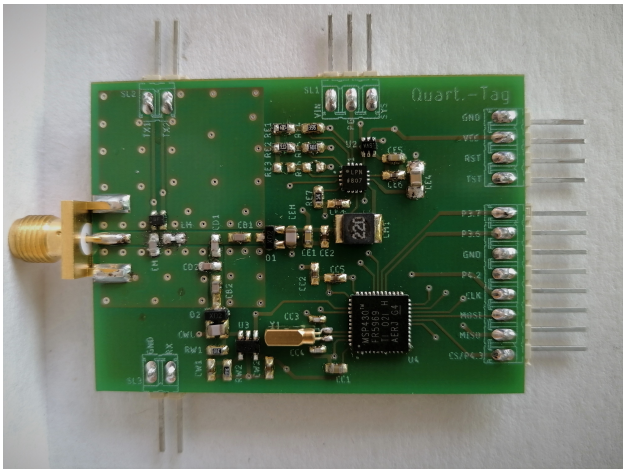

Fig. 1. Passive, computational UHF RFID tag using vector backscatter communication.

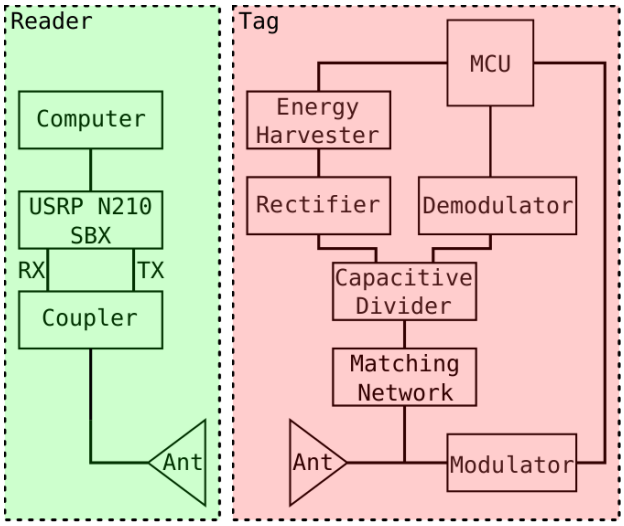

Fig. 2. Visualization of the architecture of the proposed RFID system.

III. Design and Implementation

The following section gives a detailed description of both the design and implementation of the proposed tag using vector backscatter modulation and the corresponding SDR reader.

A. Passive, computational RFID tag with a vector backscatter modulator

The proposed transponder, shown in Fig. 1, consists of the modules presented in Fig. 2 (Tag), and, is based on the designs proposed in [11], [12]. Given this tag architecture, the communication logic is performed by the incorporated MSP430FR5969 microcontroller unit (MCU), which allows to easily adapt the protocol layer by reprogramming the MCU. The incoming interrogator message is demodulated, decoded and processed according to the EPC-C1G2 protocol. Subsequently, a corresponding response message is output at the TX ports of the tag. Considering a 2-bit modulation type, the logic TX signals are output at 2 separate general purpose input output (GPIO) pins, TX1 and TX2. The backscatter communication, according to the EPC-C1G2 can be encoded in either FM0 or Miller encoding, where for the proposed design, FM0 encoding was chosen. Each FM0 message sent by the tag is prepended by the 6-bit EPC-C1G2 compliant FM0 preamble. This standard preamble is sent via the TX1 pin, whereas the TX2 pin is pulled high after the 9th half-bit of the preamble, to allow the reader to estimate the channel for the additional load modulation states (see Fig. 3). Hence, during this custom preamble, all load modulation states are present for at lest 2 half-bits. The two TX pins are directly connected to the gates of a dual-gate N-channel MOSFET (TOSHIBA 3SK293) which is used as the backscatter modulator. Its drain-source path is connected from the RF input to ground. Thus, a change in the gate voltage will result in a change of the conductance in the drain-source path, which further results in a change of the reflection coefficient. Table I explains the relationship between the logic signals at the gates and the corresponding RF behavior at the antenna port.

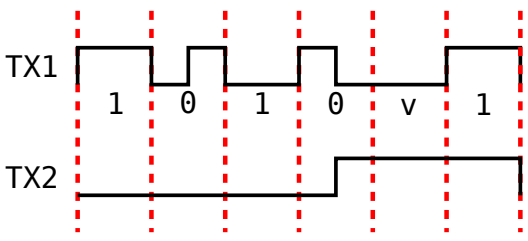

Fig. 3. Usage of the EPC-C1G2 preamble with two TX channels.

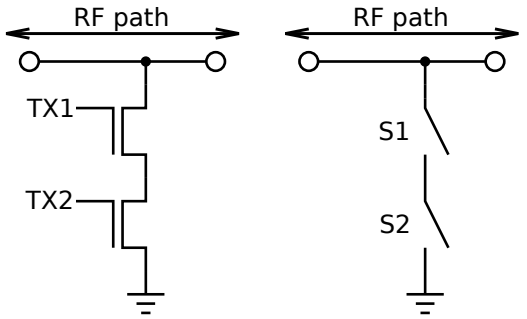

Fig. 4. Schematic and equivalent circuit of the proposed dual-gate MOSFET modulator.

TX1	TX2	S1	S2	Behavior
0	0	open	open	open circuit
0	1	open	closed	open circuit
1	0	closed	open	open ended stub
1	1	closed	closed	shorted stub

TABLE I
Logic table of the proposed dual-gate MOSFET modulator.

The resulting constellation, measured on the USRP when connecting the tag directly (without antenna) to the SMA port of the USRP with an output power of $P_{\mathrm{OUT}} = 0\,\mathrm{dBm}$ is shown in Fig. 5. It can be seen that the ”00” and ”01” states refer to a similar reflection coefficient, as in both cases, the channel controlled by gate 1 is not conducting, thus, representing a open circuit. A larger mismatch is present for the ”10” state. Here, the first PNP junctions resistance is lowered, showing the behaviour of a open ended stub. When both gates are pulled high, the dual-gate MOSFET represents a short circuit to ground, obtaining a maximum mismatch. The explained behavior results in only 3 achievable impedance states. However, based on the possible signal transitions in FM0 coded 2-bit sequences as shown in Fig. 6 and considering the proposed demodulator implementation on the reader side, all four signal states can be detected. Furthermore, considering that ”00” represents the absorbing state, ”01” also refers to a matched impedance state, thus, the resulting constellation significantly decreases the power loss during backscatter communication, omitting one of the key drawbacks of vector backscatter modulation presented in [7].

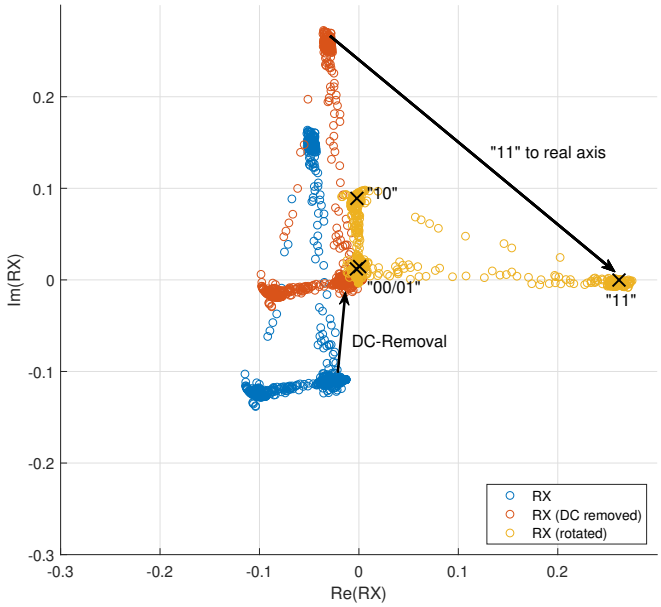

Fig. 5. Constellation Processing of the RX signal on the USRP prior to the decoding.

B. SDR UHF RFID reader

The corresponding SDR UHF Reader design is implemented on an Ettus Research USRP N210 and represents an alteration and improvement of the implementations presented in [13] and [14]. The used SDR framework is GNU Radio, where the out-of-tree modules were programmed in C++ and the modules connected using Python. To add the possibility of operating with a single antenna or connecting the RFID tag directly to a subminiature A (SMA) port, a directional coupler (Mini-Circuits ZFDC-15-10-S+) was added to the setup as shown in Fig. 2. However, the main modification compared to the SDR reader design previously presented in [13] is the implementation of the quaternary FM0 demodulator.
Before demodulating the signal based on its constellation, the incoming signal is preprocessed as follows. These steps are visualized in Fig. 5.

- DC offset removal during the time where the reader is waiting for a tag response (absorbing state).
- Channel estimation for the different load modulation states, given the custom FM0 preamble.
- Rotation of the constellation to map the 00 and 11 states onto the real axis.

The 16 possible signal transitions between FM0 symbols are shown in Fig. 6. These, only yield 4 different pulse shapes at the bit transition (T1 - T4). At the end of a symbol, only transitions between ”00” ↔ ”11” or ”01” ↔ ”10” and vice versa exist. The resulting waveforms corresponding to the four mentioned transitions are:

TX1	TX2	prev1	prev2	Transition
Data1	Data1	0	0	T1
		1	1	T2
		1	0	T3
		0	1	T4
Data1	Data0	0	0	T1
		1	0	T2
		1	1	T3
		0	1	T4
Data0	Data1	1	0	T1
		0	1	T2
		0	0	T3
		1	1	T4
Data0	Data0	1	1	T1
		0	0	T2
		0	1	T3
		1	0	T4

TABLE II
LOGIC TABLE OF THE PROPOSED SDR DEMODULATOR FOR DECODING THE QUATERNARY FM0 SIGNAL

$$T_{1,k} = \begin{cases} 11, & -\frac{L}{2} < k \leqslant 0 \\ 00, & 0 \leqslant k < \frac{L}{2} \end{cases}, \; T_{2,k} = \begin{cases} 00, & -\frac{L}{2} < k \leqslant 0 \\ 11, & 0 \leqslant k < \frac{L}{2} \end{cases},$$
$$T_{3,k} = \begin{cases} 01, & -\frac{L}{2} < k \leqslant 0 \\ 10, & 0 \leqslant k < \frac{L}{2} \end{cases}, \; T_{4,k} = \begin{cases} 10, & -\frac{L}{2} < k \leqslant 0 \\ 01, & 0 \leqslant k < \frac{L}{2} \end{cases}, \quad (1)$$

with $T_{i,k}$ representing the pulse shape, L the symbol duration and k the time samples. The signal states (11, 00, 01, 10) refer to the states of the two separate TX channels. Considering the signal states as indicated in Fig. 5, transitions T_1 and T_2 refer to a large change of the real part, and T_3 and T_4 correspond to a large change of the imaginary part. The data symbols are then decoded using the logic presented in Table II. The stored variables *prev1* and *prev2* represent the states of TX1 and TX2 during the half-bit before the previous bit transition, respectively. For example, for the transition highlighted with a black rectangle in Fig. 6 the previous bit states are $prev1 = prev2 = 0$, and the signal transition identified due to a negative step in the real part is $T1$. Thus, the decoded message, according to the corresponding logic combination in Table II refers to a Data1 sent on both TX channels.

IV. RESULTS

To investigate the digital communication performed by the microcontroller, the proposed platform allows to access the RX and the two TX pins of the tag. Furthermore, the SDR reader provides the possibility to export the incoming and outgoing IQ signal data for offline processing. The following section presents an investigation of a typical tag identification procedure using the presented RFID system. This so called inventory round consists of the following commands alternating between reader and tag: Query - RN16 - ACK - EPC.
Fig. 7 shows a visualization of both the TX and RX signals at the tag acquired using the digital inputs of an oscilloscope. Furthermore, the real and imaginary parts of the RX signal received, digitalized preprocessed on the USRP are visualized.

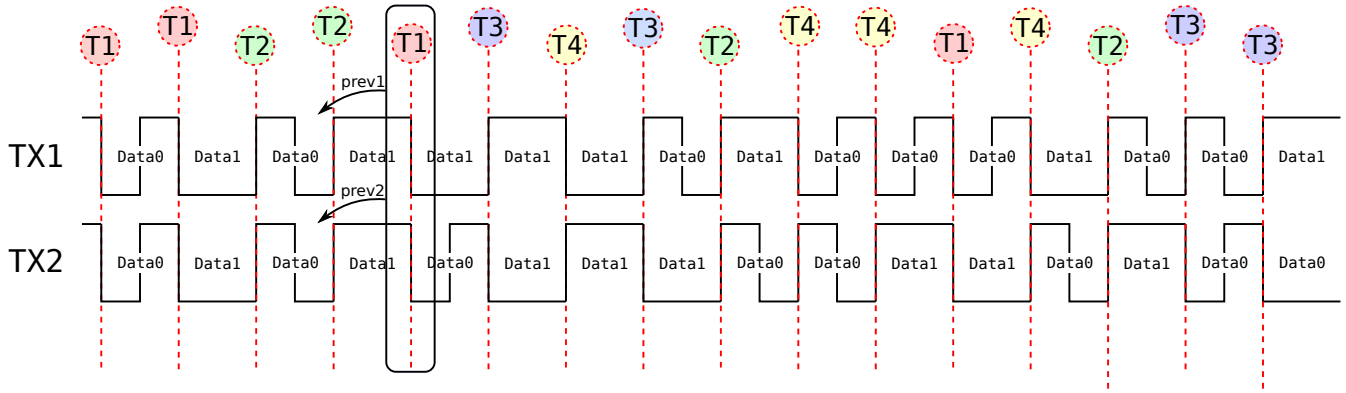

Fig. 6. Visualization of all 16 possible symbols and the resulting 4 signal transitions (T1, T2, T3, T4) at bit transitions.

It can be seen that the SDR's RX signal represents a superposition of both the reader commands and the backscattered tag response. The preamble transmitted on the 2 different TX channels further yields the 4-state preamble visible in the reader's RX signal. TX1's first signal transition represents the start of the preamble, where as the first signal transition of TX2 appears between the seventh and eigth half bit of the preamble as shown in Fig. 3. A comparison of the Query commands on the reader and the tag proves the correct demodulation of the message on the tag.

The same platform's microcontroller can be reprogrammed, such that an EPC-C1G2 compliant communication using binary modulation is achieved. In this case, the message transmitted by the tag is output on both TX channels to allow for a better modulation depth. Fig. 8 shows the tag response to an EPC-C1G2 ACK command for both binary and quaternary backscattering. During the backscattered response, the 3 possible signal states are clearly visible. Furthermore, Fig. 8 allows a direct comparison of the backscatter response length for equivalent messages. Considering a 128-bit response after the custom preamble, the quaternary backscatter solution yields a tag response shortened by a factor of 1.91.

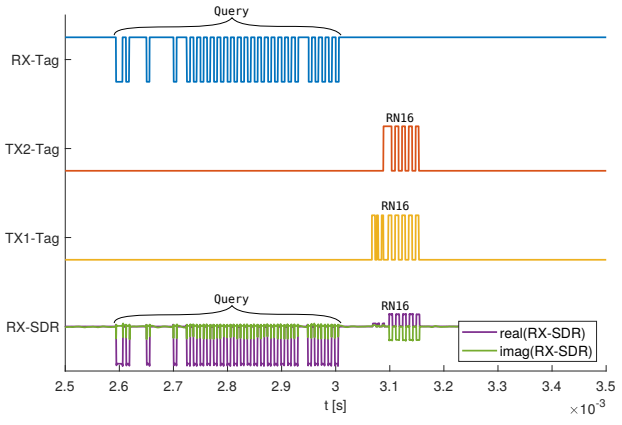

Fig. 7. RX/TX signaling for a Query command with RN16 response.

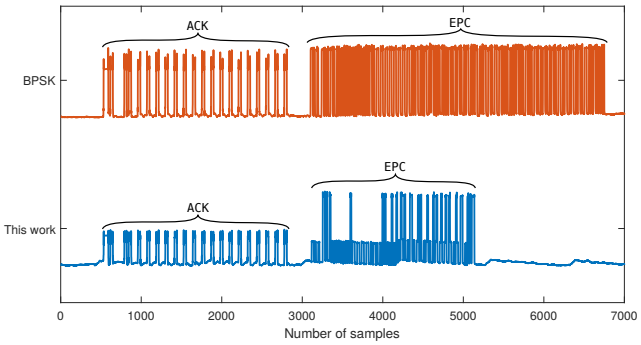

Fig. 8. Comparison of standard BPSK response and the response of the proposed tag, considering an ACK command and the corresponding tag response.

V. Conclusion

In this work, we have presented the design and implementation of a passive computational UHF RFID platform using vector backscatter communication. Both the design of the tag and the implementation of the compatible SDR reader have been explained in detail, and their performance has been investigated. The firmware based implementation of the EPC-C1G2 communication protocol provides easy adaptability, where the dual channel modulator further allows the usage of the platform with both binary and quaternary backscatter modulation. Experimental results using the EPC-C1G2 communication protocol prove the applicability and further yield a comparison to the typically used BPSK backscatter modulation. For the investigated 128-bit tag-to-reader message, a shortening of the response length by a factor of 1.91 has been achieved.

References

[1] K. Finkenzeller, *RFID handbook: fundamentals and applications in contactless smart cards, radio frequency identification and near-field communication*. John wiley & sons, 2010.

[2] R. C. Hansen, "Relationships between antennas as scatterers and as radiators," *Proceedings of the IEEE*, vol. 77, no. 5, pp. 659–662, 1989.

[3] F. Fuschini, C. Piersanti, F. Paolazzi, and G. Falciasecca, "Analytical approach to the backscattering from uhf rfid transponder," *IEEE Antennas and Wireless Propagation Letters*, vol. 7, pp. 33–35, 2008.

[4] "EPC™ Radio-Frequency Identity Protocols Generation-2 UHF RFID Standard."

[5] S. J. Thomas, E. Wheeler, J. Teizer, and M. S. Reynolds, "Quadrature amplitude modulated backscatter in passive and semipassive uhf rfid systems," *IEEE Transactions on Microwave Theory and Techniques*, vol. 60, no. 4, pp. 1175–1182, 2012.
[6] X. Jia, Q. Feng, T. Fan, and Q. Lei, "RFID technology and its applications in Internet of Things (IoT)," in *2012 2nd International Conference on Consumer Electronics, Communications and Networks (CECNet)*, 2012, pp. 1282–1285.
[7] C. Boyer and S. Roy, "Coded qam backscatter modulation for rfid," *IEEE Transactions on Communications*, vol. 60, no. 7, pp. 1925–1934, 2012.
[8] J. Rosenthal, E. Kampianakis, A. Sharma, and M. S. Reynolds, "A 6.25 mbps, 12.4 pj/bit dqpsk backscatter wireless uplink for the neurodisc brain-computer interface," in *2018 IEEE Biomedical Circuits and Systems Conference (BioCAS)*. IEEE, 2018, pp. 1–4.
[9] J. Rosenthal, A. Pike, and M. S. Reynolds, "A 1 mbps 158 pj/bit bluetooth low energy (ble) compatible backscatter communication uplink for wireless neural recording in an animal cage environment," in *2019 IEEE International Conference on RFID (RFID)*. IEEE, 2019, pp. 1–6.
[10] J. Rosenthal and M. S. Reynolds, "A dual-band shared-hardware 900 mhz 6.25 mbps dqpsk and 2.4 ghz 1.0 mbps bluetooth low energy (ble) backscatter uplink for wireless brain-computer interfaces," in *2020 IEEE International Conference on RFID (RFID)*. IEEE, 2020, pp. 1–6.
[11] A. P. Sample, D. J. Yeager, P. S. Powledge, A. V. Mamishev, and J. R. Smith, "Design of an rfid-based battery-free programmable sensing platform," *IEEE transactions on instrumentation and measurement*, vol. 57, no. 11, pp. 2608–2615, 2008.
[12] D. Fabbri, E. Berthet-Bondet, D. Masotti, A. Costanzo, D. Dardari, and A. Romani, "Long range battery-less uhf-rfid platform for sensor applications," in *2019 IEEE International Conference on RFID Technology and Applications (RFID-TA)*. IEEE, 2019, pp. 80–85.
[13] N. Kargas, F. Mavromatis, and A. Bletsas, "Fully-coherent reader with commodity sdr for gen2 fm0 and computational rfid," *IEEE Wireless Communications Letters*, vol. 4, no. 6, pp. 617–620, 2015.
[14] M. Buettner and D. Wetherall, "A software radio-based uhf rfid reader for phy/mac experimentation," in *2011 IEEE International Conference on RFID*. IEEE, 2011, pp. 134–141.
[15] D. J. Yeager, A. P. Sample, J. R. Smith, and J. R. Smith, "Wisp: A passively powered uhf rfid tag with sensing and computation," *RFID handbook: Applications, technology, security, and privacy*, pp. 261–278, 2008.
[16] R. Correia and N. B. Carvalho, "Design of high order modulation backscatter wireless sensor for passive iot solutions," in *2016 IEEE Wireless Power Transfer Conference (WPTC)*. IEEE, 2016, pp. 1–3.
[17] R. Correia, A. Boaventura, and N. B. Carvalho, "Quadrature amplitude backscatter modulator for passive wireless sensors in iot applications," *IEEE Transactions on Microwave Theory and Techniques*, vol. 65, no. 4, pp. 1103–1110, 2017.
[18] F. Muralter, L. Arjona, H. Landaluce, and A. Perallos, "A modular, passive, computational uhf rfid research platform," *IEEE Transactions on Microwave Theory and Techniques*, vol. 65, no. 4, pp. 1103–1110, 2017.
[19] F. Muralter, H. Landaluce, R. Del-Rio-Ruiz, and A. Perallos, "Selecting impedance states in a passive computational rfid tag backscattering in psk," *IEEE Microwave and Wireless Components Letters*, vol. 29, no. 10, pp. 680–682, 2019.
[20] S. J. Thomas and M. S. Reynolds, "A 96 mbit/sec, 15.5 pj/bit 16-qam modulator for uhf backscatter communication," in *2012 IEEE International Conference on RFID (RFID)*. IEEE, 2012, pp. 185–190.

Copyright

CHAPTER 4 Conclusions and Future Work

This chapter summarizes the conclusions drawn as part of the original scientific work presented in Chapter 3. Furthermore, identified gaps and opportunities that possibly yield further improvements and advances in the area of computational UHF RFID are discussed.

4.1 Conclusions

The scientific work presented as part of this Ph.D. thesis discusses the steps taken to design and implement a passive computational UHF RFID platform using vector backscattering.

4.1.1 State of the Art

To obtain a thorough understanding of the State of the Art in passive computational UHF RFID, several commercial and research platforms have been investigated to identify the gaps and needs to further improve this technology. Only very few existing designs allow for the alteration of the protocol layer, which considering the development of an adapted backscatter modulation approach is a must. Furthermore, the available methodologies for measuring the input impedance of a UHF RFID chip are limited due to the nonlinear character of passive RFID chips and the fact that the typically used dipole antennas are balanced devices.

4.1.2 UHF RFID impedance measurement

The impedance measurement of UHF RFID chips poses a well known problem, mainly, due to the rectifying and energy harvesting circuitry. The rectifying Schottky diodes are low Q factor devices and their input impedance, being the main influence on the chip impedance, varies strongly as a function of input power and frequency. Thus, measuring the input impedance of an UHF RFID chip yields a difficult task. As a result, achieving a good impedance matching at power levels around the power threshold also poses problems. Furthermore, the nonlinear behavior of these devices results in a reflection of not only the fundamental frequency, but also reflected power at harmonic frequencies.

In the incorporated scientific works, we have proposed an alternative approach to measuring the harmonic reflected power of a UHF RFID chip using a DSO and a novel signal processing methodology. The results have been compared and validated to the commonly used Vector Network Analyzer (VNA) based

method. The results of the harmonic reflection coefficients for commercially available UHF RFID chips, have shown that, for matching an RFID chip at the chip sensitivity, which corresponds to low power levels, the power reflected at the harmonic frequencies can be neglected. However, for power levels above the chip sensitivity, the response message backscattered by the tag, was detectable also at the harmonic frequencies.
Another improvement presented as part of this thesis, yields an alternative approach for measuring the chip impedance, by using a transmission line transformer test fixture. The proposed method uses the transmission line transformer as both, a balanced-to-unbalanced converter (BALUN) and a prematching network to compensate the high reactance of the RFID chip's energy harvesting section. Compared to the typically used single-ended method, the impedances measured with the proposed approach have achieved better results when used to design matching networks using a Smith chart approach.

4.1.3 **Modular UHF RFID research platform**

To the best of our knowledge, none of the existing passive, computational UHF RFID platforms provide the possibility to access certain modules of the chip architecture without redesigning the whole tag. We have proposed a platform, which allows to access all modules (Rectifier, Energy Harvester, Demodulator, Modulator and MCU) separately. Each of the modules can be substituted or adapted, without altering the rest of the architecture, thus, yielding a more flexible platform for developing new RFID solutions. The proposed platform was then used to develop a UHF RFID tag using vector backscatter modulation. The 2-bit backscatter modulator was implemented using a dual gate MOSFET. To decode the 3-state FM0 modulated signal, a new approach based on a shifted examination of the transmitted waveform was used. The complete platform consisting of both, the vector backscattering RFID tag and the SDR reader was merged using a slightly modified EPC-C1G2 communication protocol.

4.2 Future Work

The work presented as part of this thesis has fruited in the development of a passive, computational UHF RFID platform using vector backscatter modulation. This new addition to the backscattering of passive UHF RFID tags results in a set of new possibilities to further improve the capabilites of RFID systems. This section presents some ideas, concepts and plans for future progress in the area of passive, computational UHF RFID.

Due to the achieved shorter backscatter response time, the duration of tag operation is shortened, which could result in a lower power consumption. However, the need of additionally feeding power to the second gate of the MOSFET, thus, driving two General Purpose Input Output (GPIO) pins increases the power consumption. A future plan is to investigate the effect of multi-state modulators and their corresponding communication routines, on the overall power consumption during backscatter communication.
Given the developed passive, computational UHF RFID platform using vector backscatter modulation the usage of the four backscattered states, considering novel approaches in the protocol layer can yield a significantly better communication performance. One such proposal could be using two states according to the EPC-C1G2 and the other two for simultaneous data transmission. This step would need further adaptions to the protocol layer, as the reader would have to understand, whether or not, a data message is submitted.
The easy and cheap deployment of a dual-gate MOSFET as a quaternary load modulator can possibly be expanded to higher order modulation types. However, the desired constellations would have to be adapted for better reflection coefficient separation.
As RF energy harvester's efficiencies are increasing rapidly and novel low power sensors are being developed on a daily basis, this addition to backscatter communication might help RFID sensing gain more attention in the IoT, which in return would further increase the research focus and yield faster progress.

Declaration

I herewith declare that I have produced this work without the prohibited assistance of third parties and without making use of aids other than those specified; notions taken over directly or indirectly from other sources have been identified as such. This work has not previously been presented in identical or similar form to any examination board.

The dissertation work was conducted from 2018 to 2021 under the supervision of Dr. Hugo Landaluce and Dr. Asier Perallos at the University of Deusto.

Bilbao,

This dissertation was finished writing in Bilbao on May 13, 2021

This page is intentionally left blank